UNIVERSITY OF CALIFORNIA

Santa Barbara

Genetic Regulation of Retinal Development

A dissertation submitted in partial satisfaction

of the requirement for the degree Doctor of Philosophy

in Molecular, Cellular, and Developmental Biology

by

Bridget Kulesh

Thesis Committee:

Professor Benjamin E. Reese, Chair

Professor Stuart Feinstein

Professor Kathy Foltz

Professor Dennis O. Clegg

December 2022

The dissertation of Bridget Kulesh is approved.

_____

Stuart Feinstein

_____

Kathy Foltz

_____

Dennis O. Clegg

_____

Benjamin E. Reese, Committee Chair

December 2022

Genetic Regulation of Retinal Development

By

Bridget Kulesh

ACKNOWLEDGEMENTS

This dissertation would not be possible without the support of the faculty and students in the MCDB department at UCSB, many who I am lucky enough to call my friends. Their continued encouragement provided much of the motivation when I didn't think there was a light at the end of the tunnel. Numerous people deserve special recognition and thanks.

First, I would like to thank my mentor, Ben Reese, who allowed me to complete a fourth rotation my first year of graduate school. His passion for research pushed me to be a better scientist, both in the lab and as an academic writer. I would also like to thank Patrick Keeley, as a coworker, office mate, mentor, and close friend. You were always available to provide help and advice to me when I asked (and sometimes when I didn't, but still needed it), and would not have been as successful as I was without your guidance. I would also like to thank my committee for their continual support, especially during the COVID pandemic, when the university was working remotely. None of this would have been possible without the love from the "Davenport Girls" (Haley Smith, Christine Tchounwou, Claire (Tran) Banovetz, and Aneta Jelowicki), who helped keep me grounded during graduate school, and reminded me to have fun every once in a while. A special thanks to everyone in the Santa Barbara volleyball community, both players and coaches, many whom have become lifelong friends. To my parents, Joanne and David, and my brother, Andrew, who's love and support I could always feel from 3,000 miles away. Finally, to Jason, who may not have always understood what I was working on, but nevertheless supported me through the ups and downs of graduate school.

CURRICULUM VITAE

Bridget Kulesh

December 2022

EDUCATION:

Doctor of Philosophy	Molecular, Cellular, and Developmental Biology University of California, Santa Barbara December 2022 (expected)
Master of Science	Cellular and Microbial Biology The Catholic University of America May 2015
Bachelor of Science	Biology, Honors in Biology and Theology, *Summa Cum Laude* The Catholic University of America May 2014

PUBLICATIONS:

Kulesh B, Reese BE, Keeley PW. (2022). Contraction of axonal and dendritic fields in *Sox5*-deficient cone bipolar cells is accompanied by axonal sprouting and dendritic hyper-innervation of pedicles. *Frontiers in Neuroanatomy*. 16(944706): 1-13.

Benbow SJ, Wozniak KM, **Kulesh B**, Savage A, Slusher BS, Littlefield BA, Jordan MA, Wilson L, Feinstein SC. (2017). Microtubule-Targeting Agents Eribulin and Paclitaxel Differentially Affect Neuronal Cell Bodies in Chemotherapy-Induced Peripheral Neuropathy. *Neurotox Res.* 32(1):151-162.

Furman C, Mehla J, Ananthaswamy N, Arya N, **Kulesh B**, Kovach I, Ambudkar SV, Golin J. (2013). The deviant ATP-binding site of the multidrug efflux pump Pdr5 plays an active role in the transport cycle. *J. Biol Chem*. 288(42): 30420-30431.

PRESENTATIONS:

Kulesh, B., Keeley, P.W., & Reese, B.E. "*Dixdc1* modulates AII amacrine cell number in the mouse retina" The Association for Research in Vision and Ophthalmology (ARVO). 2019.

Kulesh, B., Keeley, P.W., & Reese, B.E. "Candidate gene analysis of 2 QTL modulating AII amacrine cell number in mouse retina" The Association for Research in Vision and Ophthalmology (ARVO). 2018.

Kulesh, B., Joly, S.P., & Golin, J. “Using suppressors to find proteins that interact with *Pdr5*” The Catholic University of America Biology Graduate Student Research Symposium. 2015.

TEACHING EXPERIENCE:

Teaching Assistant for Molecular Genetics Spring 2022
Department of Molecular, Cellular, and Developmental Biology,
University of California, Santa Barbara

Teaching Assistant for Developmental Neurobiology Spring 2021
Department of Molecular, Cellular, and Developmental Biology,
University of California, Santa Barbara

Graduate Mentor for Summer Institute in Mathematics and Science (SIMS) Summer 2019 & 2020
Center for Science and Engineering Partnerships (CSEP),
University of California, Santa Barbara

Teaching Associate for Biology Mentoring and Engagement II Winter 2020
Department of Molecular, Cellular, and Developmental Biology,
University of California, Santa Barbara

Teaching Assistant for Biology Mentoring and Engagement III Spring 2017 & 2019
Department of Molecular, Cellular, and Developmental Biology,
University of California, Santa Barbara

Teaching Assistant for Biology Mentoring and Engagement II Winter 2017-2019 & 2021
Department of Molecular, Cellular, and Developmental Biology,
University of California, Santa Barbara

Teaching Assistant for Biology Mentoring and Engagement I Fall 2016-2022
Department of Molecular, Cellular, and Developmental Biology,
University of California, Santa Barbara

Teaching Assistant for Introduction to Biology Laboratory Fall 2015 & Summer 2016
Department of Molecular, Cellular, and Developmental Biology,
University of California, Santa Barbara

Teaching Assistant for Investigations in Molecular Cell Biology Lecture and Laboratory Spring 2014 & 2015
Department of Biology, The Catholic University of America

Teaching Assistant for General Microbiology Laboratory Fall 2013 & 2014
Department of Biology, The Catholic University of America

AWARDS AND HONORS**:**

Jane Altman Memorial Fellowship 2021
Department of Molecular, Cellular, and Developmental Biology,
University of California, Santa Barbara

Doreen J. Putrah Cancer Research Foundation Conference Fellowship 2019
Department of Molecular, Cellular, and Developmental Biology,
University of California, Santa Barbara

UCSB Quarter Fellowship 2018
Department of Molecular, Cellular, and Developmental Biology,
University of California, Santa Barbara

Senior Biology Academic Achievement Award 2014
Department of Biology, The Catholic University of America

Landmark Conference Volleyball Senior Scholar Athlete 2013
The Catholic University of America

Phi Beta Kappa Honors Society 2014
The Catholic University of America

Phi Eta Sigma Freshman Honors Society 2010
The Catholic University of America

ABSTRACT

Genetic Regulation of Retinal Development

by

Bridget Kulesh

The development of the central nervous system (CNS), which includes the brain, requires the coordination of numerous intricate processes. Due to its complexity, the brain can be a difficult tissue to use to investigate the genes that are involved in regulating these processes. The retina, which is a simpler tissue in the CNS, can be utilized to study the mechanisms that underlie proper development and maintenance. The murine retina, in which numerous cell types have been studied, provides researchers with a model to study. In this dissertation, three genes and their involvement in retinal development will be evaluated. In the first chapter, we utilize 26 recombinant inbred (RI) strains in order to elucidate genes, as well as their genetic variants, that regulate the size of a neuronal cell population, the AII amacrine cell. In the second chapter, we investigate the genetic regulation of neuronal migration during retinal development. The final chapter describes the analysis of a cell-type specific transcription factor that regulates the morphology of that cell. Studying the genes that regulate the development of the retina provides insight to how the nervous system develops, the knowledge of which should ultimately contribute to the design of successful therapeutics, particularly those involving cell and gene replacement strategies.

TABLE OF CONTENTS

LIST OF FIGURES AND TABLES

I**NTRODUCTION**

The central nervous system (CNS) is a complex structure required for a variety of functions, such as memory, cognition, and motor control. The “control center” of the CNS, the brain, contains billions of neurons forming trillions of synaptic connections. Numerous populations of neurons are necessary to control such a complex system. However, investigating the brain and its development can be an arduous undertaking because of its size and complexity. Fortunately, the CNS includes a much smaller and organized tissue, which comes from the developing forebrain: the retina (Hamburger and Hamilton, 1951, Figure 1). Determining the mechanisms involved in regulating retinal development has been critical in providing further insights into proper development and various functions of the CNS, as well as discovering much-needed therapies for many debilitating neurological diseases.

As early as the 1890’s, Santiago Ramón y Cajal was using then-novel staining techniques to characterize the five major classes of retinal cells, and to distinguish individual types contained within each class, based on their morphologies. As new experimental techniques were developed, researchers began to further differentiate cells based on their physiological responses to stimuli. More recently, retinal cells have been profiled based on gene expression, culminating in an estimated 130 neuronal cell types in the murine retina, which fall under one of five neuronal cell classes (Jeon, Strettoi and Masland 1998, Macosko et al. 2015, Shekhar et al. 2016, Tran et al. 2019).

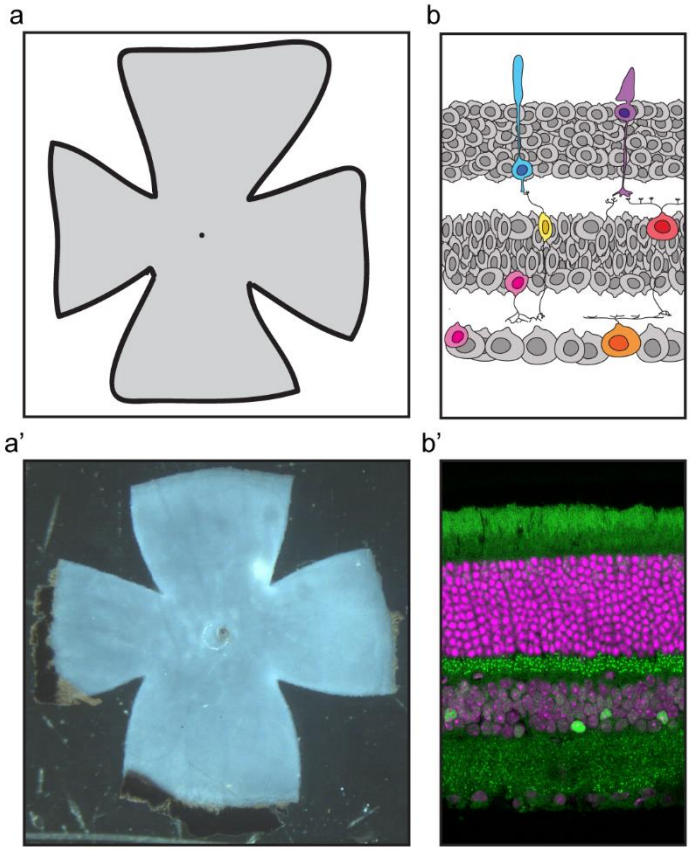

Figure 1: Retinal wholemounts and sections. a : Cartoon representation of a hemispheric retinal wholemount with radial cuts, so that it may lie flat. b: Cartoon representation of a retinal section, with all three nuclear and two plexiform layers visible. a' & b': Examples of (a) a retinal wholemount and (b) a retinal section.

The retina is an attractive model to study neuronal development

The retina is a thin piece of tissue that arises from the developing forebrain, located in the back of the eye. The role of the retina is to transduce light responses into a neural signal and process it, before undergoing further interpretation by the brain. The retina consists of three nuclear layers, where the cells reside, and two plexiform layers, where their processes form synaptic connections (Figure 2a). The outer nuclear layer (ONL) is comprised of the two types of photoreceptor cells: rods and cones. In the murine retina, 97% of the photoreceptor population is comprised of rods (Jeon et al. 1998). Photoreceptors are responsible for converting light into a neural signal and passing it along to the various cells in the retina, which will further process the signal. Bipolar cells, located in the inner nuclear layer (INL), receive the information from their presynaptic partners, the photoreceptors, in the outer plexiform layer (OPL). Bipolar cells are classified as either rod or cone bipolar cells, depending on which photoreceptor they preferentially form synaptic connections with. There are 14 bipolar cell types that synapse with cones, and one with rods. Interestingly, the murine retina's photoreceptor population is predominantly rods (Shekhar et al. 2016). The signal is then transmitted to ganglion cells through connections in the inner plexiform layer (IPL). The axons of ganglion cells form a bundle that make up the optic nerve, which exits the back of the eye and transmits the signal to the brain. Horizontal and amacrine cells, additional interneurons located in the INL, are responsible for providing feedback and further processing of the visual signal.

The retina has become a useful tool in studying neural development in various model organisms. As mentioned earlier, the retina is an outgrowth from the developing

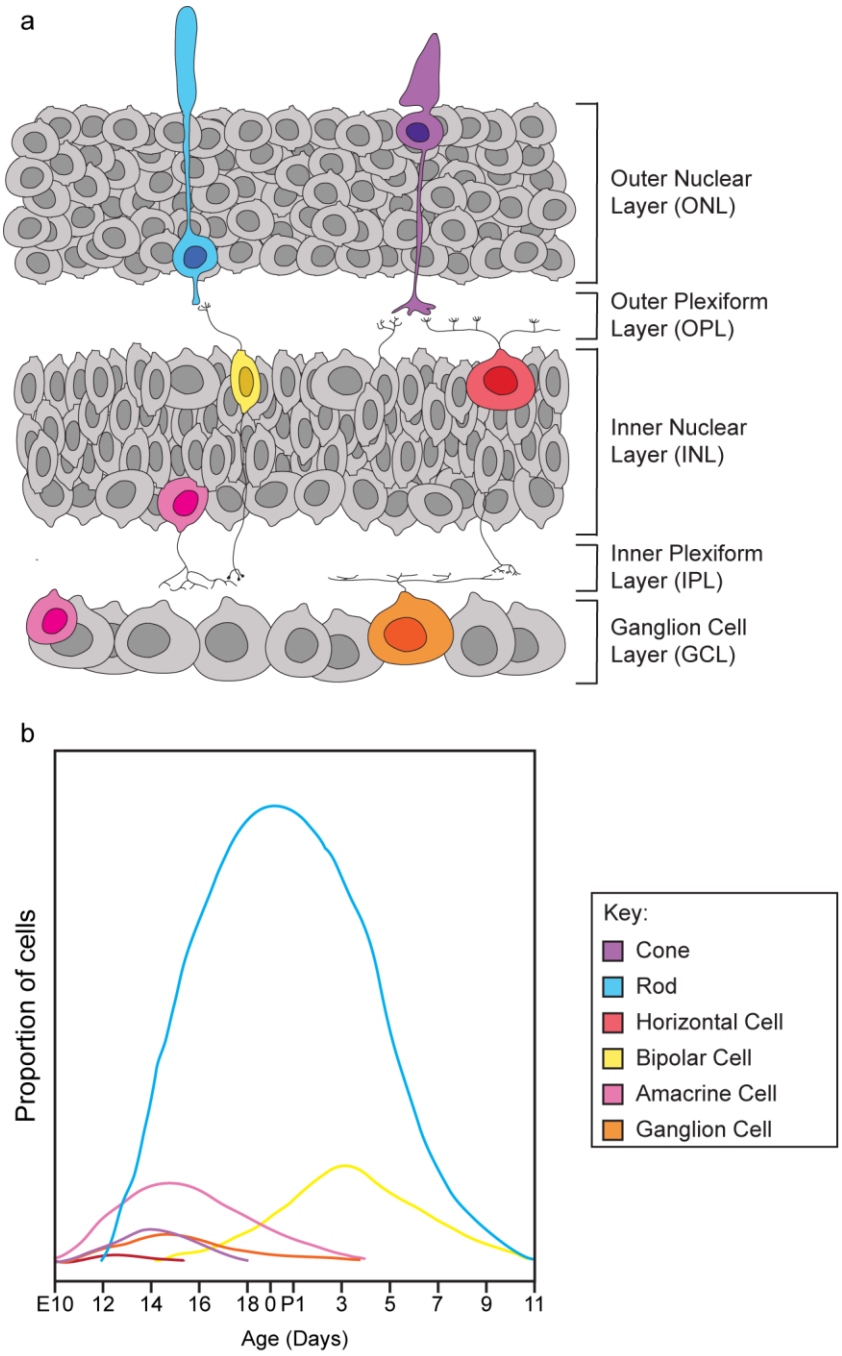

Figure 2: Neuronal cell classes and development. a: The retina is comprised of five neuronal cell classes: Photoreceptors (rods and cones), horizontal cells (HCs), bipolar cells (BCs), amacrine cells (ACs), and retinal ganglion cells (RGCs). These cells are organized into three nuclear layers, and synapse with one another in the two plexiform layers. b: The proportion of cell classes that are born from embryonic day 10 (E10) to postnatal day 11 (P11). The sizes of the curves are meant to convey the variation in absolute number between the cell types, believed to reflect the precise species-specific specification of cell number in a mouse, an issue addressed in Chapter 1. Modified from Young 1985.

forebrain, and thus is part of the CNS. Many of the developmental processes that occur in the retina are therefore similar to those underlying the development of the brain. The retina's laminar architecture provides researchers with a structure that contains distinct layers that are populated by known cell types, enabling entire cell populations to be studied, which can be difficult to study in the brain, in which three dimensions must be considered.

The five neuronal cell classes that make up these layers have been extensively studied, as well as the various types within each of them. They have been characterized by their morphologies, synaptic partners, and gene expression. Understanding the genes that determine the fates of the different classes, and that drive the differentiation of the individual types within a class, is a starting point for understanding the cellular and molecular mechanisms that underlie the formation of neuronal circuitry.

Retinal development follows a set of sequential steps

The development of the brain follows a set of consecutive phases, and retinal development is no different. The processes include: 1) proliferation, 2) fate determination, 3) cellular migration, 4) morphological differentiation and synaptogenesis, and 5) cell death. Each cell class undergoes these processes, though not all simultaneously or to the same extent. Additionally, the precise molecular mechanisms behind each of these steps differs between cell classes.

1) Proliferation

The early murine retina is a pseudostratified tissue made up of dividing retinal progenitor cells (RPCs) (Cepko et al. 1996). Each cell contains processes that attach

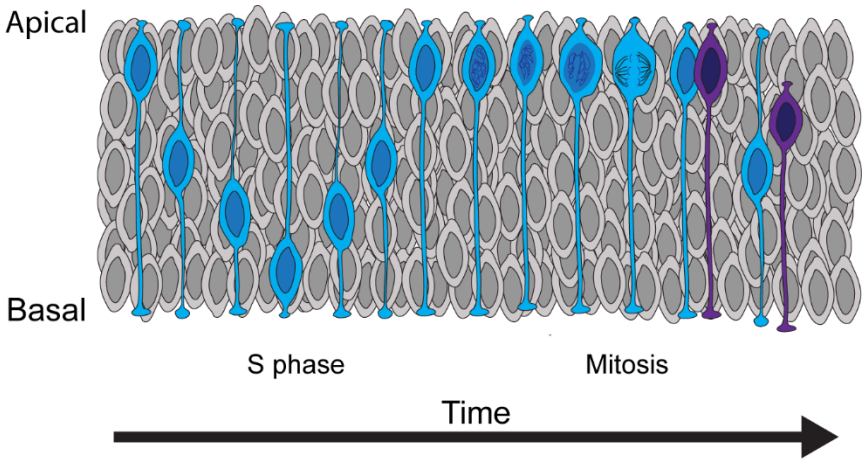

Figure 3: Proliferation via interkinetic nuclear migration. Progenitor cells translocate from the apical surface at the outer limiting membrane (OLM) towards the basal surface of the developing retina, where they will undergo S phase. The cells then translocate back to the apical surface, where mitosis occurs, resulting in either 1) two daughter cells that will returns to the cell cycle (blue) or 2) asymetric division, where one cell will return to the cell cycle (blue) and one that begins differentiating (purple). The to- and fro- nature of interkinetic nuclear migration is believed to be unique to proliferating progenitor cells, but post-mitotic photoreceptors also engage in such behavior, considered in Chapter 2.

to both the apical and basal membranes of the retinal neuroepithelium, corresponding to the ventricular surface and the basement membrane of the developing CNS, respectively. Early in embryogenesis, these cells begin dividing, via interkinetic nuclear migration, to increase the total cell population (Baye and Link 2008). Proliferating cell nuclei translocate towards the basal side of the neuroepithelium during G1, enter S phase and duplicate their DNA, and move back to the apical surface during G2 (Figure 3). These cells then undergo mitosis at the ventricular surface, which will become the future outer limiting membrane (OLM) (Sidman 1961).

2) Fate Determination

As the population of RPCs increases, there is a transition of these cells towards a neurogenic phase, where cell divisions will be asymmetrical, with one cell returning to the cell cycle, and the other withdrawing from it, beginning to migrate and differentiate (Figure 4). Researchers have utilized BrdU and [^{3}H]thymidine labeling at different times in development in order to determine the “birth dates” of each cell type (Carter-Dawson and LaVail 1979b, Dräger 1985, Harman and Ferguson 1994, Reese, Thompson and Peduzzi 1994, Cepko et al. 1996, Voinescu et al. 2009). Neurogenic windows vary between the different cell types, ranging from embryonic day 10 through postnatal day 11 in the mouse (Young 1985, Cepko et al. 1996, Petridou and Godinho 2022, Figure 1b). The neurogenetic windows for each of the different cell types overlap (Sidman 1961, Carter-Dawson and LaVail 1979b, Young 1985), and different cell types can arise from a single progenitor, suggesting that the RPCs are multipotent (Turner and Cepko 1987, Wetts and Fraser 1988, Turner, Snyder and Cepko 1990,

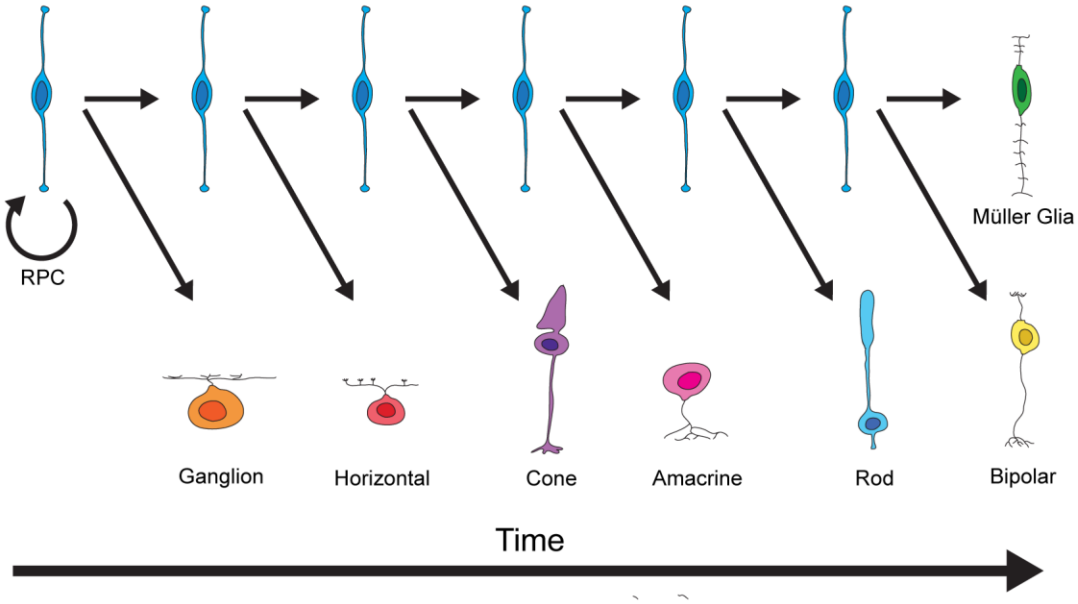

Figure 4: Retinal progenitor cells are multipotent, but competence windoes follow a unidirectional sequence. Retinal progenitor cells (RPCs) initally undergo symmetrical divisions, which expands the cell population. As the population increases, there is a transition to a neurogenic phase, where divisions become asymmetrical: one cell returns to the cell cycle, and the other withdraws and begins to differentiate. The differentiation of cells, including neuronal morphology, is under the control of transcription factors uniquely expressed by cell-types, examined in Chapter 3. Modified from Reese 2011.

Reese, Harvey and Tan 1995, Harris 1997). Retinal progenitor cells are unable to differentiate into any cell type at any time point, and instead progress through competence windows (Rapaport and Dorsky 1998, Livesey and Cepko 2001, Figure 4). The changing environmental cues and intrinsic gene expression push RPCs towards particular cell types at specific points in development (Holt et al. 1988, Cepko et al. 1996, Livesey and Cepko 2001). The order in which cells are born follows a similar progression amongst all vertebrates.

Despite the similarity in this developmental program, the number of cells produced varies greatly between the cell types when comparing different species, which is thought to provide a retinal organization suited to the needs of each species. For example, whereas 3% of the photoreceptor population in mice are cones, in the ground squirrel there are nearly 6 times as many cones as there are rods (Kryger et al. 1998, Keeley et al. 2014), a difference critical for their nocturnal versus diurnal lifestyles. While precision in the specification of cell number might therefore be regarded as critical for achieving the needs of an individual species, we shall see below in Chapter 1that this assumption about the precision by which neuronal number is specified within a species is incorrect.

3) Migration

After a cell's fate is determined, it begins to migrate to its final location, and the three nuclear layers begin to form. Because ganglion cells are the earliest born, they migrate first and form the ganglion cell layer, followed by the INL, and finally, the ONL. Cells use different mechanisms in order to migrate towards their correct layer: glial-guided migration, free migration, or nuclear translocation (Figure 5). For example,

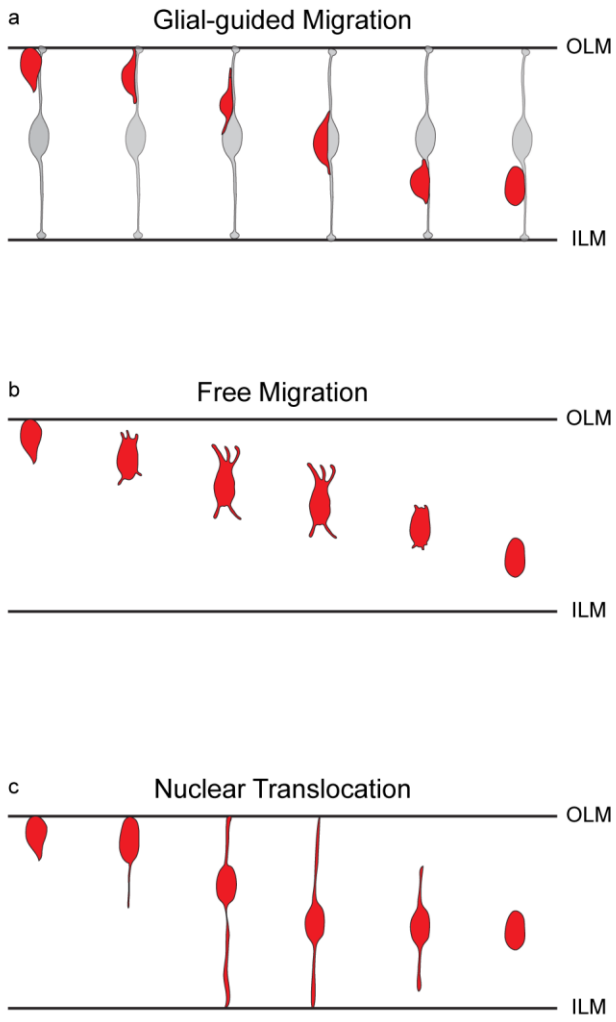

Figure 5: Migration models for differentiating retinal cells. As a cell adopts its fate, it must migrate to the correct nuclear layer, either via glial-guided migration (a), free migration (b), nuclear translocation (c), or some combination of them. Ganglion cells migrate to the ganglion cell layer (GCL) by migrating on neuroepithelial cells (a). Horizontal and amacrine cells begin utilizing a bipolar migration, and then release their attachments to the OLM and ILM and reach their final destination through free migration (b). Photoreceptor cells utilize nuclear translocation (c).

retinal ganglion cells release their attachment from the OLM and migrate along other neuroepithelial cells (Snow and Robson 1994, Zolessi et al. 2006). Other newly born cells, such as photoreceptors, do not need to migrate as far to their final location, and are loosely organized so that earlier born rods are located more basally in the ONL and later born rods will be located towards outer limiting membrane (Carter-Dawson and LaVail 1979b). Interestingly, cones follow a different migration pattern than the rod photoreceptors. After being born, cone nuclei migrate deeper into the ONL, but instead of remaining there, migrate back up towards the ventricular surface in close proximity to the OLM (Rich, Zhan and Blanks 1997, Razafsky et al. 2012), a behavior not unlike that of the interkinetic nuclear migration characteristic of progenitor cells (Figure 3).

Horizontal cells, amacrine cells, and bipolar cells all must reach the developing inner nuclear layer. Interestingly, they seem to do this utilizing different migration processes. Initially, all these cells undergo bipolar migration to the apicobasal center of the retina (Chow et al. 2015). From there, both horizontal cells and amacrine cells lose their attachments at the ILM and OLM, and freely migrate to their final position while maintaining an amoeboid-like, or multipolar morphology (Edqvist and Hallböök 2004, Chow et al. 2015, Amini et al. 2022). Horizontal cells migrate in a bi-directional manner; they migrate basally into the retina, overshooting their final location in the retina, before moving apically to the outermost portion of the INL (Edqvist and Hallböök 2004, Poché et al. 2007).

4) Final Differentiation and Synaptogenesis

As the cells began adopting their cellular fates, they express an array of cell-type specific genes, which first promote class-specific migration, and then guide their morphological differentiation and ability to recognize correct synaptic partners. Axons and dendrites begin to form, identifying extrinsic signals from both their homotypic neighboring cells, as well as their target cells so that they stratify to the correct layer to form synaptic connections. Additionally, for some cell types, these signals promote the formation of orderly “mosaics”, in which cells are non-randomly positioned within the plane of the retina (Wässle and Riemann 1978, Wässle et al. 2009, Reese 2012, Reese and Keeley 2015, Keeley, Eglen and Reese 2020).

The organization of the processes of these cells, in relation to their homotypic neighbors, is important in ensuring that there is complete coverage across the retina. Some cell types, such as the Type 7 CBC, extend their processes up to those of their homotypic neighbors without overlapping, or tile (Wässle et al. 2009). Interestingly, these tiling dendritic arbors change with the density of the cell type, occupying more space when there is a lower density of cells and decreasing in size when there is a higher density (Lee et al. 2011). Not all cells do this however, as some cells do not stop growing outwards once they meet another dendrite and thus generate a degree of dendritic overlap. Such dendritic coverage can vary conspicuously: horizontal cells in the mouse retina exhibit a “coverage factor” (i.e. the number of overlapping dendritic arbors at any point on the retina) of ~6, while starburst amacrine cells have coverage factors ~30. Curiously, whereas the horizontal cells are constrained by their homotypic neighbors, changing in areal size when the number of horizontal cells is

modulated (Raven et al. 2005, Poché et al. 2008) cholinergic amacrine cells do not (Farajian et al. 2004, Whitney et al. 2008).

5) Cell Death

Some, but not all, cell types overproduce cells, and then refine their final cell number through apoptosis (Linden and Reese 2006). The genes *Bax* and *Bcl2* have been shown to antagonize one another, with expression of *Bax* promoting cell death (Oltvai, Milliman and Korsmeyer 1993, Vekrellis et al. 1997). Previous studies have shown that programmed cell death occurs within the retina, and that removal of the *Bax* gene results in a thicker retinal tissue (Péquignot et al. 2003). Several cell types have been identified as undergoing this process, including some bipolar cells, amacrine cells and ganglion cells (Mosinger Ogilvie et al. 1998, Whitney et al. 2009, Lee et al. 2011, Keeley et al. 2014a, Keeley et al. 2021). As expected then, overexpression of the *Bcl-2* gene results in increased cell numbers for a variety of these same cell types (Bonfanti et al. 1996, Strettoi and Volpini 2002).

Using the model organism *Mus musculus* to study retinal development

Neural development has been studied in numerous organisms, from invertebrates such as the fruit fly to larger vertebrate organisms, such as primates (Dacey 1999, Cagan 2009). Our laboratory utilizes the model organism *Mus musculus*, or house mouse, in order to study the various mechanisms that promote retinal development, using both forward and reverse genetic approaches. Although there are differences between the mouse and human retina, such as mice being dichromatic and humans being trichromatic and containing a fovea, these mammals share 99% of the same genes (Peters et al. 2007). This homology provides

researchers with a model organism in which normal and pathological development can be studied, as well as degenerative conditions in various retinal diseases. The genomes of numerous laboratory and recombinant inbred mouse strains have been sequenced, and thus the genetic differences that cause complex phenotypes to arise can be determined via Quantitative Trait Locus (QTL) mapping (Peters et al. 2007). Additionally, the mouse genome can be modified, so that endogenous gene expression is removed, enabling researchers to investigate the role of that gene in development or maintenance of a particular tissue. When the gene is critical in the development and proper function of many organs, however, removing that gene may result in lethality to the embryo. Conditional knockout mice, in which the gene is knocked out in a time and/or tissue-specific manner, has been designed to circumvent this problem (Babinet 2000).

Along with the genetic tools that can be used, mice are an accessible and convenient *in vivo* model. They have relatively short gestation periods (around 19 days) and can have litters with as many as 12 pups. The murine retina continues to develop postnatally, with several cell types still undergoing neurogenesis, migrating, and forming connections with their synaptic partners after birth. Manipulation of the retina postnatally, such as overexpression of a gene using *in vivo* electroporation, allows researchers to influence these different developmental mechanisms and observe changing phenotypes (Matsuda and Cepko 2004, Kautzman et al. 2018). Numerous cell types in the murine retina have been extensively studied and characterized, providing researchers with a fundamental understanding of retinal architecture and functional roles of these cells. The morphology, stratification, and

synaptic partners of various retinal cell types have already been described, permitting an assessment of the role of a particular gene in creating those features following either loss- or gain-of-function experimental manipulations. Newer techniques, such as single cell sequencing, has provided additional information regarding gene expression of individual cell types throughout development and adulthood (Macosko et al. 2015, Shekhar et al. 2016, Tran et al. 2019). Cell-type specific expression of genes has given researchers the ability to label individual cell populations in the retina, either via immunofluorescence techniques or utilizing promoters of the cell-specifically expressed genes to constitutively drive expression of fluorescent proteins in those cells (Jusuf, Harris and Poggi 2013).

Dissertation overview

The overall goal of this research was to further our understanding of genetic factors implicated in retinal development. We utilized both forward and reverse genetic screens to connect various phenotypes to the genes that regulate them. Chapter 1 is concerned with the determinants that influence the size of a single neuronal population. The sizes of various neuronal cell types in the mouse retina have been shown to vary across different strains of mice (Keeley et al., 2014b), suggesting that genetic variants contribute to the variability by modulating developmental processes such as neurogenesis, fate determination, differentiation, and cell death. Here, we utilized Quantitative Trait Locus (QTL) mapping to identify genomic loci where genetic variants contribute to the modulation of AII amacrine cell number. By parsing such genomic loci using bioinformatic resources, those genes containing high priority variants were identified and further ranked based on known expression and functions.

One such gene, *Dixdc1*, was studied, first determining the effect that removing *Dixdc1* had on cell number, and then by investigating two gene variants.

Chapter 2 is concerned with the control of correct neuronal positioning across the depth of the retina. As described earlier, different cell types utilize various modes of migration. Here, we examined rod photoreceptor positioning, which is controlled via somal translocation. The machinery involved in somal translocation had recently been identified, but transcriptional regulatory control had not been explored. We utilized an *in vivo* electroporation technique in order to overexpress a transcriptional co-regulator, *Zmiz2*, in the developing retina and observed the effect on positioning.

Chapter 3 investigates the morphological differentiation of bipolar cells in the developing retina. Bipolar cells extend dendrites and axons into the OPL and IPL, respectively, where they form arbors that reach a specific size and depth. Here, we investigate the role of a bipolar-specific transcription factor, *Sox5*, and its role in axonal and dendritic arbor size. We selectively removed expression of *Sox5* in Type 7 cone bipolar cells (CBCs), and profiled axonal and dendritic arbor size, axonal branch lamination, and connective partners.

CHAPTER 1

DIXDC1 Modulates AII Amacrine Cell Number

ABSTRACT

Differences in heritable traits arise from sequence variants that influence the expression or function of contributing genes. We utilized a forward-genetic approach to identify genes that influence AII amacrine cell population size in the retina, and to define critical sequence variants modulating their contributions. Two genetically distinct inbred mouse strains, A/J and B6/J strains, their F1 progeny, and a set of recombinant inbred (RI) strains derived from them were used to identify genomic loci regulating AII amacrine cell number. While there was little variation in AII amacrine cell number within each strain, there was conspicuous variation between the strains. Simple and composite interval quantitative trait loci (QTL) mapping revealed genomic regions that contributed to the observed phenotypic changes at Chrs 9 and 19, and consomic chromosome substitution strains confirmed that variants on these chromosomes contributed to the variation in AII amacrine cell number. Each gene within the defined regions of the QTLs was investigated in detail for: 1) the presence of single nucleotide polymorphisms (SNPs) and insertions and deletions (InDels) that could influence expression or function; 2) evidence of expression in developing and mature retina or nervous system; and 3) known biological functions that might be expected to modulate cell number. One candidate gene, *Dixdc1*, showed a significant increase in AII amacrine cell number when knocked out. High priority sequence variants in *Dixdc1* were identified, being the likely sources of variation in gene

expression, ultimately contributing to the final number of AII amacrine cells. Differential expression of a *Dixdc1* truncated transcript, thought to arise from a splice-region disrupting InDel, was determined via microarray, RT-PCR, and quantitative PCR analyses. An *in vitro* functional assay revealed that the truncated protein product resulting from translation of this transcript was unable to modulate *β*-catenin signaling, suggesting some novel function, which could play a critical role in the variation in AII amacrine cells between strains.

INTRODUCTION

The AII amacrine cell is a unique retinal interneuron originally appreciated for its role in transmitting scotopic rod photoreceptor signaling via the rod bipolar cells to retinal ganglion cells by way of ON and OFF cone bipolar cell (Bloomfield and Dacheux 2001). Additional roles of AII amacrine cells have since been determined, such as mediating cross-over inhibition between ON and OFF pathways (Demb and Singer 2012). AII amacrine cells are narrow-field bistratified amacrine cells with a set of lobular terminals distributed to the OFF stratum of the IPL, and arboreal dendrites distributed into the ON stratum of the IPL. The lobular terminals form inhibitory glycinergic synapses upon the terminals of OFF cone bipolar cells and the dendrites of OFF retinal ganglion cells (Kolb and Famiglietti 1974, Famiglietti and Kolb 1975, Strettoi, Raviola and Dacheux 1992, Hartveit and Veruki 2012, Marc et al. 2014). The arboreal dendrites receive glutamatergic input from multiple rod bipolar cell terminals, as well as form gap junctions with ON-alpha retinal ganglion cell dendritic arbors and ON cone bipolar cell terminals, and with one another. Because of the AII amacrine cell's small arbor area (30-70µm), these are one of the more numerous types of amacrine cells. Although AII amacrine cells are one of the most studied amacrine cell types, what controls the size of the population has not been extensively examined (Keeley et al. 2014b).

Our laboratory previously profiled the number of AII amacrine cells (Figure 1a, b) in a set of recombinant inbred mouse strains, derived from the B/6J and A/J strains, in order to detect the genes and genomic variants that control AII amacrine cell number. Across the AXB/BXA RI strains, there was a noticeable variation in average

total number, from a low of 57,141 cells to a high of 86,557 cells, a 51% increase (Figure 1c). These results suggested that there were unique variants between the two parental strains that were responsible for the variation in cell number. Quantitative Trait Loci (QTL) mapping identified three prospective genomic loci, on Chrs 9, 11, and 19 ($p < 0.05$, Figure 1d). When controlling for the variation associated on Chr 9 via composite interval mapping, the peak at Chr 19 surpassed the significant threshold (Figure 1e). The inverse was additionally seen: when controlling for Chr 19, Chr 9 surpassed the significant value (Figure 1f). Cell number increased when strains contained the *A* haplotype at either of the loci on Chrs 9 and 19 and was the highest when the strain contained *A* haplotypes at both loci (Figure 1g). In order to experimentally determine whether the presence of *A* alleles on Chrs 9 and 19 increased cell number, our laboratory utilized consomic strains (also known as chromosome substitution strains), in which the entire *A* haplotype was introgressed onto the B6/J genetic background. Both substitution strains showed a significant increase from the cell number measured in B6/J parental strains (Figure 1h).

This study begins with the identification of the genomic regions on Chrs 9 and 19 that would be further investigated. The genes encompassed by these regions were determined, and all of the variants found discriminating the B6/J and A/J strains were recorded. Each variant was critically evaluated and was classified as a high-priority variant if it was predicted to change function or expression of the protein it encoded. Further analysis was done on genes with high-priority variants, exploring their expression patterns in development and maturity, as well as known biological and developmental functions. Among the 21 final candidate genes, *Dixdc1,* a known

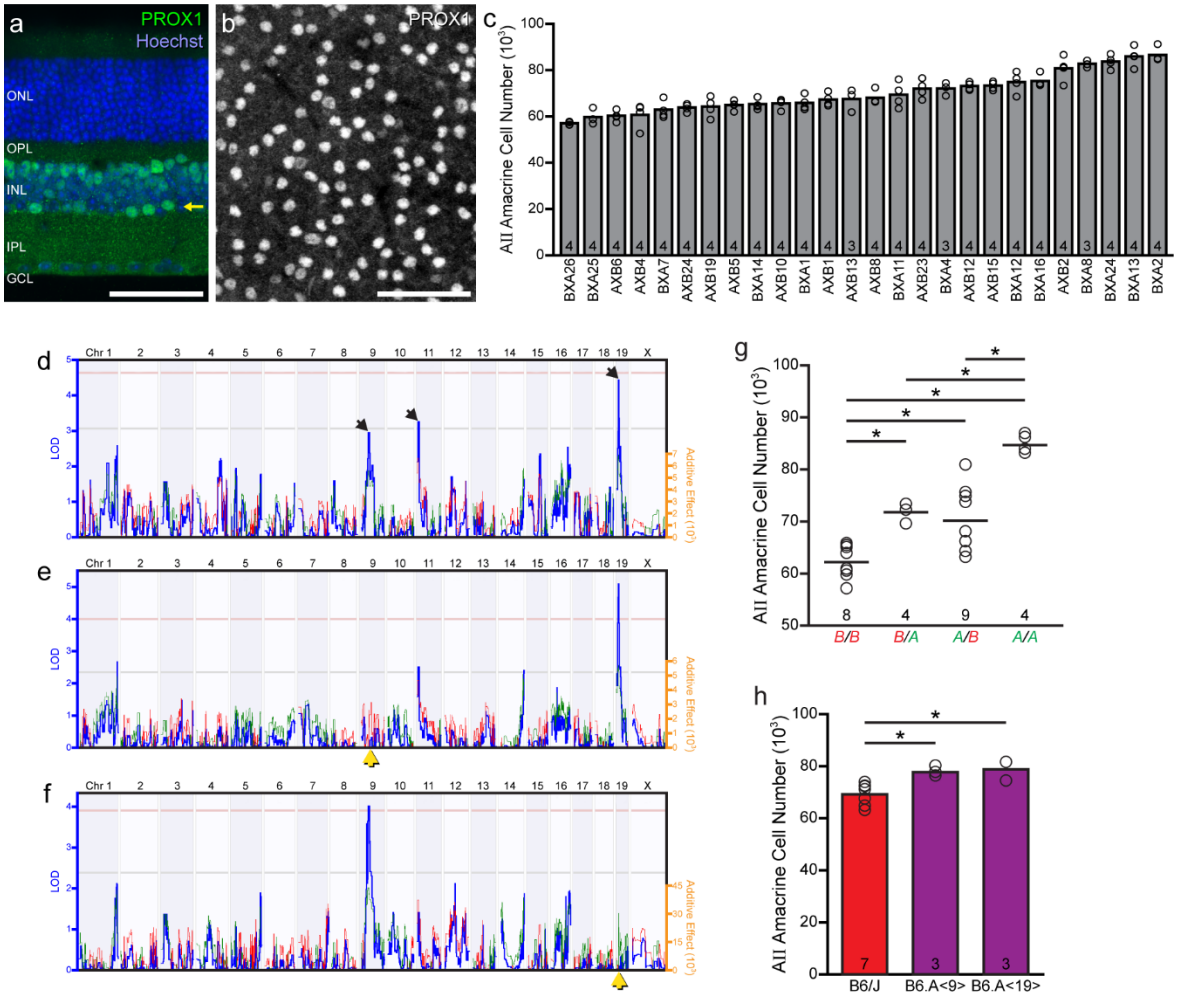

Figure 1: AII amacrine cell population size is genetically controlled a: Cross-section showing the stratification of AII somata, immunolabeled using PROX1 antibodies, at the INL/IPL boundary. b: Wholemount preparation showing the somal distribution of AII cells labeled using PROX1 within this stratum. c: The total number of AII amacrine cells varied across the 26 RI strains of the AXB/BXA strain set, by nearly 30,000 cells. d: Mapping the variation in AII amacrine cell number revealed three suggestive or near-suggestive genomic loci, on Chrs 9, 11 and 19. The blue trace plots the logarithm of the odds (LOD) score, indicated along the left Y axis. The pink and grey horizontal dashed lines indicate significant and suggestive thresholds, respectively, for the LOD score determined through 1000 permutation tests of the strain data. The red and green traces plot the additive effect of *A* or *B* alleles at that genomic locus upon AII cell number, indicated along the right Y axis. e & f: Composite interval mapping, controlling for the effect of the variation attributed to the QTL on Chr 9 (e), or on Chr 19 (f) (yellow arrows), raised the LRS score for the Chr 19 locus, or the Chr 9 locus, respectively, above the significant threshold. g: The four RI strains harboring the *A* haplotype at both loci have on average ~84,000 AII amacrine cells, whereas the seven RI strains containing the *B* haplotype at both loci have ~62,000 cells. Strains having *A* at one locus and *B* at the other locus contain intermediate numbers of AII amacrine cells (one-way ANOVA and post-hoc Tukey tests). h: Consomic mouse strains, bearing the *A* haplotype for Chr 9 or Chr 19 introgressed upon a B6/J genetic background, each contained roughly 9,000-10,000 more AII amacrine cells than did B6/J mice (one-way ANOVA and post-hoc Tukey tests). n = the number of retinas sampled (c & h) or number of RI strains with each haplotype combination at the respective loci on Chr 9 and 19 (g). Calibration bar = 50 µm.

modulator of Wnt-*β* catenin signaling, was chosen for further evaluation. We examined *Dixdc1* loss of function in a murine model and detected a statistically significant increase in AII amacrine cell number in the knockout (KO). We next investigated the expression of a truncated form of the *Dixdc1* transcript, thought to arise from a splicing variant, and determined that the mRNA levels this transcript varied between the two strains. Finally, we attempted to determine whether the truncated DIXDC1 protein could modulate Wnt-*β* catenin signaling. The truncated DIXDCI was unable to do so, suggesting a novel role for this truncated isoform.

METHODS

Mouse Strains and Tissue Preparation

The following strains were obtained from the Jackson Laboratory and bred in the Animal Resource Center at the University of California, Santa Barbara: C57BL/6J (Stock Number: 000664) and A/J (Stock Number: 000646). B6.129-*Dixdc1*^{tm1Bnrc}/J (Stock Number: 029504), additionally obtained through the Jackson Laboratory, was originally generated in the laboratory of Benjamin N. Cheyette (Kivimäe et al. 2011). Mice were genotyped via PCR using the following forward and reverse primers: 5'-CTCGTGCTTTACGGTATCGC-3', 5'-ACTGTTGTCTGGGTGATGGA-3', and 5'-ACCTTTGGGAGGAACTGTTGA-3'; wildtype allele (WT) amplicon size was 236bp, and knockout (KO) was 300bp.

In order to collect retinal tissue, 4-8 week old mice were given a lethal dose of sodium pentobarbital (120mg/kg). After no reaction was seen following a tail pinch, an intracardial perfusion was performed using 4mL of 0.9% saline, followed by 4% paraformaldehyde in 0.1M sodium phosphate buffer (pH 7.2-7.4) for 15 minutes. Eyes were carefully removed from the orbits and fixed in paraformaldehyde for an additional 15 minutes. Retinas were dissected out of the eye and four relieving radial cuts were made so that the hemispheric retina could lie flat.

Eyes from developmental mice were collected following euthanasia via decapitation (P1 and P5) or a lethal dose of sodium pentobarbital (P10). Retinas were immediately dissected out of the eyecup and stored in RNAl*ater* (Thermofisher Scientific, AM7020). All procedures were approved by the Institutional Animal Care and Use Committee (IACUC) at the University of California, Santa Barbara.

Quantitative Trait Loci (QTL) Mapping

AII amacrine cell number was previously determined by our laboratory for B6/J, A/J, F1, and 26 RI strains using identical collection and harvesting techniques and entered into GeneNetwork (ID 10179) in the AXB/BXA published phenotypes dataset (Keeley et al. 2014b). GeneNetwork implements standard methods for simple and composite interval mapping to identify QTLs, while also estimating the genome-wide *p* value of a false-positive error by randomly permuting the strain data. 1000 random permutations were used to determine the suggestive ($p < 0.67$) and significant ($p < 0.05$) thresholds for the logarithm of the odds (LOD) score, being an index of the strength of the linkage between the variation in AII amacrine cell number and genomic locus. The parental strains were excluded, and variability observed in the individual retinas within each strain was included.

Candidate Gene Analysis

Using the trace of the LOD score, the span of the chromosome in which the trace was higher than 1.5 LOD from the maximum LOD on Chrs 9 and 19 was determined, and a comprehensive list of genes within these regions was constructed. In order to ascertain the genomic variants that influenced AII amacrine cell number, all candidate gene single nucleotide polymorphisms (SNPs), insertions/deletions (InDels), and structural variants (SVs) between B6/J and A/J strains were determined, using Release-1505 (GRCm38) of the Sanger Mouse Genomes Project (https://www.sanger.ac.uk/sanger/Mouse_SnpViewer). Any gene that did not have a variant between the two genomes, and therefore could not be the source of AII amacrine cell number, was removed from the candidate gene analysis. The remaining

variants were classified as functional or regulatory variants and analyzed using the set of parameters described below (Appendices 1 & 2).

Missense Variants. Missense variants were defined as differences in nucleic acid sequences between strains that resulted in a change in amino acid sequence. Variants between the two strains was determined using NCBI dbSNP Short Genetic Variations database (https://www.ncbi.nlm.nih.gov/SNP/snp_ref). Changes in amino acid sequence that resulted in a difference in the side chain properties (i.e. polar amino acid in one strain and a hydrophobic amino acid in another) or found in an annotated domain or membrane spanning region (www.uniprot.org) and could impact protein function was recorded.

Frameshift Variants. Frameshift variants were defined as insertions or deletions in nucleic acid sequence that resulted in a disruption of the reading frame, causing the downstream sequence to be read incorrectly. Because frameshift mutations can cause catastrophic changes in protein sequence, all variants were further investigated.

Inframe (+/-) Variants. Inframe variants were characterized as insertions or deletions in nucleic acid sequences that did not disrupt the translational reading frame. Variants that added or removed an amino acid located in an annotated domain or membrane spanning region (www.uniprot.org) were prioritized.

Stop (+/-) Variants. The addition or removal of a stop codon impacts the amount of mRNA that will be translated. All stop variants were further evaluated.

Splice Variants. The SNP/InDel sequence of both B6/J and A/J strains was compared to those of 6 other organism sequences (frog, possum, human, fish, cow,

and chicken) and classified as having none (0), low (1-2), medium (3-4) or high (5-6) homology depending on how many species contained the same sequence. Additionally, the sequence surrounding the SNP/InDel (250bp up and downstream) was similarly analyzed.

3' UTR Variants. The 3' untranslated region (UTR) contains sites where microRNAs bind and decrease gene expression. Predicted microRNA binding sites (www.microrna.org) were compared to SNPs/InDels listed for each candidate gene to determine whether there was a change in sequence in a binding site that would prevent miroRNAs from correctly binding.

5' UTR Variants. The SNP/InDel sequence of both B6/J and A/J strains was compared to those of 6 other organism sequences (frog, possum, human, fish, cow, and chicken) and classified as having none (0), low (1-2), medium (3-4) or high (5-6) homology depending on how many species contained the same sequence. Additionally, the sequence surrounding the SNP/InDel (250bp up and downstream) was similarly analyzed.

Structural Variants. Structural variants were characterized based on its location (if it was in the intron of a candidate gene), and if the sequence surrounding the SNP/InDel (250bp up and downstream) was homologous to at least 3 of the 6 compared organism sequences.

Upstream Variants. SNP/InDel locations were compared to the start of any known or predicted isoform sequences using NCBI gene (https://www.ncbi.nlm.nih.gov/gene/). Those that were within 500bp of the start of the gene were recorded.

Candidate Gene Expression and Functional Analysis

Information regarding the expression patterns and known functions of genes that contained at least one of the SNPs/InDels of interest was collected using public databases. Functional information regarding these genes was found on DAVID Functional Annotation Bioinformatics Microarray Analysis (https://david.ncifcrf.gov/) and NCBI Gene (https://www.ncbi.nlm.nih.gov/gene). Various expression datasets were used to determine developmental and adult gene expression including the GeneNetwork adult whole eye and retina microarray gene expression databases (http://www.genenetwork.org, GN Accession #GN210 and #GN302, respectively); SAGE database of developmental and adult retinal gene expression (http://cepko.med.harvard.edu, Blackshaw et al. 2004); gene expression data of AII amacrine cells at P7 (Kay, Chu and Sanes 2012); and single cell gene expression data for adult AII amacrine cells (Macosko et al. 2015). Genes that had been shown to be expressed during retinal development, modulate biological processes likely to affect cell number, and contained multiple high-priority variants were regarded as the highest priority for further consideration.

Immunofluorescence

In order to prevent non-specific binding of antibodies, whole retinas or sections were protein blocked in 5% Normal Donkey Serum (NDS) for three hours, followed by a series of three washes in cold phosphate-buffered saline (PBS, pH 7.2-7.4). Samples were incubated in primary antibodies (Table 1), for three days. After an additional three washes in cold PBS, secondary antibodies diluted 1:200 were added. Samples were incubated overnight, and again, washed three times. Incubations were

executed at 4ºC with gentle agitation. All solutions were made up in 1% Triton in PBS. Additionally, Neurotrace 530 (Invitrogen) was used at a dilution of 1:250 and Hoechst33342 at 1: 1,000 (Invitrogen, #H3570).

Retinal Sectioning

Dissected retinas were embedded in 5% agarose in 0.1M phosphate buffer. Retinal sections 200µm thick were cut using a vibratome and stored in 0.1M phosphate buffer. *Dixdx1*-KO and littermate CTRL sections were examined for visual differences in retinal architecture using antibodies listed in Table 1.

Cell Counts

Eight fields (4 central and 4 peripheral) were sampled in each whole mounted retina, using a ×40 objective. Cell soma or processes, identified using specifically labeled antibodies (listed in Table 1), were counted within each field and their average density calculated. AII amacrine cell nuclei were identified using antibodies to PROX1 in a sample field of 0.057 mm^2; horizontal cell nuclei were identified as large PROX1+ nuclei in the outermost region of the INL in a sample field of 0.101 mm^2; cholinergic amacrine cell bodies were identified as CHAT+ cells in both the INL and GCL in a sample field of 0.176 mm^2; VGLUT3+ amacrine cell bodies were identified in the INL in a sample field of 0.045 mm^2; rod bipolar cells were identified from PKC+ axon stalks coursing through the inner plexiform layer (IPL) in a sample field of 0.011 mm^2; and Type 2 cone bipolar cells were identified from SYT2+ axon stalks in the IPL in a sample field of 0.045 mm^2. Total retinal area was determined and used to calculate total cell number for each retinal sample. Fields were coded and assorted before being given to a counter who was blind to the genotype of each retina. The entire population of

dopaminergic amacrine cells within each retina was quantified from retinal whole mounts by using the Olympus fluorescence microscope and systematically scanning across the entire retina to identify every TH+ cell using the BioQuant software.

Quantitative PCR (qPCR)

Fresh retinas were dissected from the eyes of P1, P5, P10 and adult B6/J and A/J mice. Developmental samples came from retinas from an entire litter (3-4 mice). Qiagen RNeasy Mini Kit was used for collection and purification of RNA. A cDNA library was produced from these samples using iScript cDNA Synthesis Kit. Expression levels of each gene was determined using Sso Advanced Universal SYBR Green Supermix. Each experiment was run in triplicate using the BioRadCFX96 qPCR Instrument. Primers were designed for the housekeeping genes *β*-2 microglobulin (*β2m*) and Glyceraldehyde 3-phosphate dehydrogenase (*Gapdh*), commonly used in our laboratory (Keeley et al. 2012), and for *Dixdc1,* including primers that recognize all transcripts (using the common 3'UTR), and a novel alternatively spliced *Dixdc1* transcript discussed below. Annealing temperature, amplicon size, and primer sequences for each of the genes can be found in Table 2.

Luciferase Assay

Three expression plasmids were created to test the effect of DIXDC1 protein variants on *β*-catenin signaling *in vitro*. mRNA was extracted from B6/J brain tissue, and cDNA of full length Dixdc1 was produced using the previously described protocol. Primers containing adaptors for restriction enzyme sites Xho1 (F Primer) and NotI (R primer) were used to amplify *Dixdc1* mRNA NM_001374656 (Forward: 5'-CCGCTCGAGCGCCTTTGTGTACAGAGGGAA-3'; Reverse*:* 5'-

AAGGAAAAAAGCGGCCGCTCAGTGGGCTAAGGACAAGC-3'). Purified amplicons were cloned into the multiple cloning site of the pTargeT Mammalian Expression Vector (#A1410; Promega), which uses a CMV enhancer/promoter to drive expression of the coding sequence and contains a SV40 late poly(A) tail to improve transcript stability. Sanger sequencing revealed that the cloned transcript of *Dixdc1* matched the RefSeq annotated transcript NM_001374656. The C-terminus region of *Dixdc1* was removed using Q5 Site-Directed Mutagenesis Kit (NEB Biolabs, #E0554S) with the primers F: 5'-GTTTTCCATGATGACGATGC-3'; and R: 5'-CTGCTTTGAAGGGCGAATG-3'. Q5 Site-Directed Mutagenesis Kit (NEB Biolabs, #E0554S) was also used to create the *Dixdc1* missense variant, in which aa252 was changed from an isoleucine to a threonine, with the following forward and reverse primers: F: 5'-CTGAAGGAATgGAGAACAGAAC-3' and R: 5'-AGGGAATGATCACGAAATC-3'. In addition to the DIXDC1 expression plasmids, a plasmid that expresses murine Disheveled 2 (DVL2) under a CMV promoter was also cloned (Addgene, #123587, originally from (Choi et al. 2019) to simulate Wnt signaling in transfected cells.

For each experiment, HEK293T cells were seeded on a 24-well plate, coated with gelatin, at a density of $2x10^6$ cells/well. Cells were grown in in DMEM: F12 medium with 20% Iron Fortified Calf Bovine Serum (Fisher Scientific, #11320033; Fisher Scientific #16010167) and penicillin/streptomycin**.** The cells were then co-transfected 48 hours after plating with several plasmids using TurboFect (Thermo Fisher Scientific, #R0531). Each well received a combination of four types of plasmids: 1) a DIXDC1 expression plasmid (control, full length, truncated, or missense), 2) a

DVL2 expression plasmid (control or protein expressing), 3) the *β*-catenin reporter firefly luciferase-expressing plasmid (Super 8x TOPFlash, Addgene, #12456), and 4) the transfection control *Renilla* luciferase-expression plasmid (pRL-null; Promega, #E2271). Except for the latter, which was transfected at 20ng per well, all plasmids were transfected at molar equivalents such that the total mass of transfected plasmids did not exceed 1,000ng per well. Two days post-transfection, protein lysates were collected from each well using Glo Lysis Buffer (Promega, #E2661) and transferred in equal volumes (45µL) to four wells of a 96-well plate; two wells were used to assess firefly luciferase luminescence using Steady-Glo reagent (Promega, #E2510), and two well were used to assess *Renilla* luciferase luminescence using *Renilla*-Glo reagent (Promega, #E2710). Luminosity readings were taken using a Tecan Spark plate reader and were normalized as follows: technical repeats were averaged, and then firefly luciferase values were normalized by *Renilla* luciferase values per well. For each of the four DIXDC1 conditions, the wells receiving DVL2-encoding plasmids were normalized by the average value for the wells that did not receive the plasmid, to determine the increase over baseline β-catenin signaling caused by activating the WNT pathway. This normalization was performed for each of six plates, as each plate contained HEK293T from a different passage. Each well was treated as an independent biological sample, resulting in 18 total wells per condition; one well from the missense DIXDC1 condition was excluded as it was an extreme outlier, resulting from abnormally low *Renilla* luminosity values.

Statistics

Student's two-tailed t-tests were used to assess statistical significance for all comparisons between *Dixdc1*-KO and littermate CTRL mice. The levels of *Dixdc1* transcript expression determined from qPCR experiments were assessed for statistical significance between strains of mice, across developmental ages, and for any interaction between strain and age, using two-way ANOVAs followed by post-hoc Tukey tests. Differences in *β*-catenin signaling across conditions in the *in vitro* luciferase assay were assessed using a one-way ANOVA followed by a post-hoc Tukey test. An alpha threshold of 0.05 was used for determining statistical significance in all cases, indicated by an asterisk.

RESULTS

Analysis of loci at Chromosomes 9 and 19 identified candidate genes that modulate AII amacrine cells

The QTL mapping identified genomic loci on Chrs 9 and 19 that affect AII amacrine cell number. AII amacrine cell number increased with *A* alleles at both loci, and consomic strains validated that Chrs 9 and 19 contained variants that increased cell number. In order to compile the initial list of candidate genes, the highest points of the QTL peaks on Chrs 9 and 19 were identified. From there, any gene within the range of 1.5 LOD from the peak was recorded (Figure 2a, b). The range on Chr 9 included 157 genes, while the range on Chr 19 contained 182 genes (Figure 2a, b, top).

The variation in cell number arises from differences in the genome between the two parental strains. Therefore, any gene that did not contain variants between parental strains was removed from the list, since it could not contribute to cell number differences. The variants for the remaining genes were extensively analyzed, using the protocol for each variant type that was listed in the Methods section (Figure 2c). The genes that contained high priority variants were further researched, with the focus being on their known expression and functions. Genes that were expressed during retinal or neuronal development were of greatest interest. Additionally, genes known to modulate biological processes that might affect cell number, such as proliferation, fate determination, and apoptosis, were investigated further. Appendices 1 and 2 list all genes present at each locus, their total variants for each gene, and the number of

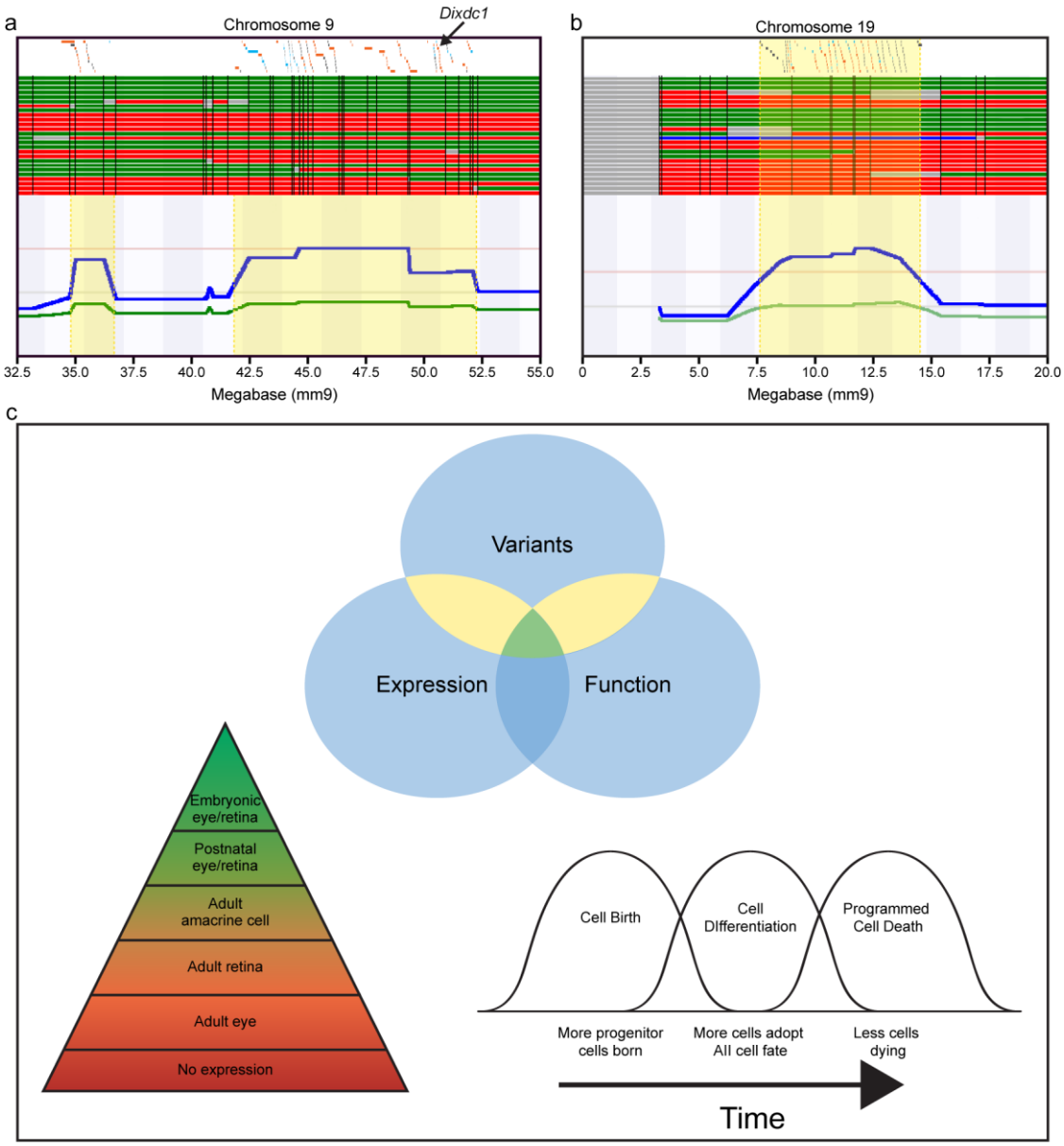

Figure 2: Candidate gene analysis was performed at each QTL. a & b : All of the genes within the respective QTLs on Chr 9 (a) and Chr 19 (b), indicated across the top of each map, were first interrogated for the presence of sequence variants. Those containing no sequence variants, shaded in grey, were eliminated from further consideration. Genes that contained variants, but none categorized as high priority, were shaded in blue, and those with interesting variants were shaded in orange. The haplotype map for each strain is indicated across the bottom. Other conventions as in Figure 3. c: Bioinformatic analyses of the remaining genes at the two QTL were conducted to identify candidate genes warranting further interest. High-priority candidate genes at the Chr 9 and Chr 19 loci were identified and shaded in orange, with their features abridged here from Supplementary Tables 1 and 2.

variants of interest. A final list of twenty-one priority candidate genes, including eleven from the Chr 9 locus and ten from the Chr 19 locus, was compiled. *Dixdc1,* however, was regarded as of particular interest out of these 21 genes, explained below.

Dixdc1 overview

Dix domain containing 1 (Dixdc1) is a positive regulator of the Wnt signaling pathway (Shiomi et al. 2003, Liu et al. 2011). *Dixdc1* has been shown to play a role in neuronal proliferation and migration in the developing neocortex (Singh et al. 2010), and dendritic development and synapse function (Martin et al. 2018, Guo et al. 2018), and multiple sequence-disrupting single nucleotide variants in *Dixdc1* have been associated with mental illness and autism (Martin et al. 2018). Studies in zebrafish demonstrated a reduction in eye size following overexpression of *Dixdc1* during development (Shiomi et al. 2003), while loss of *Dixdc1* in the mouse has been shown to delay retinal angiogenesis (Kim et al. 2022). *Dixdc1* expression during murine development had been previously characterized using several techniques. RT-PCR of murine embryos showed that *Dixdc1* was expressed as early as E9.5 (Shiomi et al. 2005). A number of tissues were profiled via *in situ* hybridization, revealing expression in the CNS as early as E9.5 (Soma et al. 2006), and profiling of the mouse retina revealed expression confined to the inner retina as early as E13.5 (Shiomi et al. 2005), and continued through the prenatal period (Soma et al. 2006), when amacrine cells are being generated (Voinescu et al. 2009). We consequently profiled knockout mice to assess a potential role for *Dixdc1* in the regulation of AII amacrine cell number.

Dixdc1-KO mice show increased numbers of AII amacrine cells

We first examined whether removal of *Dixdc1* modulated the trait of interest, AII amacrine cell number. AII amacrine cell density was determined in *Dixdc1*-KO and littermate CTRLs, and total cell number calculated from the density and retinal areas (Figure 3a, b). There was a significant increase in the number of cells in the KO condition, by almost 6,000 cells (Figure 3c). To determine whether this effect was specific to AII amacrine cells, additional cell type populations were profiled: cholinergic amacrine cells, VGluT3 amacrine cells, dopaminergic amacrine cells, rod bipolar cells, one type of cone bipolar cell (Type 2 cone bipolar cell), and horizontal cells. Only the dopaminergic amacrine cell population showed a significant change in population size, being an increase of comparable magnitude to that observed for AII cells, by about 11% (Figure 3d-j). No change in the overall size of the retina was observed, nor were there any observable abnormalities in the cellular or synaptic architecture of the retina (Figure 3k, l). We next validated this effect upon AII cells by sampling additional *Dixdc1* KO and littermate control (WT) retinas at P10, when AII amacrine cells could first be visualized via immunofluorescence. As in maturity, we found a comparable increase in AII amacrine cells, by 12.5% ($p < 0.001$, Figure 3m-o). Additionally, we quantified horizontal cell number, which was not influenced by the removal of *Dixdc1*, and saw that population was unchanged ($p = 0.921$, Figure 3p).

High priority variants of *Dixdc1*

The RefSeq database lists three annotated mRNA transcripts, each coding for the full-length DIXDC1 protein (Figure 4a), that is, isoforms which contain all of the known functional domains, including a calponin homology domain, an actin binding domain, two coiled coil domains, and a DIX domain (Shiomi et al. 2005, Wang et al.

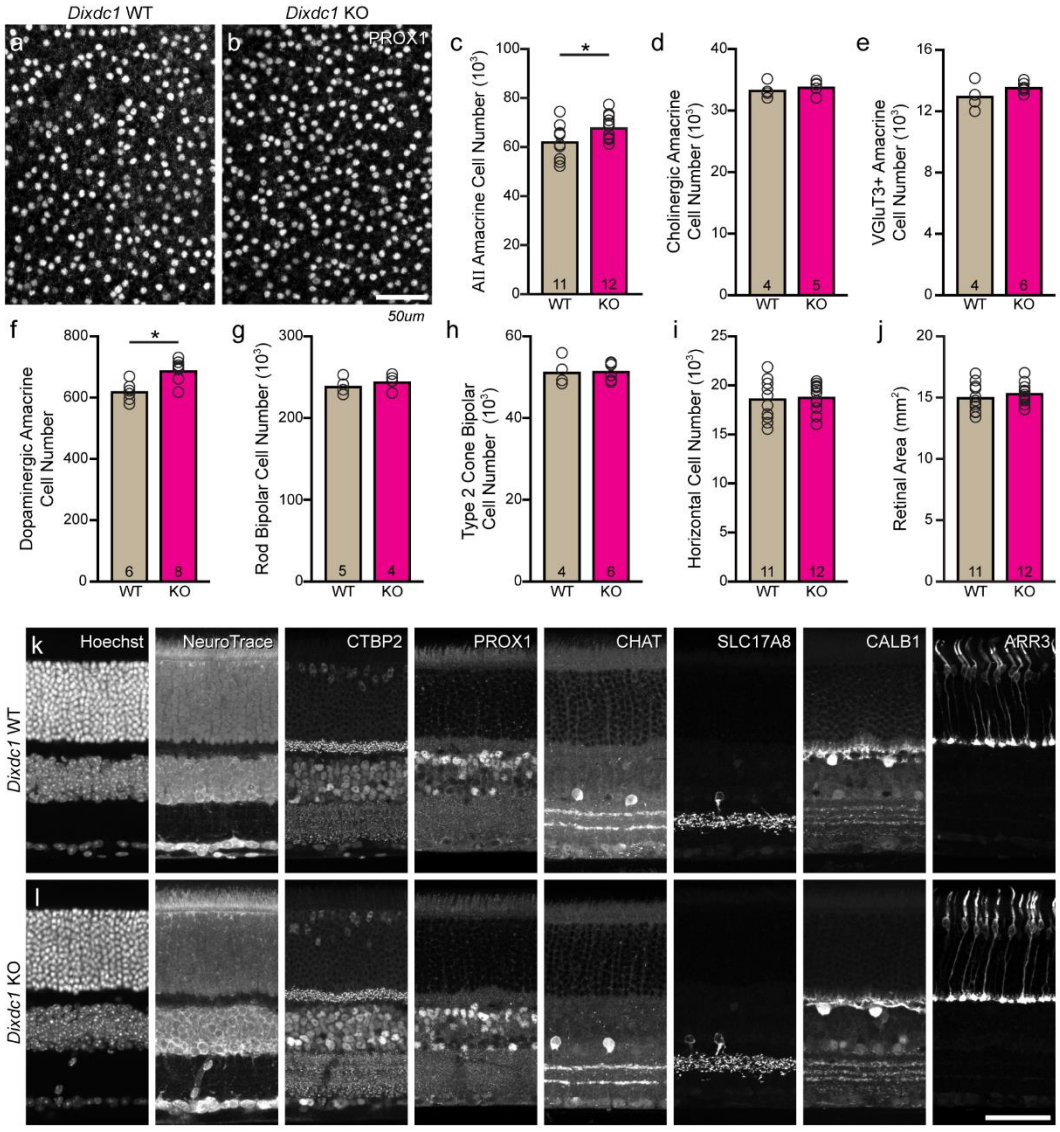

Figure 3: *Dixdc1* modulated AII amacrine cell number. a-c: *Dixdc1*-KO retinas had a significant increase in the size of their AII amacrine cell population, by about 10%. d-i: Of six other sampled retinal populations, only the dopaminergic amacrine cells were significantly different, showing a comparable increase in size. j: The areal size of the retina was unaltered in *Dixdc1*-KO mice. k: Both the cellular and synaptic architecture of the retina were unaffected. n = the number of retinas sampled in c-j. Calibration bar in k = 50 µm.

2006). Other isoforms are known to arise from the use of multiple promoters and alternative splicing, coding for proteins that lack various portions of the N-terminal region (Shiomi et al. 2005), and thus altering DIXDC1 function. Amongst the twenty-two sequence variants in *Dixdc1* discriminating the B6/J from A/J genomes, twelve high priority variants were identified, including: one missense variant, one splice variant, two 5'UTR variants and eight 500bp upstream variants. The splice variant was of particular interest, as it lies within a region of high homology, with B6/J containing the evolutionarily conserved sequence. This variant lies within the polypyrimidine tract at the 3′ end of the second intron (Figure 4a, b, c); the location of this InDel is close to the donor splice site and may influence the function of the splicing machinery during mRNA processing. Additionally, the missense variant was interesting, as a nonpolar isoleucine within the actin-binding domain of the B6/J strain was changed to a polar threonine in the A/J strain (Figure 4d).

B6/J and A/J mouse retinas express a *Dixdc1* transcript that includes a portion of the second intron

The RI strain set AXB/BXA has been previously profiled transcriptionally via microarray analysis, including *Dixdc1* (Whitney et al. 2011). The whole eye mRNA expression database included two probes for *Dixdc1*, one that recognized the 3' UTR (ILMN_2665301, Figure 4a), and one that recognized a portion of the second intron, which we predicted to be retained (ILMN_1214173, Figure 4a & b). Searching various databases revealed that, indeed, two protein coding *Dixdc1* transcripts were expected to terminate within this very intron. These “truncated” transcripts contained a STOP codon in the intronic sequence, so translation of these transcripts would be expected

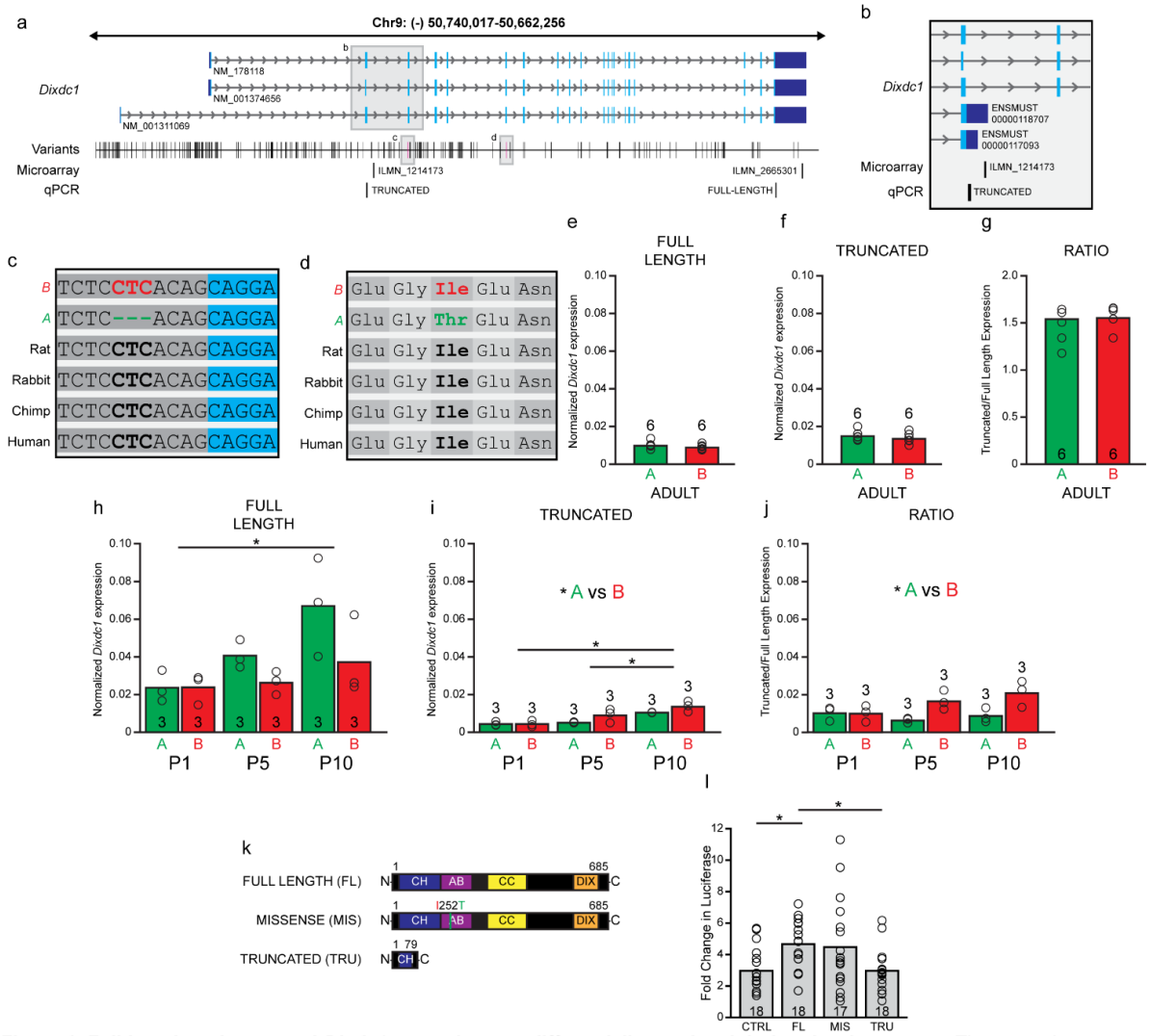

Figure 4: Full-length and truncated *Dixdc1* transcripts are differentially regulated during development. a: The genomic structure of *Dixdc1*. Three transcripts are annotated in the RefSeq database, each with 20 exons and ~77 kb in size. A/J and B6/J genomes are discriminated by many sequence variants, including one missense variant and one splice region InDel that are of particular interest. The positions of two microarray probes are indicated, one probe recognizing the 3′UTR of the three annotated transcripts, and one probe that is complementary to a portion of the second intron. The positions of the qPCR primers are indicated at the very bottom. b: Magnified region encompassing the second intron. Two transcripts that terminate within this intron were identified in the Ensembl database (release 102), one of which is recognized by the microarray probe. c: The splice variant, a three-nucleotide InDel, is in the second intron near the splice donor site. d: The missense variant results in an amino acid substitution from nonpolar isoleucine to a polar threonine within the actin binding domain of *Dixdc1*. B6/J carries the evolutionarily conserved sequence in each case. e, f, g: qPCR analysis reveals the truncated transcripts to be the dominant form in maturity, showing comparable levels of each transcript in both strains. h, i, j: During postnatal development, the full-length transcripts are more prevalent, with expression of both transcripts increasing significantly as a function of age. Strain differences in expression were observed at later ages, yielding significant differences in the proportion of truncated to full-length transcripts, with B6/J retinas exhibiting a larger proportion than A/J retinas. k: A luciferase expression assay compared the effectiveness of a full-length DIXDC1 isoform (NP_835219; translated from NM_001374656), an identical DIXDC1 isoform but now containing the missense mutation, and a truncated DIXDC1 isoform similar to that expected to be translated from the truncated transcripts, upon DVL2-mediated β-catenin signaling. Function domains were determined from UniProt (uniport.org) annotations; CH = calponin homology domain, AB = actin binding domain, CC = coiled coil domain, DIX = DIX domain. l: The missense isoform showed no functional effect of the mutation, augmenting β-catenin signaling to similar levels as full-length DIXDC1, while the truncated isoform was ineffective at modulating β-catenin signaling in either direction, with luciferase expression levels identical to controls. n = the number of adult retinas in F, the number of pooled samples from postnatal retinas in G, and the number of wells in H.

to yield a truncated protein product lacking most of the C-terminal domains of DIXDC1. Interestingly, there was varying levels of expression across parental and RI strains of the intron probe. In order to confirm the inclusion of this intronic sequence in *Dixdc1* transcripts, we designed primers for RT-PCR that could identify transcripts that excised the intron (termed canonical transcript) and those were truncated in the second intron (termed truncated transcript). Both B6/J and A/J parental strain retinal mRNAs exhibited the presence of both canonical and truncated transcripts.

B6/J and A/J retinas differentially express the canonical and truncated *Dixdc1* transcripts in development

We designed probes to quantify, via qPCR, the expression levels of all transcripts that contained the 3'UTR versus the truncated transcripts, both in adult and developmental retinas (Figure 4a, e-j). We first compared adult retinal mRNA in B6/J and A/J parental strains and found the *Dixdc1* truncated transcript was unexpectedly predominant in both strains, relative to the canonical transcript, accounting for about 60% of the total transcripts present. Both strains expressed similar amounts of the full-length ($p = 0.27$) as well as truncated ($p = 0.42$) transcripts (Figure 4e & f), yielding comparable ratios of truncated to full-length transcripts ($p = 0.92$, Figure 4g).

We next examined mRNA levels during postnatal development (P1, P5, and P10), during which AII amacrince cells are concluding their neurogenesis and differentiating (Voinescu et al. 2009, Gamlin et al. 2020). The canonical transcript was the dominant form in both strains at all ages, and we observed a progressive increase in both *Dixdc1* transcripts during the first 10 postnatal days, with a two-way ANOVA detecting a significant main effect of age (Figure 4h; full-length, $p = 0.020$; truncated,

$p < 0.001$). A significant main effect of strain was also detected for the truncated transcripts ($p = 0.027$), with the B6/J strain exhibiting higher expression than the A/J strain; although no significant effect of strain was observed for the full-length transcripts ($p = 0.062$), the A/J strain appeared to have a higher expression than the B6/J strain at the later postnatal ages (Figure 4i). These opposing effects seen between the strains resulted in a ratio of truncated to full-length transcripts that also differed, yielding a significant main effect of strain ($p = 0.005$) with B6/J having a higher relative abundance of truncated transcripts. The efficiency of this splicing event may be altered transiently after birth due to the presence of the splice region InDel; as development proceeds beyond P10, the abundance of full-length transcripts decreases and the truncated transcripts become the dominant form, and differences between the strains in the ratio of these transcripts are no longer present (Figure 4j).

The truncated transcript does not promote *β*-catenin signaling

The truncated *Dixdc1* transcript was detected via microarray analysis, RT-PCR, and qPCR. Bioinformatic database Enselbl predicted that this transcript contained a 3' UTR, suggesting that it is not immediately degraded, and is in fact, translated. Whether or not this truncated protein could exhibit a functional role in Wnt signaling was unknown. In order to test this hypothesis, we transfected a plasmid containing the canonical or truncated transcripts into HEK cells, in order to determine the effect on Wnt-*β*-catenin signaling via an *in vitro* via luciferase assay (Figure 4k). HEK cells were also transfected with plasmids expressing a *β*-catenin reporter construct and *Disheveled2* (*Dvl*), an effective activator of this *β*-catenin reporter in transfected cells. We also examined any potentially functional consequence of the missense variant

mentioned above, by comparing plasmids expressing the full-length transcript used above with plasmids expressing this same construct now containing the *A* missense variant at this locus (Figure 4k).

A one-way ANOVA confirmed significant differences across the four conditions ($p < 0.01$, Figure 4l). Tukey's post-hoc testing confirmed that canonical DIXDC1 significantly increased DVL-induced *β*-catenin signaling relative to controls lacking any *Dixdc1* transcript ($p < 0.05$), as to be expected. The substitution of the *A* missense variant in that full-length *Dixdc1* transcript yielded comparable DVL-induced *β*-catenin signaling relative to controls ($p < 0.05$), suggesting that the presence of this variant does not alter DIXDC1 function. Finally, substituting the truncated *Dixdc1* transcript in place of the full-length transcript yielded levels of DVL-induced *β*-catenin signaling that were significantly lower ($p < 0.05$), being comparable to those achieved in the control condition lacking any *Dixdc1* transcript. We conclude, consequently, that any truncated protein that is produced *in vivo* should be ineffective in either promoting or reducing WNT-β-catenin signaling, but whether it might possess any other functional significance, such as acting as a dominant negative isoform, as well as whether a truncated protein is translated remains to be determined.

DISCUSSION

In vertebrates, the number of neurons in a population is not a fixed trait, but is controlled by the coordination of processes that regulate the production, differentiation and survival of the cells. Each of these processes, in turn, are modulated by a variety of genes, containing an assortment of sequence variants that influence the expression or function of such genes. The retina is a prime example of how neuronal populations vary in their sizes: every cell type examined to date shows considerable variability across mouse strains (Keeley et al. 2014b), but the genetic contributors have yet to be elucidated for most of them. The current study focused on one type of retinal neuron, the AII amacrine cell, seeking to identify candidate genes and evaluate their sequence variants that control cell number. The graded variation in cell number across recombinant strains suggested the presence of multiple variants that would contribute to cell number. We mapped the variation to QTLs on Chrs 9, 11, 19, and composite interval mapping confirmed the QTLs on Chr 9 and 19. Chromosome substitution strains validated the presence of genomic variants on the two chromosomes.

The comprehensive bioinformatic analysis provided us with a systematic way of analyzing candidate genes and utilizing numerous databases in order to investigate variants that affect phenotypes of interest. While this approach may be somewhat time-consuming, it results in a more precise list of candidate genes that can then be experimentally validated. The continual addition of new databases will improve this analysis, so that genes and variants may be found more quickly, and experimentally tested.

We examined one such candidate gene, *Dixdc1*, which when knocked out, selectively increased AII amacrine cell numbers by about 10%. Retinal expression of *Dixdc1* is present prenatally (Shiomi et al. 2005, Soma et al. 2006), during the period of AII amacrine cell genesis (Voinescu et al. 2009), as well as postnatally (shown here), when AII amacrine cells differentiate (Gamlin et al. 2020). Full-length *Dixdc1* transcripts, as well as truncated *Dixdc1* transcripts, are expressed in developing mouse retina, and strain differences in the ratio of full-length to truncated *Dixdc1* transcripts were detected postnatally, largely after the neurogenetic period, suggesting that the role played by *Dixdc1* in modulating cell number occurs after their production. We investigated a truncated form of *Dixdc1* and determined that this transcript was expressed in adult and developmental retinas. To determine whether *Dixdc1* variants have a functional role, we designed an *in vitro* luciferase assay to test two of the high-priority variants, the splice variant, as well as a missense variant (in which aa278 in B6/J mice is a nonpolar isoleucine, and in the A/J is a polar threonine). We tested whether the truncated protein and/or the missense protein could influence Wnt-*β*-catenin signaling. The full-length DIXDC1 isoform possessing the amino acid substitution was found to activate β-catenin similarly to the canonical full-length isoform, leading us to dismiss its role *in vivo*. Instead, we addressed whether the truncated isoform might have biological activity in the same assay, finding it neither augmented nor attenuated DVL2-mediated activation of β-catenin signaling; this is perhaps unsurprising given this isoform lacks most of the functional domains, including the DIX domain. As such, we infer that any effect produced by the decline in the efficiency of splicing caused by this splice-region disrupting InDel is likely due to

the reduction in functional (full-length) DIXDC1, in turn affecting AII amacrine cell number. Because the presence of the *B* haplotype at the Chr 9 QTL is correlated with lower numbers of AII amacrine cells (Figures 1g & h) and higher expression of the truncated transcripts (Figure 4), we expect that an increase in non-functional over functional DIXDC1 isoforms would lead to fewer AII amacrine cells. Yet the effect of knocking out *Dixdc1* function entirely was shown to directly elevate, not reduce, AII cell number. Given the prevalence of the truncated over the full-length transcripts in maturity, these results may intimate a novel function of the truncated DIXDC1 protein independent of the WNT-signaling pathway that itself may modulate AII amacrine cell number.

Wnt signaling is critical in the proper development of the eye, influencing RPE, lens, and retinal vasculature development, promoting dorso-ventral patterning of the retina, as well as being involved in cell proliferation and fate determination (Fujimura 2016). Wnt signaling has been mapped in developing retinas and is activated in RGCs and in the inner INL where amacrine cells are positioned by postnatal day 7, suggesting that this signaling is involved in the development of RGCs and amacrine cells (Liu et al. 2006). *Dixdc1* is not necessary for Wnt signaling to occur, but the addition of *Dixdc1* further promotes it (Shiomi et al. 2003). The removal of a functional protein, therefore, may not completely disrupt proper development, but influence to a lesser degree processes such as proliferation and fate determination, thereby affecting cell number.

Table 1: List of primary antibodies, source, working dilution, and cell type labeled

Animal	Antibody	Cell Type Identified	Dilution	Company Name
Mo Monoclonal	CtBP2	Ribbon Synapses (Cone)	1:500	BD Transduction (612044)
Gt Polyclonal	VGlut3	VGLUT3 AC	1:500	Santa Cruz (sc-26031)
Mo Monoclonal	PKC	RBC	1:500	Milipore (05-983)
Sp Polyclonal	TH	Dopaminergic AC	1:1,000	Milipore (AB1542)
Mo Monoclonal	Syt2	Type 2 CBC	1:200	ZIRC (ZDB-ATB-081002-25)
Rb Polyclonal	Prox1	AII AC and HC	1:1,000	BioLegend (PRB-238C)
Gt Polyclonal	ChAT	Cholinergic AC	1:200	Millipore (AB144P)
Rb Polyclonal	Calbindin	HC and AC	1:10,000	Calbio (PC253L)

Table 2: List of primer sequences and attributes used for quantitative PCR

Gene	Primers (5'-3')	Product Length	Melting Temperature
Gapdh	5'-AATGTGTCCGTCGTGGATCTGA-3' 5'-AGTGTAGCCCAAGATGCCCTTC-3'	117bp	63°C
β2m	5'-GGAGAATGGGAAGCCGAACATAC-3' 5'-AGAAAGACCAGTCCTTGCTGAAG-3'	143bp	63°C
Dixdc1 3'UTR	5'-TGCATCCACTTCCAGGTTCC-3' 5'-AACCGAAGGCCTTAACCACC-3'	86bp	61.5°C
Dixdc1 Intron-retaining	5'-ACAGACCTCACTCTCCAGTCT-3' 5'-AACAGCGTCGGGAAATACCTA-3'	161bp	63°C

Appendix A: Candidate genes and their variants on Chr 9, in order of most to least total variants

Symbol	Total	High Priority Variants									
		Mis.	frame	inframe +/-	stop +/-	Splicing	Structural variants	3'	5'	500 up	Total
Sorl1	48	2	0	0	0	2	0	0	0	0	4
Zbtb16	37	0	0	0	0	0	1	0	3	0	4
Nxpe2	33	5	0	0	0	0	0	10	0	1	16
Cadm1	29	0	0	0	0	2	1	4	0	3	10
Ttc12	28	1	0	0	0	1	0	6	0	2	10
Tirap	26	0	0	0	0	0	0	3	0	1	4
Sc5d	22	1	0	0	0	1	0	0	0	0	2
Dixdc1	22	1	0	0	0	1	0	0	2	8	12
1110032A03Rik	22	1	0	0	0	3	0	2	2	3	11
Ube4a	21	1	0	0	0	0	0	5	0	4	10
Ankk1	21	1	0	0	0	0	0	0	1	10	12
Nxpe4	20	4	0	0	0	0	2	10	1	6	23
Arhgef12	19	1	0	0	0	1	0	0	0	0	2
Alg9	18	0	0	0	0	0	0	2	3	2	7
Cdon	17	2	0	0	0	3	1	0	1	1	8
Ncam1	15	0	0	0	0	0	1	1	0	3	5
Rdx	15	0	0	0	0	1	0	3	0	5	9
Dcps	14	0	0	0	0	0	0	0	4	8	12
Cd3e	14	0	0	0	0	1	0	0	0	9	10
Tmprss13	13	2	0	0	0	1	0	0	0	6	9
Nnmt	12	0	0	0	0	1	0	2	1	6	10
St3gal4	11	0	0	0	0	1	1	4	0	0	6
Fdxacb1	11	1	0	0	0	0	0	0	1	4	6
Srpr	10	1	0	0	0	0	0	0	1	1	3
Ddx6	10	0	0	0	0	0	0	0	0	0	0
Htr3a	10	0	0	0	0	0	1	1	0	2	4
4933407I05Rik	10	0	0	0	0	0	0	0	0	10	10
Tecta	9	3	0	0	0	1	0	0	0	0	4
Sik3	9	1	0	0	0	0	0	2	0	0	3
Ppp2r1b	9	0	0	0	0	0	0	4	0	10	14
Scn2b	8	0	0	0	0	0	0	0	0	7	7
Scn4b	8	0	0	0	0	0	0	0	0	1	1
Gm5617	8	0	0	0	0	0	0	2	1	6	9
Tmprss4	7	0	0	0	0	0	0	0	0	4	4
BC049352	7	0	0	0	0	0	0	0	1	5	6
Drd2	7	0	0	0	0	0	0	0	0	5	5
2310030G06Rik	7	0	0	0	0	1	0	1	0	3	5
Trim29	5	0	0	0	0	1	0	0	0	0	1

Cxcr5	5	0	0	0	0	0	0	0	0	0	0
Usp28	5	0	0	0	0	0	0	0	0	3	3
Zc3h12c	5	0	0	0	0	0	0	0	0	0	0
Foxred1	4	0	0	0	0	0	0	0	0	3	3
Tlcd5	4	0	0	0	0	0	0	0	0	0	0
Pou2f3	4	0	0	0	0	0	0	0	0	0	0
Usp2	4	0	0	0	0	0	0	0	0	0	0
Cbl	4	0	0	0	0	0	0	0	0	0	0
Gm4791	4	0	0	0	2	0	0	0	0	2	4
Htr3b	4	0	0	0	0	0	0	0	0	2	2
Zw10	4	1	0	0	0	1	0	0	0	1	3
2310003N18Rik	4	0	0	0	0	0	0	0	0	4	4
Cryab	4	0	0	0	0	0	0	0	1	3	4
Rpusd4	3	0	0	0	0	0	0	0	0	1	1
Hspb2	3	1	0	0	0	0	0	0	0	2	3
Thy1	3	0	0	0	0	0	0	0	0	0	0
Cd3g	3	0	0	0	0	0	0	0	0	0	0
Cd3d	3	0	0	0	0	0	0	0	0	2	2
1700003G13Rik	3	0	0	0	0	0	0	0	0	3	3
Fxyd6	3	0	0	0	0	1	0	0	0	0	1
Dscaml1	3	1	0	0	0	0	1	0	0	0	2
Apoa1	3	2	0	0	0	0	0	0	0	1	3
Apoc3	3	1	0	0	0	0	0	0	0	2	3
Tmprss5	3	0	0	0	0	0	0	1	0	0	1
Dlat	3	0	0	0	0	0	0	0	0	1	1
Btg4	3	0	0	0	0	0	0	0	0	0	0
Pou2af1	3	0	0	0	0	0	0	0	0	3	3
4833427G06Rik	3	0	0	0	0	0	0	0	3	0	3
Kirrel3	2	0	0	0	0	0	0	0	0	1	1
9230113P08Rik	2	0	0	0	0	0	0	0	0	2	2
Grik4	2	0	0	0	0	0	0	0	0	0	0
Oaf	2	0	0	0	0	0	0	0	0	0	0
Rnf26	2	0	0	0	0	0	0	0	0	0	0
Mcam	2	0	0	0	0	0	0	0	0	0	0
Trappc4	2	0	0	0	0	1	0	0	0	0	1
4833428L15Rik	2	0	0	0	0	0	0	0	0	1	1
Gm4894	2	0	0	0	1	0	0	0	0	0	1
AU019823	2	0	0	0	0	0	0	0	0	1	1
Fdx1	2	0	0	0	0	1	0	0	0	0	1
4933422A05Rik	1	0	0	0	0	0	0	0	0	1	1
Hyls1	1	0	0	0	0	0	0	2	0	0	2
Gm5615	1	0	0	0	0	0	0	0	0	0	0
Tbcel	1	0	0	0	0	0	0	0	0	0	0

Nectin1	1	1	0	0	0	0	0	0	0	0	1
Tmem24	1	0	0	0	0	0	0	0	0	0	0
Dpagt1	1	0	0	0	0	0	0	0	0	0	0
H2afx	1	0	0	0	0	0	0	0	0	0	0
Hmbs	1	0	0	0	0	0	0	0	0	0	0
Hyou1	1	0	0	0	0	0	0	0	0	0	0
Upk2	1	0	0	0	0	0	0	0	0	0	0
Phldb1	1	1	0	0	0	0	0	0	0	0	1
Kmt2a	1	0	0	0	0	0	0	0	0	1	1
Fxyd2	1	0	0	0	0	0	0	0	0	1	1
2900052N01Rik	1	0	0	0	0	0	0	0	0	1	1
Rexo2	1	0	0	0	0	0	0	0	0	1	1
Rbm7	1	0	0	0	0	0	0	0	0	1	1
Plet1os	1	0	0	0	0	0	0	0	0	1	1
Plet1	1	0	0	0	0	0	0	0	0	0	0
Bco2	1	0	0	0	0	0	0	0	0	0	0
Pih1d2	1	0	0	0	0	0	0	0	0	0	0
1810046K07Rik	1	0	0	0	0	1	0	0	0	0	1
Arhgap20	1	0	0	0	0	0	0	0	0	1	1
Gm6981	1	0	0	0	0	0	0	0	0	1	1
4930546K05Rik	**0**	**-**	**-**	**-**	**-**	**-**	**-**	**-**	**-**	**-**	**-**
4930581F22Rik	**0**	**-**	**-**	**-**	**-**	**-**	**-**	**-**	**-**	**-**	**-**
4931429L15Rik	**0**	**-**	**-**	**-**	**-**	**-**	**-**	**-**	**-**	**-**	**-**
9230110F15Rik	**0**	**-**	**-**	**-**	**-**	**-**	**-**	**-**	**-**	**-**	**-**
Abcg4	**0**	**-**	**-**	**-**	**-**	**-**	**-**	**-**	**-**	**-**	**-**
Amica1	**0**	**-**	**-**	**-**	**-**	**-**	**-**	**-**	**-**	**-**	**-**
Apoa4	**0**	**-**	**-**	**-**	**-**	**-**	**-**	**-**	**-**	**-**	**-**
Apoa5	**0**	**-**	**-**	**-**	**-**	**-**	**-**	**-**	**-**	**-**	**-**
Arcn1	**0**	**-**	**-**	**-**	**-**	**-**	**-**	**-**	**-**	**-**	**-**
Atp5l	**0**	**-**	**-**	**-**	**-**	**-**	**-**	**-**	**-**	**-**	**-**
Bace1	**0**	**-**	**-**	**-**	**-**	**-**	**-**	**-**	**-**	**-**	**-**
BC049987	**0**	**-**	**-**	**-**	**-**	**-**	**-**	**-**	**-**	**-**	**-**
Bcl9l	**0**	**-**	**-**	**-**	**-**	**-**	**-**	**-**	**-**	**-**	**-**
Bud13	**0**	**-**	**-**	**-**	**-**	**-**	**-**	**-**	**-**	**-**	**-**
C1qtnf5	**0**	**-**	**-**	**-**	**-**	**-**	**-**	**-**	**-**	**-**	**-**
Ccdc153	**0**	**-**	**-**	**-**	**-**	**-**	**-**	**-**	**-**	**-**	**-**
Ccdc84	**0**	**-**	**-**	**-**	**-**	**-**	**-**	**-**	**-**	**-**	**-**
Cep164	**0**	**-**	**-**	**-**	**-**	**-**	**-**	**-**	**-**	**-**	**-**
Cldn25-ps	**0**	**-**	**-**	**-**	**-**	**-**	**-**	**-**	**-**	**-**	**-**
D630033O11Rik	**0**	**-**	**-**	**-**	**-**	**-**	**-**	**-**	**-**	**-**	**-**
D730048I06Rik	**0**	**-**	**-**	**-**	**-**	**-**	**-**	**-**	**-**	**-**	**-**
Ddx25	**0**	**-**	**-**	**-**	**-**	**-**	**-**	**-**	**-**	**-**	**-**
Foxr1	**0**	**-**	**-**	**-**	**-**	**-**	**-**	**-**	**-**	**-**	**-**

Gm684	**0**	**-**	**-**	**-**	**-**	**-**	**-**	**-**	**-**	**-**	**-**
Gm6980	**0**	**-**	**-**	**-**	**-**	**-**	**-**	**-**	**-**	**-**	**-**
Ift46	**0**	**-**	**-**	**-**	**-**	**-**	**-**	**-**	**-**	**-**	**-**
Il10ra	**0**	**-**	**-**	**-**	**-**	**-**	**-**	**-**	**-**	**-**	**-**
Il18	**0**	**-**	**-**	**-**	**-**	**-**	**-**	**-**	**-**	**-**	**-**
Kirrel3os	**0**	**-**	**-**	**-**	**-**	**-**	**-**	**-**	**-**	**-**	**-**
Layn	**0**	**-**	**-**	**-**	**-**	**-**	**-**	**-**	**-**	**-**	**-**
Mfrp	**0**	**-**	**-**	**-**	**-**	**-**	**-**	**-**	**-**	**-**	**-**
Mizf	**0**	**-**	**-**	**-**	**-**	**-**	**-**	**-**	**-**	**-**	**-**
Mpzl2	**0**	**-**	**-**	**-**	**-**	**-**	**-**	**-**	**-**	**-**	**-**
Mpzl3	**0**	**-**	**-**	**-**	**-**	**-**	**-**	**-**	**-**	**-**	**-**
Nlrx1	**0**	**-**	**-**	**-**	**-**	**-**	**-**	**-**	**-**	**-**	**-**
Pafah1b2	**0**	**-**	**-**	**-**	**-**	**-**	**-**	**-**	**-**	**-**	**-**
Pate2	**0**	**-**	**-**	**-**	**-**	**-**	**-**	**-**	**-**	**-**	**-**
Pate4	**0**	**-**	**-**	**-**	**-**	**-**	**-**	**-**	**-**	**-**	**-**
Pcsk7	**0**	**-**	**-**	**-**	**-**	**-**	**-**	**-**	**-**	**-**	**-**
Pdzd3	**0**	**-**	**-**	**-**	**-**	**-**	**-**	**-**	**-**	**-**	**-**
Pts	**0**	**-**	**-**	**-**	**-**	**-**	**-**	**-**	**-**	**-**	**-**
Pus3	**0**	**-**	**-**	**-**	**-**	**-**	**-**	**-**	**-**	**-**	**-**
Rnf214	**0**	**-**	**-**	**-**	**-**	**-**	**-**	**-**	**-**	**-**	**-**
Rps25	**0**	**-**	**-**	**-**	**-**	**-**	**-**	**-**	**-**	**-**	**-**
Sdhd	**0**	**-**	**-**	**-**	**-**	**-**	**-**	**-**	**-**	**-**	**-**
Sidt2	**0**	**-**	**-**	**-**	**-**	**-**	**-**	**-**	**-**	**-**	**-**
Sik2	**0**	**-**	**-**	**-**	**-**	**-**	**-**	**-**	**-**	**-**	**-**
Slc37a4	**0**	**-**	**-**	**-**	**-**	**-**	**-**	**-**	**-**	**-**	**-**
Tagln	**0**	**-**	**-**	**-**	**-**	**-**	**-**	**-**	**-**	**-**	**-**
Tex12	**0**	**-**	**-**	**-**	**-**	**-**	**-**	**-**	**-**	**-**	**-**
Timm8b	**0**	**-**	**-**	**-**	**-**	**-**	**-**	**-**	**-**	**-**	**-**
Tmem25	**0**	**-**	**-**	**-**	**-**	**-**	**-**	**-**	**-**	**-**	**-**
Treh	**0**	**-**	**-**	**-**	**-**	**-**	**-**	**-**	**-**	**-**	**-**
Ttc36	**0**	**-**	**-**	**-**	**-**	**-**	**-**	**-**	**-**	**-**	**-**
Vps11	**0**	**-**	**-**	**-**	**-**	**-**	**-**	**-**	**-**	**-**	**-**
Zpr1	**0**	**-**	**-**	**-**	**-**	**-**	**-**	**-**	**-**	**-**	**-**

Appendix B: Candidate Genes and their variants on Chr 19, in order of most to least total variants

Symbol	Total	High Priority Variants									
		Mis.	frame	inframe +/-	stop +/-	Splicing	Structural variants	3'	5'	500 up	Total
Fam111a	82	46	0	0	0	0	1	2	0	2	51
Stx3	70	1	0	0	0	2	0	12	3	16	34
Olfr1418	33	1	0	0	0	0	0	0	0	12	13
Ms4a6d	30	3	0	0	0	1	1	2	0	5	12
Ms4a6b	24	3	0	0	0	0	0	2	0	6	11
Olfr1419	20	0	0	0	0	0	0	0	0	11	11
Ms4a10	16	2	0	0	0	0	0	0	1	7	10
Olfr1433	16	3	0	0	0	0	0	0	0	7	10
Cd6	14	0	0	0	0	0	0	10	0	0	10
Lpxn	14	0	0	0	0	1	1	0	1	6	9
Olfr1441	14	2	0	0	0	0	0	0	0	6	8
Mpeg1	13	2	0	0	0	0	0	3	0	2	7
Tmem258	13	0	0	0	0	0	0	0	0	7	7
Ms4a15	12	0	0	0	0	0	0	2	0	4	6
1700025F22Rik	12	0	0	0	0	0	1	0	0	5	6
Zfp91	11	0	0	0	0	0	0	0	2	4	6
4930524O05Rik	11	0	0	0	0	0	0	0	0	6	6
Mrpl16	10	0	0	0	0	0	0	3	0	2	5
Olfr235	10	1	0	0	0	0	0	0	1	3	5
Patl1	10	1	0	0	0	1	0	1	0	1	4
Ms4a4d	9	1	0	0	0	0	0	2	0	1	4
Pfpl	9	1	0	0	0	0	0	1	0	2	4
Olfr1417	8	0	0	0	0	0	0	0	0	4	4
Vwce	8	2	0	0	0	1	0	0	0	0	3
Fads2	8	1	0	0	0	2	0	0	0	0	3
Ms4a14	8	3	0	0	0	0	0	0	0	0	3
Osbp	7	0	0	0	0	1	0	1	0	1	3
Ms4a5	7	1	0	0	0	1	0	0	0	1	3
Ms4a13	7	0	0	0	0	0	0	0	0	3	3
Best1	7	0	0	0	0	1	0	0	0	2	3
2210404E10Rik	7	0	0	0	0	0	0	0	0	3	3
4930526L06Rik	7	0	0	0	0	0	0	0	0	3	3
Ms4a3	7	1	0	0	0	0	0	2	0	0	3
Olfr1436	7	3	0	0	0	0	0	0	0	0	3
Ms4a1	6	1	0	0	0	0	0	1	0	0	2
Fads1	6	0	0	0	0	0	0	1	0	1	2
Ttc9c	6	1	0	0	0	0	0	0	0	1	2
Asrgl1	6	1	0	0	0	0	0	0	0	1	2

Tut1	5	0	0	0	0	0	0	0	0	2	2
Oosp2	5	0	0	0	0	0	0	0	0	2	2
Ppp1r32	4	1	0	0	0	0	0	0	0	1	2
EG240549	4	0	0	0	0	0	0	0	0	2	2
Fth1	4	0	0	0	0	0	0	0	0	2	2
Gif	4	0	0	0	0	0	0	0	0	2	2
Slc15a3	4	0	0	0	0	1	0	0	1	0	2
Zbtb3	3	1	0	0	0	0	0	0	0	1	2
Dagla	3	0	0	0	0	1	0	0	0	1	2
Dtx4	3	0	0	0	0	0	0	1	0	0	1
Syt7	3	1	0	0	0	0	0	0	0	0	1
Sdhaf2	3	1	0	0	0	0	0	0	0	0	1
Ms4a2	3	1	0	0	0	0	0	0	0	0	1
Rab3il1	3	0	0	0	0	1	0	0	0	0	1
Lrrc10b	3	0	0	0	0	0	0	0	0	1	1
Ccdc86	3	0	0	0	0	0	0	0	0	1	1
Hnrnpul2	3	1	0	0	0	0	0	0	0	0	1
Mta2	3	0	0	0	0	0	0	0	0	1	1
Pga5	2	1	0	0	0	0	0	0	0	0	1
Tmem138	2	0	0	0	0	0	0	0	0	1	1
Ahnak	2	0	0	0	0	0	0	0	0	1	1
Dak	2	1	0	0	0	0	0	0	0	0	1
Fads3	2	0	0	0	0	0	0	0	0	1	1
Fen1	2	0	0	0	0	0	0	0	0	1	1
1700017D01Rik	2	0	0	0	0	0	0	0	0	1	1
1810009A15Rik	2	0	0	0	0	0	0	0	0	1	1
5730408K05Rik	2	0	0	0	0	0	0	0	0	1	1
Bscl2	2	0	0	0	0	0	0	0	0	1	1
Cpsf7	2	0	0	0	0	0	0	0	0	1	1
Ddb1	1	0	0	0	0	1	0	0	0	0	1
Eml3	1	0	0	0	0	0	0	0	0	1	1
Ms4a8a	1	0	0	0	0	0	0	0	0	1	1
Olfr1420	1	0	0	0	0	0	0	0	0	1	1
Olfr1424	1	0	0	0	0	0	0	0	0	1	1
Olfr1425	1	0	0	0	0	0	0	0	0	1	1
Olfr1431	1	0	0	0	0	0	1	0	0	0	1
Olfr1437	1	0	0	0	0	0	0	0	0	1	1
Olfr1453	1	0	0	0	0	0	0	0	0	1	1
Oosp3	1	1	0	0	0	0	0	0	0	0	1
Rom1	1	0	0	0	0	0	0	0	0	1	1
Ubxn1	1	0	0	0	0	0	0	0	0	1	1
Zp1	1	0	0	0	0	0	0	0	0	1	1
A430093F15Rik	1	0	0	0	0	0	0	0	0	0	0

Myrf	1	0	0	0	0	0	0	0	0	0	0
Zfp91-cntf	1	0	0	0	0	0	0	0	0	0	0
B3gat3	1	0	0	0	0	0	0	0	0	0	0
Olfr1443	1	0	0	0	0	0	0	0	0	0	0
Oosp1	1	0	0	0	0	0	0	0	0	0	0
Cyb561a3	1	0	0	0	0	0	0	0	0	0	0
Eef1g	1	0	0	0	0	0	0	0	0	0	0
Ganab	1	0	0	0	0	0	0	0	0	0	0
Gng3	1	0	0	0	0	0	0	0	0	0	0
Incenp	1	0	0	0	0	0	0	0	0	0	0
Ms4a4b	1	0	0	0	0	0	0	0	0	0	0
Ms4a7	1	0	0	0	0	0	0	0	0	0	0
Olfr1465	1	0	0	0	0	0	0	0	0	0	0
Prpf19	1	0	0	0	0	0	0	0	0	0	0
Ptgdr2	1	0	0	0	0	0	0	0	0	0	0
Stxbp3b	1	0	0	0	0	0	0	0	0	0	0
Vps37c	1	0	0	0	0	0	0	0	0	0	0
1700092M07Rik	**0**	**-**	**-**	**-**	**-**	**-**	**-**	**-**	**-**	**-**	**-**
9830166K06Rik	**0**	**-**	**-**	**-**	**-**	**-**	**-**	**-**	**-**	**-**	**-**
Cd5	**0**	**-**	**-**	**-**	**-**	**-**	**-**	**-**	**-**	**-**	**-**
Chrm1	**0**	**-**	**-**	**-**	**-**	**-**	**-**	**-**	**-**	**-**	**-**
Cntf	**0**	**-**	**-**	**-**	**-**	**-**	**-**	**-**	**-**	**-**	**-**
EG383436	**0**	**-**	**-**	**-**	**-**	**-**	**-**	**-**	**-**	**-**	**-**
Glyat	**0**	**-**	**-**	**-**	**-**	**-**	**-**	**-**	**-**	**-**	**-**
Gm2518	**0**	**-**	**-**	**-**	**-**	**-**	**-**	**-**	**-**	**-**	**-**
Gm6252	**0**	**-**	**-**	**-**	**-**	**-**	**-**	**-**	**-**	**-**	**-**
Gm8630	**0**	**-**	**-**	**-**	**-**	**-**	**-**	**-**	**-**	**-**	**-**
Hrasls5	**0**	**-**	**-**	**-**	**-**	**-**	**-**	**-**	**-**	**-**	**-**
Ints5	**0**	**-**	**-**	**-**	**-**	**-**	**-**	**-**	**-**	**-**	**-**
Keg1	**0**	**-**	**-**	**-**	**-**	**-**	**-**	**-**	**-**	**-**	**-**
Lrrn4cl	**0**	**-**	**-**	**-**	**-**	**-**	**-**	**-**	**-**	**-**	**-**
Ms4a18	**0**	**-**	**-**	**-**	**-**	**-**	**-**	**-**	**-**	**-**	**-**
Ms4a4c	**0**	**-**	**-**	**-**	**-**	**-**	**-**	**-**	**-**	**-**	**-**
Ms4a6c	**0**	**-**	**-**	**-**	**-**	**-**	**-**	**-**	**-**	**-**	**-**
Nxf1	**0**	**-**	**-**	**-**	**-**	**-**	**-**	**-**	**-**	**-**	**-**
Olfr1423	**0**	**-**	**-**	**-**	**-**	**-**	**-**	**-**	**-**	**-**	**-**
Olfr1426	**0**	**-**	**-**	**-**	**-**	**-**	**-**	**-**	**-**	**-**	**-**
Olfr1427	**0**	**-**	**-**	**-**	**-**	**-**	**-**	**-**	**-**	**-**	**-**
Olfr1428	**0**	**-**	**-**	**-**	**-**	**-**	**-**	**-**	**-**	**-**	**-**
Olfr1440	**0**	**-**	**-**	**-**	**-**	**-**	**-**	**-**	**-**	**-**	**-**
Olfr1442	**0**	**-**	**-**	**-**	**-**	**-**	**-**	**-**	**-**	**-**	**-**
Olfr1444	**0**	**-**	**-**	**-**	**-**	**-**	**-**	**-**	**-**	**-**	**-**
Olfr1445	**0**	**-**	**-**	**-**	**-**	**-**	**-**	**-**	**-**	**-**	**-**

Olfr1446	**0**	**-**	**-**	**-**	**-**	**-**	**-**	**-**	**-**	**-**	**-**
Olfr1447	**0**	**-**	**-**	**-**	**-**	**-**	**-**	**-**	**-**	**-**	**-**
Olfr1448	**0**	**-**	**-**	**-**	**-**	**-**	**-**	**-**	**-**	**-**	**-**
Olfr1449	**0**	**-**	**-**	**-**	**-**	**-**	**-**	**-**	**-**	**-**	**-**
Olfr1450	**0**	**-**	**-**	**-**	**-**	**-**	**-**	**-**	**-**	**-**	**-**
Olfr1451	**0**	**-**	**-**	**-**	**-**	**-**	**-**	**-**	**-**	**-**	**-**
Olfr1454	**0**	**-**	**-**	**-**	**-**	**-**	**-**	**-**	**-**	**-**	**-**
Olfr1457	**0**	**-**	**-**	**-**	**-**	**-**	**-**	**-**	**-**	**-**	**-**
Olfr1459	**0**	**-**	**-**	**-**	**-**	**-**	**-**	**-**	**-**	**-**	**-**
Olfr1461	**0**	**-**	**-**	**-**	**-**	**-**	**-**	**-**	**-**	**-**	**-**
Olfr1462	**0**	**-**	**-**	**-**	**-**	**-**	**-**	**-**	**-**	**-**	**-**
Olfr1463	**0**	**-**	**-**	**-**	**-**	**-**	**-**	**-**	**-**	**-**	**-**
Olfr1466	**0**	**-**	**-**	**-**	**-**	**-**	**-**	**-**	**-**	**-**	**-**
Olfr1467	**0**	**-**	**-**	**-**	**-**	**-**	**-**	**-**	**-**	**-**	**-**
Olfr1469	**0**	**-**	**-**	**-**	**-**	**-**	**-**	**-**	**-**	**-**	**-**
Olfr1471	**0**	**-**	**-**	**-**	**-**	**-**	**-**	**-**	**-**	**-**	**-**
Olfr1472	**0**	**-**	**-**	**-**	**-**	**-**	**-**	**-**	**-**	**-**	**-**
Olfr1474	**0**	**-**	**-**	**-**	**-**	**-**	**-**	**-**	**-**	**-**	**-**
Olfr1475	**0**	**-**	**-**	**-**	**-**	**-**	**-**	**-**	**-**	**-**	**-**
Olfr1477	**0**	**-**	**-**	**-**	**-**	**-**	**-**	**-**	**-**	**-**	**-**
Olfr1480	**0**	**-**	**-**	**-**	**-**	**-**	**-**	**-**	**-**	**-**	**-**
Olfr1484	**0**	**-**	**-**	**-**	**-**	**-**	**-**	**-**	**-**	**-**	**-**
Olfr1487	**0**	**-**	**-**	**-**	**-**	**-**	**-**	**-**	**-**	**-**	**-**
Olfr1489	**0**	**-**	**-**	**-**	**-**	**-**	**-**	**-**	**-**	**-**	**-**
Olfr1490	**0**	**-**	**-**	**-**	**-**	**-**	**-**	**-**	**-**	**-**	**-**
Olfr1491	**0**	**-**	**-**	**-**	**-**	**-**	**-**	**-**	**-**	**-**	**-**
Olfr1494	**0**	**-**	**-**	**-**	**-**	**-**	**-**	**-**	**-**	**-**	**-**
Olfr1495	**0**	**-**	**-**	**-**	**-**	**-**	**-**	**-**	**-**	**-**	**-**
Olfr1496	**0**	**-**	**-**	**-**	**-**	**-**	**-**	**-**	**-**	**-**	**-**
Olfr1497	**0**	**-**	**-**	**-**	**-**	**-**	**-**	**-**	**-**	**-**	**-**
Olfr1499	**0**	**-**	**-**	**-**	**-**	**-**	**-**	**-**	**-**	**-**	**-**
Olfr1500	**0**	**-**	**-**	**-**	**-**	**-**	**-**	**-**	**-**	**-**	**-**
Olfr1501	**0**	**-**	**-**	**-**	**-**	**-**	**-**	**-**	**-**	**-**	**-**
Olfr1502	**0**	**-**	**-**	**-**	**-**	**-**	**-**	**-**	**-**	**-**	**-**
Olfr1504	**0**	**-**	**-**	**-**	**-**	**-**	**-**	**-**	**-**	**-**	**-**
Olfr1505	**0**	**-**	**-**	**-**	**-**	**-**	**-**	**-**	**-**	**-**	**-**
Olfr262	**0**	**-**	**-**	**-**	**-**	**-**	**-**	**-**	**-**	**-**	**-**
Olfr76	**0**	**-**	**-**	**-**	**-**	**-**	**-**	**-**	**-**	**-**	**-**
Polr2g	**0**	**-**	**-**	**-**	**-**	**-**	**-**	**-**	**-**	**-**	**-**
Scgb1a1	**0**	**-**	**-**	**-**	**-**	**-**	**-**	**-**	**-**	**-**	**-**
Slc22a19	**0**	**-**	**-**	**-**	**-**	**-**	**-**	**-**	**-**	**-**	**-**
Slc22a27	**0**	**-**	**-**	**-**	**-**	**-**	**-**	**-**	**-**	**-**	**-**
Slc22a28	**0**	**-**	**-**	**-**	**-**	**-**	**-**	**-**	**-**	**-**	**-**

Slc22a29	**0**	**-**	**-**	**-**	**-**	**-**	**-**	**-**	**-**	**-**	**-**
Slc22a30	**0**	**-**	**-**	**-**	**-**	**-**	**-**	**-**	**-**	**-**	**-**
Slc22a6	**0**	**-**	**-**	**-**	**-**	**-**	**-**	**-**	**-**	**-**	**-**
Slc22a8	**0**	**-**	**-**	**-**	**-**	**-**	**-**	**-**	**-**	**-**	**-**
Slc3a2	**0**	**-**	**-**	**-**	**-**	**-**	**-**	**-**	**-**	**-**	**-**
Snhg1	**0**	**-**	**-**	**-**	**-**	**-**	**-**	**-**	**-**	**-**	**-**
Stx5a	**0**	**-**	**-**	**-**	**-**	**-**	**-**	**-**	**-**	**-**	**-**
Taf6l	**0**	**-**	**-**	**-**	**-**	**-**	**-**	**-**	**-**	**-**	**-**
Tle4	**0**	**-**	**-**	**-**	**-**	**-**	**-**	**-**	**-**	**-**	**-**
Tmem109	**0**	**-**	**-**	**-**	**-**	**-**	**-**	**-**	**-**	**-**	**-**
Tmem132a	**0**	**-**	**-**	**-**	**-**	**-**	**-**	**-**	**-**	**-**	**-**
Tmem179b	**0**	**-**	**-**	**-**	**-**	**-**	**-**	**-**	**-**	**-**	**-**
Tmem216	**0**	**-**	**-**	**-**	**-**	**-**	**-**	**-**	**-**	**-**	**-**
Tmem223	**0**	**-**	**-**	**-**	**-**	**-**	**-**	**-**	**-**	**-**	**-**
Wdr74	**0**	**-**	**-**	**-**	**-**	**-**	**-**	**-**	**-**	**-**	**-**

CHAPTER 2

Zmiz2 Overexpression Displaces Rod Photoreceptors to the Cone Stratum

ABSTRACT

After retinal cells exit the mitotic cycle, they migrate from the neuroblast layer (NBL) to various depths of the developing retina, creating the three nuclear layers that form the retinal architecture. Immature rod and cone photoreceptors retain an attachment at the ventricular surface and translocate their nuclei through a basally-directed process to occupy a position across the depth of the outer nuclear layer (ONL). Cone photoreceptors exhibit a puzzling pattern of nuclear translocation, first traveling through the ONL, only to translocate back towards the outer limiting membrane (OLM). Recent studies have identified the intracellular machinery mediating this process, but the transcriptional regulatory control is still largely undefined (Razafsky et al. 2012). Here we describe a potential role for the transcriptional co-regulator, *Zmiz2*, in modulating photoreceptor positioning. Previously, *Zmiz2* mRNA expression in the retina had been profiled using *in situ* hybridization in maturity. We utilized an antibody that recognized ZMIZ2, and showed expression was accentuated in cones during the second postnatal week in development, at which time cones are translocating through the ONL. To interrogate the role of *Zmiz2* in photoreceptor development, we designed a *Zmiz2*-encoding plasmid and overexpressed *Zmiz2* mRNA into postnatal day two (P2) murine retinas. Successfully transfected cells included rod photoreceptors, as well as Müller glia, bipolar cells, and amacrine cells, all of which are known to continue to be generated

postnatally. There was no change in the proportion of cells located in the INL versus the ONL when compared to retinas electroporated with control plasmids. Interestingly, *Zmiz2*-overexpressing rods in the ONL showed a propensity to become positioned closer to the OLM. Although these cells exhibited positioning typical of cones, they did not express two different genes used to identify cones (Ctbp2 and mouse Cone Arrestin), confirming that they had not adopted a cone fate. The mispositioning of these rods appeared to emerge late in development, as there was no difference in the distribution of GFP-positive cells in the ONL between the *Zmiz2*-overexpressing cells and control cells at postnatal day 5, 10, and 15. We suggest that endogenous *Zmiz2* expression in photoreceptors participates in the regulation of nuclear translocation to ensure correct cellular positioning in maturity.

INTRODUCTION

As neuroblasts exit the mitotic cycle and commit to a particular cell fate, they migrate to their appropriate depth within the developing retina, ensuring the creation of three nuclear layers. Developing cells that will occupy the GCL and INL separate from the ventricular surface and migrate via radial migration or somal translocation, moving basally until they reach their cell-specific layer (Prada et al. 1987, Snow and Robson 1994, Baye and Link 2008, Chow et al. 2015). Interestingly, photoreceptors remain attached to the ventricular surface and extend a process into the developing retina, thereby giving their somas a path to translocate along (Johnson et al. 1999). Rod photoreceptors, which comprise 97% of the ONL population in the murine retina, begin being produced after cones, with their peak at the day of birth (Young 1985). Their somal positioning across the depth of the ONL is not tightly linked to birth order, aside from a slight trend for prenatally born rods to become positioned within the inner half of the ONL and postnatally generated rods to be positioned within the outer half of the ONL (Carter-Dawson and LaVail 1979b). Cones follow a drastically different path, undergoing active nuclear translocation into the ONL, only to return towards the OLM, where they will be positioned in the mature retina (Rich, Zhan and Blanks 1997, Aghaizu et al. 2021).

While several studies have provided insight into the machinery involved in this process, much less is known about the regulatory mechanisms controlling nuclear translocation and positioning in post-mitotic cells (Razafsky et al. 2012, Jimeno et al. 2016, Aghaizu et al. 2021). Protein Inhibitor of Activated STAT (PIAS) proteins are transcriptional co-regulators that use diverse mechanisms to modify transcriptional

activity (Shuai and Liu 2005, Sharrocks 2006). Zinc finger MIZ-type containing 2 (*Zmiz2,* previously called *Zimp7*; Huang et al. 2005, Beliakoff and Sun 2006) is a PIAS-like protein that is expressed by photoreceptors in maturity (Akimoto et al. 2006), but little is known of its functions within the developing nervous system. *Zmiz2* is known to augment T-cell factor (TCF) and Wnt-β-catenin-mediated transcription (Lee et al. 2013), the latter modulating a variety of developmental processes (Mulligan and Cheyette 2012, Rosso and Inestrosa 2013). Our laboratory previously profiled the expression of *Zmiz2* in the mature retina, utilizing *in situ* hybridization. Labeling was present in all three nuclear layers, notably in the INL and GCL, but also in the ONL above background levels seen with control sense riboprobes (unpublished data, Figure 1a, a', b, b').

In this study, we report the retinal expression of ZMIZ2 during development and in maturity via immunofluorescence, and the effect of its overexpression upon photoreceptor positioning during postnatal development. ZMIZ2 expression was seen in all three nuclear layers in the mature retina, although it was less pronounced in the ONL. There was increased signal in somata located in the outer ONL, believed to be cone nuclei. *Zmiz2* was overexpressed in murine retinas on the day after birth (P2), and successfully electroporated cells could be visualized via GFP expression. *Zmiz2* overexpression did not change the cell fate, but affected the somal location of rod photoreceptors, mis-positioning them to the outer ONL. Electroporated retinas were taken at various developmental timepoints in order to determine whether cell somas were able to translocate into the ONL, before moving back towards the outer ONL. GFP-positive somata were seen throughout the depth of the ONL at P5, 10, and 15,

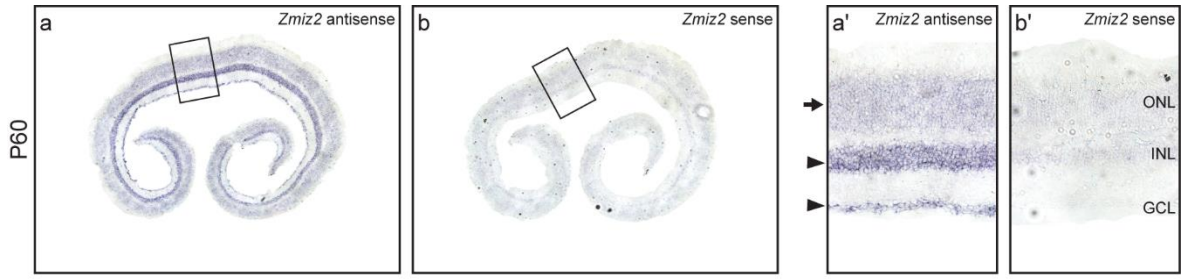

Figure 1: *Zmiz2* antisense riboprobes confirmed retinal expression in maturity. a & b: Entire cross-sections of retinas at P60 showed elevated signal relative to sense (control) riboprobes. a' & b': Higher magnification views of central retina. Note the pronounced signal in the GCL and INL in maturity (a', filled arrowheads). Signal was also present in the ONL (a', filled arrow. Calibration bar = 250 μm for panels a & b, and = 50 μm for panels a'-b'.

suggesting that overexpression of *Zmiz2* did not prevent somata from initially translocating and promoted cells to migrate back to the outer ONL. This phenotype mirrors that of normal cone development, suggesting that *Zmiz2* is involved in regulating proper localization of cone somata.

METHODS

Mouse strains and Tissue Preparation

The mouse line Crl:CD1(ICR) (Strain #022) was obtained from the Charles River Laboratory. C57BL/6J (B6/J) mice obtained from The Jackson Laboratory (Strain #000664) were bred for histological analysis. All animals were housed and bred in the Animal Resource Center at University of California, Santa Barbara and protocols were approved by the IACUC. Electroporated and developmental eyes (P5, P10, P15, P21) were drop-fixed in 4% paraformaldehyde for 30 minutes after euthanasia via intraperitoneal injection of sodium pentobarbital (120mg/kg) and removal of the eyes from their orbits. Adult retinas were fixed via intracardial gravity perfusion for 15 minutes with 4% paraformaldehyde, followed by immersion fixation for 15 minutes.

In Vivo Electroporation

The pCAGIG expression plasmid (Addgene, #11150) was originally deposited by the laboratory of Connie Cepko (Matsuda and Cepko 2004). Ubiquitous gene expression (*Zmiz2* and *gfp*) was controlled by a chicken β-actin promoter with CMV enhancer. *Zmiz2* clone MMM1013-202858381 (Dharmacon, BC060652) was inserted using restriction enzymes EcoRI and NotI.

The electroporation protocol followed that described by Connie Cepko (Matsuda and Cepko 2004). In summary, postnatal day 2 (P2) CD1 pups were placed on ice. Once there was no reaction via tail pinch, the pup was placed onto a dissecting microscope and its eyelid was cleaned with 70% ethanol. The eyelid was then cut with a syringe needle (27 gauge), followed by a puncture of the nasal cornea. From there,

0.7µL of plasmid (1.5µg/µL) was injected into the subretinal space using a Hamilton syringe. After the injection, tweezer type electrodes (Harvard University, 10mm SS electrode, disc tip, #45-0119) soaked in phosphate-buffered saline (PBS) were placed around the head and pulses were applied (4 pulses at 60V, 50ms duration with 950ms intervals) using an Electro Square Porator (BTX, Model 830). One to two drops of 0.5% proparacaine was dripped onto the eye and then the pup was placed on a pad in a warm water bath to recover. Once fully recovered, pups were returned to the dam and left to develop until the desired age.

Retinal Sectioning

Retinas were embedded in 5% agarose in 0.1M phosphate buffer. Retinal sections 200µm thick were cut using an Pelco easySlicer (Ted Pella, Inc., Redding, CA) and stored in 0.1M phosphate buffer.

Immunofluorescence

Whole retinas or sections were protein blocked in 5% Normal Donkey Serum (NDS) for three hours, followed by a series of three washes in cold PBS. Samples were then incubated in primary antibodies for the next three days. After three washes in cold PBS, secondary antibodies (diluted 1:200) were added to the samples for an overnight incubation. Again, the samples were washed three times. All solutions were made up in 1% Triton in PBS and incubations were completed at 4ºC with gentle shaking. Primary antibodies used in this study included a mouse monoclonal CtBP2 antibody (BD Transduction, #612044, 1:500), a rabbit polyclonal GFP antibody conjugated to Alexa Fluor 488 (Invitrogen, #A21311, 1:1,000), an affinity-purified goat polyclonal GFP antibody conjugated to DyLight 488 (Rockland, #600-141-215,

1:1,000), and an affinity-purified rabbit polyclonal mCAR antibody (Millipore, #AB15282, 1:10,000). Additionally, Hoechst33342 (Invitrogen, #H3570, 1:1,000) was used to label cell nuclei and visualize the three nuclear layers. A custom affinity-purified rabbit polyclonal antibody that recognized the C-terminal region (aa714-824) was given to the laboratory by Zijie Sun (Huang et al. 2005). Secondary antibodies used to detect CtBP2, mCAR or ZMIZ2 were donkey anti-rabbit IgGs conjugated to either Alexa Fluor 546 or Alexa Fluor 488 (Invitrogen, #A10040 and #A21206, 1:200).

Electroporated Cell Analysis

Individual retinal sections that had been immunolabeled to reveal the presence of GFP in the two conditions were coded to conceal their identity and then randomly intermingled, and each labeled cell in the ONL was plotted relative to the boundaries of the ONL as revealed in the Hoechst counterstain, and that position was then expressed as a proportion of the depth through the layer for each of the P21 sampled retinas. Each labeled cell in the INL from these same retinas was classified as residing in the inner half versus the outer half of the INL. Of those 26 analyzed retinas at P21, 4 (2 in each condition) had a very low sample of cells in the inner half of the INL (as few as 1-4 cells), and so those four retinas were eliminated from the analysis of relative positioning between the ONL and INL, and within the INL itself. For each of the retinas sampled at P10 or P15, positioning was determined only for the cells in the ONL, while in the case of the P5 retinas, positioning was relative to the boundaries of the neuroblast layer (NBL).

To further describe the positioning of cells in the ONL (and at P5, the NBL), we divided the layer into four equal quarters across depth and determined the proportion

of all cells in the ONL (or NBL) residing in each of those four quarters, plotted as relative frequency histograms. The mean depth of the entire population in each retina was also determined at each sampled age. Respective figures comparing the two conditions at each age, therefore, presented sample plots of the distribution of labeled cells, followed by relative frequency histograms across the four quarters of the layer, and concluded with a comparison of the mean values for the two conditions. Data for the frequency histograms and for the comparison of population means were derived from the entire sampled population of cells in each retina, while the sampled plots of cellular positioning across depth were matched in density by randomly selecting cells from the condition with the greater number of cells to match that with the fewer number of cells. Finally, retinal wholemounts that were double-labeled for either CtBP2 or mCAR (known markers of cone somata in the mature ONL) and GFP were sampled through the entire depth of the ONL to identify whether any of the GFP-positive cells were cone photoreceptors. One sample field was chosen per electroporated retina, centered on the region with the greatest GFP expression.

Statistics

The proportion of electroporated retinas yielding effective transfection, judging by the presence of GFP labeling, was variable, as was the extent of retina transfected. All transfected retinas were sectioned, and those sections without disruption of the retinal architecture were sampled, with this sampling protocol conducted blind to condition. Consequently, the number of cells assessed for depth of positioning in the ONL or NBL per retina was considerably variable. The average depth for all sampled cells in each retina was determined, and Student's t-test was used to compare those

means at P5, P10 and P21, using a *p* value of 0.05 as the threshold to reject the null hypothesis. In the case of the P15 comparison, only two retinas electroporated with *Zmiz2*-encoding plasmids yielded effective transfection, so no statistical comparison was conducted at that age.

RESULTS

Zmiz2 is expressed in the mature and developing murine retina, and can be overexpressed via electroporation

Zmiz2 expression in the eye and retina was determined using two different bioinformatic databases. Whole mouse eye and retinal transcriptome profiling showed *Zmiz2* expression in maturity (GeneNetwork: AXB eye-GN210, and BXD retina-GN267). *Zmiz2* expression has also been observed in mature photoreceptors (Akimoto et al. 2006). Our laboratory additionally profiled expression of *Zmiz2* in mature retinal tissue, as described previously (Figure 1). Antibodies that recognize ZMIZ2 were subsequently used to determine the expression within particular cell types in developing and mature retinal tissue. In the mature retina, both the GCL and INL layers exhibited prominent staining (Figure 2a, b). The ONL contained less pronounced labeling, although there appeared to be more heavily labeled staining in a number of somata located in the outermost part of the ONL, believed to be cones based on location and density (Carter-Dawson and LaVail 1979a, Figure 2a, b, arrows). At P10, there was similar staining in all three layers, although the sparsely labeled cells that were found in the ONL near the outer limiting membrane in mature retinas were now located at variable depths of the ONL (Figure 2e, f), concurrent with the translocation of cone nuclei during development (Rich et al. 1997, Aghaizu et al. 2021). Negative control sections, in which the ZMIZ2 affinity-purified antibody was excluded, exhibited a degree of non-specific labeling, particularly within the inner retina in maturity (Figure 2c, d, g, h).

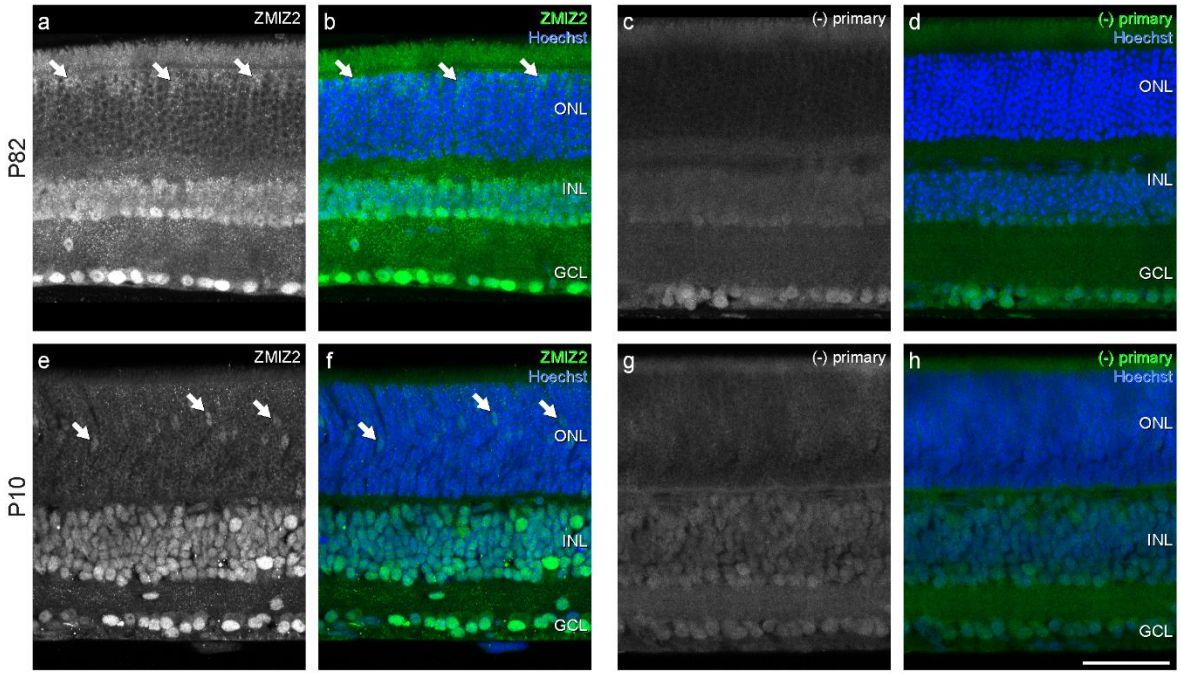

Figure 2: A polyclonal antibody to ZMIZ2 revealed immuno-positive cells across the retina. a, b, e, f: At both P82 (a, b) and P10 (e, f), labeled cells were detected in the GCL, INL and ONL. Within the ONL, more heavily labeled cells were positioned in the outermost part of the ONL in maturity, where cone somata were positioned (a, b; arrows), but lightly labeled cells can be detected throughout the layer relative to negative control sections. Note the slight background labeling present in the GCL in those negative control sections in maturity (c, d). A comparable pattern of labeling was present at P10 (e, f), with the distinction that the more heavily labeled cells in the ONL occupied variable positions across the depth of the ONL (arrows), consistent with the distribution of cone somata at this age. Also note the reduced non-specific labeling within the GCL in the negative control sections at P10 (g, h) in comparison with P82 (c, d). Calibration bar = 50 µm.

In order to investigate whether *Zmiz2* might participate in the positioning of cells across retinal depth, we overexpressed *Zmiz2* via electroporation. Plasmids (pCAGIG) encoding *gfp* with or without the coding sequence for *Zmiz2* were transfected into the murine retina one day after birth (P2), and the pups were left to develop until postnatal day 21. Successfully electroporated retinas were sectioned and GFP-positive sections were quantified, each yielding an average of 281 GFP-positive cells per retina. In both retinal sections expressing solely GFP or *Zmiz2* and GFP, the majority of electroporated cells were found in the ONL and INL, with the occasional cell in the GCL (Figure 3a, b). Based on the cells' locations and morphologies, electroporated cells included bipolar cells, amacrine cells, Müller glia, and rod photoreceptors (Figure 3c, d), as should be expected given the postnatal birthdates of these cell types and the fact that plasmid electroporation transfects proliferating, rather than post-mitotic, cells (Matsuda and Cepko 2004, Matsuda and Cepko 2007).

Electroporation of *Zmiz2*-encoding plasmids yielded GFP-positive cells that expressed heightened levels of ZMIZ2, as seen by immunofluorescence using the ZMIZ2-specific antibody (Figure 4). This signal was absent from GFP-positive cells when the ZMIZ2 antibody was removed, as well as in sections that were electroporated with the control plasmids (Figure 4c, d, g, h). Still present in the sections was the endogenous immunostaining of somata in the outer ONL (oONL), similar to that of the non-electroporated retinas (Figure 4a, b, e, f). Cells that were electroporated with *Zmiz2*-encoding plasmids, evidenced by their GFP fluorescence, therefore, effectively overexpressed the ZMIZ2 protein.

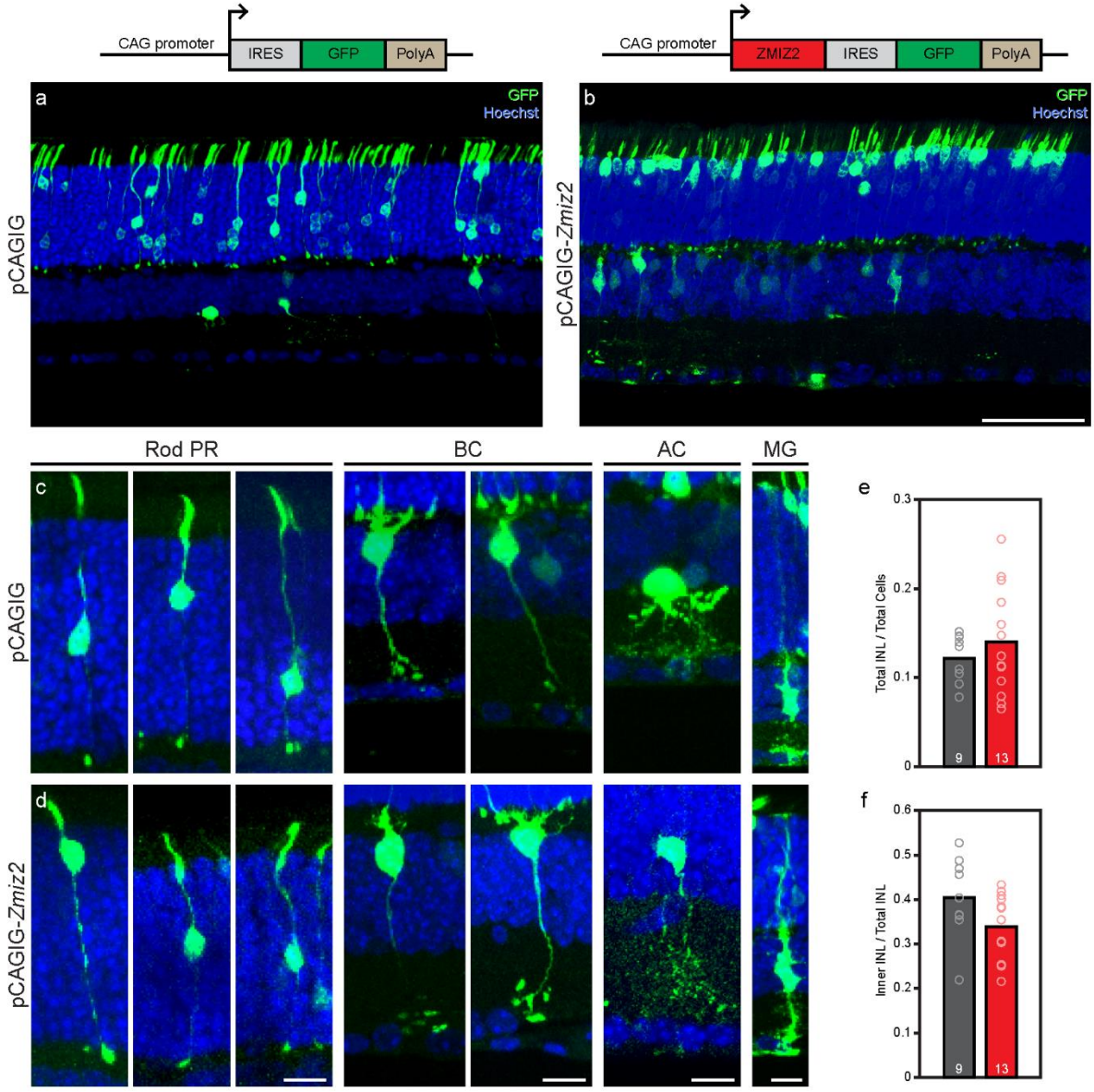

Figure 3: Electroporating control or *Zmiz2*-encoding plasmids on P2 yields GFP-positive cells in the ONL and INL at P21. a, b: Retinal sections show the mis-positioning of GFP-positive cells in the ONL in a retina overexpressing *Zmiz2* (b) within the outer-most parts of the ONL, relative to the control condition (a) where cells are found relatively evenly distributed through the ONL. The composition of the pCAGIC and pCAGIC-*Zmiz2* vectors are indicated at the top. c, d: At higher magnification, the morphologies of single GFP-positive photoreceptor, bipolar, amacrine and Müller glial cells in the *Zmiz2*-overexpressing retinas appeared normal. e, f: The proportion of all GFP+ cells positioned within the INL was unaltered (e) and nor was the proportion of GFP+ cells in the INL that were positioned within its inner half (f). Calibration bar = 50 µm for a and b, and = 10 µm for c and d.

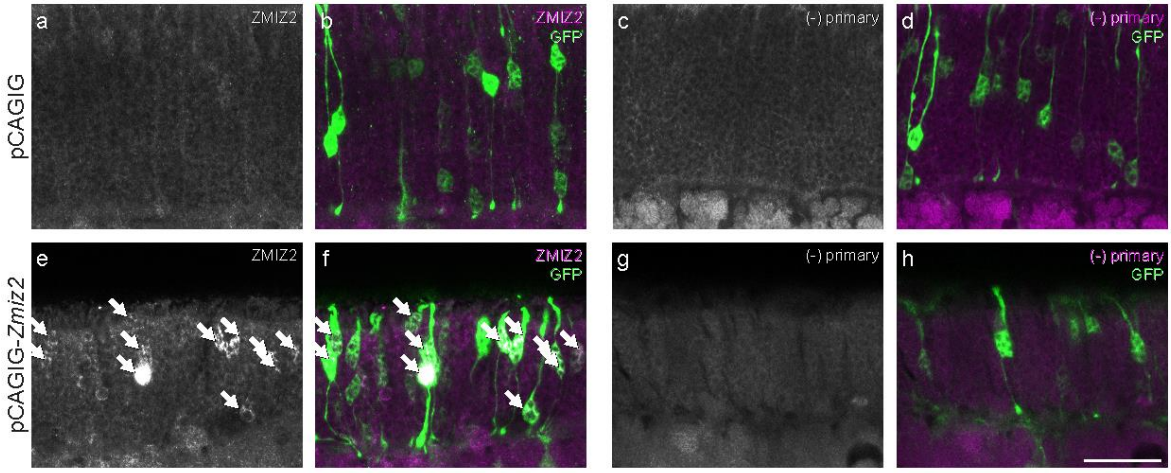

Figure 4: Electroporating *Zmiz2*-encoding plasmids on P2 yielded heightened ZMIZ2 immunolabeling in transfected cells in the ONL at P15. a, c: anti-ZMIZ2 labeling. b, d: Same sections double-labeled, showing transfected GFP+ cells and anti-ZMIZ2 labeling combined. Panels a-d show a retina transfected with control plasmids, while panels e-h show a retina transfected with *Zmiz2*-encoding plasmids. Panels on the right side (c, d; g, h) show negative control sections in which the primary antibody to ZMIZ2 had been omitted. Note the heightened ZMIZ2 labeling of the GFP-positive cells only in the *Zmiz2*-overexpressing retina (arrows in e, f), confirming that the antibody detected ZMIZ2. GFP expression in retinas transfected with *Zmiz2*-encoding plasmids therefore effectively reports *Zmiz2*-overexpression. Calibration bar = 25 µm.

Overexpression of *Zmiz2* does not change cell fate or location between nuclear layers, but does influence somal location within the ONL

Electroporation using the pCAGIG plasmid, both with and without the *Zmiz2*-encoding sequence, resulted in GFP-positive cells primarily located in the ONL and INL, as described above. We first investigated whether overexpression of *Zmiz2* affected the distribution of GFP-positive cells in the ONL versus the INL. All GFP-positive cells were classified as residing in the ONL or INL, and the proportion of cells in the INL to the total cell number was calculated for each retina. There was no change in the proportion of labeled cells in the INL in the *Zmiz2*-overexpression condition compared to the control ($p = 0.41$, Figure 3g). These results suggested that overexpression of *Zmiz2* does not change the fate of cells belonging in one layer to the other, and that there was no mis-positioning of the cells into the wrong layer. Next, we determined whether the proportion of cells within the iINL (amacrine cell stratum) and oINL (bipolar cell stratum) was altered with the overexpression of *Zmiz2*. We divided the Hoechst-labeled INL in half to classify the cell as being located in the iINL or oINL. There was no significant difference in the iINL-to-oINL ratio ($p = 0.08$, Figure 3f). Cells in the INL exhibited the characteristic features of bipolar cells, amacrine cells and Müller glia.

By contrast, within the ONL itself, there was a marked difference in the positioning of GFP-positive cells at P21 between the two conditions. Whereas retinas electroporated with only *gfp* showed labeled somata distributed at various depths throughout the ONL, experimental retinas receiving *Zmiz2*-encoding plasmids were frequently mis-positioned to the outermost portion of the ONL, many of them

contacting the OLM (Figure 3b). These cells exhibited characteristic features of photoreceptor cells, with an inner segment extending through the OLM and a basally directed process reaching the OPL. We quantified the location of all GFP-positive cells located in the outer nuclear layer as a proportion of ONL thickness and plotted the positions (Figure 5). Positioning along the X axis is arbitrary in this figure, to show the population of all cells relative to ONL depth, making clear the bias towards the outer parts of the ONL in cells overexpressing *Zmiz2* (Figure 5a, c). We further classified the entire population of GFP-positive cells in each retina as residing in one of four quarters across the depth of the ONL and expressed them as a proportion of the total population. The histograms indicated the mean percentage in each quarter, and the individual retinas were represented as thin lines (Figure 5b, d). Across the four quarters, the proportion of cells was greatest in the outer quarter in most of the *Zmiz2*-overexpressing retinas, declining as a function of distance from the OLM. Some retinas showed a more prominent trend than others (Figure 5d), but this trend was absent in the eleven retinas receiving control plasmids, where the distribution of cells was highest in the middle two quarters of the ONL, declining slightly in the outer and inner quarters (Figure 5b). The histogram in Figure 5e indicated the mean position for the entire population of cells in each individual retina, being significantly different between the two conditions ($p < 0.001$). These results suggested that *Zmiz2*-overexpressing photoreceptors, as a population, are biased to reside closer to the OLM.

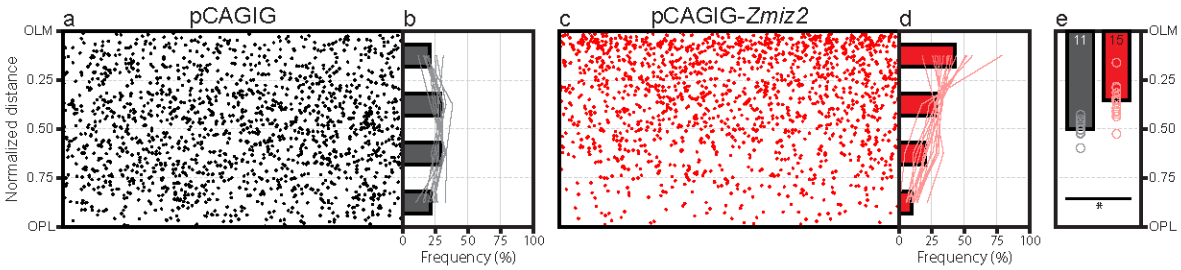

Figure 5: Overexpression of *Zmiz2* caused photoreceptor somata to be displaced to the outer parts of the ONL. a, c: Plot of the position of GFP-positive cells within the ONL at P21 from retinas that had been electroporated with control (black) or *Zmiz2*-encoding (red) plasmids on P2 (n = 1565 cells from retinas that received control plasmids versus the same number randomly drawn from 2226 cells from retinas that received *Zmiz2*-overexpressing plasmids, to balance the density in these plots). b, d: Percentage of all labeled cells in each retina positioned in each of the four quarters of the ONL extending from the OLM to the OPL. Histograms indicate the mean percentage across all retinas for that quarter, while the individual retinas are indicated by thin connecting lines across the quarters (n = 11 and 15 retinas, respectively). e: Histogram comparing the population means derived from the individual retinas contributing these cells.

Zmiz-overexpressing cells in the ONL are rod photoreceptors

We next investigated whether the overexpression of *Zmiz2* changed the fate of the rod photoreceptors to cones. Based on previously described immunofluorescence, endogenous ZMIZ2 appeared to be more highly expressed in cone photoreceptors. Additionally, somas of photoreceptors that overexpressed *Zmiz2* were located in the oONL, where cone soma normally reside. We double-labeled electroporated retinas with CtBP2, which labels cone somata in the outer parts of the ONL. Retinas from both conditions showed characteristic cone labeling in the outer ONL that complemented, but never coincided with, the GFP-positive cells in the control retinas, and only very rarely coincided in the *Zmiz2*-overexpressing retinas. We sampled double-labeled wholemount preparations to quantify the proportion of GFP-positive cells that were also CtBP2-positive, while blind to condition (Figure 6). Out of the 1,123 cells receiving the control plasmid (n = 1 retina), zero were double-labeled, while in the *Zmiz2*-overexpressing condition (n = 2 retinas), 6 double-labeled cells (e.g. figure 6b, arrow) were detected out of 757 sampled cells. CtBP2 normally also labels the ribbon synapses of both rod spherules as well as cone pedicles, and therefore may not have been as reliable an indicator of cone identity. We repeated this experiment labeling the retina for the cone-specific protein, mouse cone arrestin (mCAR). In this comparison, out of the 1189 cells receiving control plasmid (n = 2 retinas) and 1,865 cells receiving the *Zmiz2*-overexpressing plasmid (n = 5 retinas), only a single cell was detected in each condition that was plausibly double-labeled. mCAR labels the cone pedicles as well as cone somata, and an examination of the OPL showed a complementarity, rather than any colocalization, of mCAR and GFP in photoreceptor

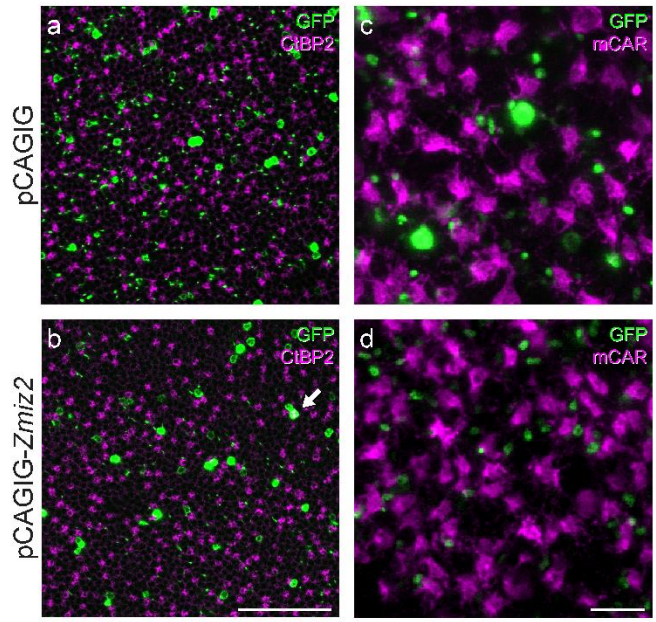

Figure 6: *Zmiz2*-overexpressing photoreceptors have not differentiated into cone photoreceptors. a, b: Z-stack reconstructions through the outermost portion of the ONL of wholemounted retinas from eyes transfected with control plasmid (a) or with *Zmiz2*-encoding plasmid (b) and labeled for CtBP2 to identify cone somata (magenta). With one exception in this field (figure 2b, arrow), none of the GFP-positive somata colocalize CtBP2. c, d: At the level of the GFP-positive rod spherules, none here colocalize mCAR, which normally label cone somata and their axons in the ONL and their pedicles terminating in the OPL (magenta). (Note the very occasional GFP-positive rod somata at the border of the OPL in the control condition). Calibration bar = 50 µm for a and b, 10 µm for c and d.

terminals. All GFP-positive terminals had the characteristics of rod spherules, while all the mCAR-positive terminals had the traits of cone pedicles, and none were double-labeled. Together these results indicate that the mis-positioned *Zmiz2*-overexpressing cells were rod rather than cone photoreceptor cells.

Overexpression of *Zmiz2* does not prevent photoreceptor somata from translocating into the ONL

As retinal electroporation around the time of birth is thought to transfect proliferating cells undergoing mitosis at the ventricular surface (the future OLM), the prior results suggested the possibility that postnatally generated rod photoreceptors that overexpress *Zmiz2* simply fail to translocate into the ONL, and instead, remain "stuck" within the outer parts of the developing NBL. In order to address this hypothesis, we performed electroporations at P2, and then harvested the retinas at P5, the earliest age that GFP could be visualized, and measured the distance of the GFP-positive cells across the depth of the neuroblast layer (Figure 7 a, b, c, d). Both the control and *Zmiz2*-overexpressing cells showed somal distributions throughout the entire depth of the neuroblast layer, and the comparison between the two conditions' average position in each of the individual retinas showed no significant difference ($p = 0.74$, Figure 7e). Overexpressing *Zmiz2* in developing photoreceptor cells did not impact their ability to initially translocate into the ONL, before mis-positioning near the OLM.

To determine when these cells translocate back towards the oONL, we repeated the experiment harvesting retinas at P10, where the ONL boundaries were defined. GFP-positive somata expressing *Zmiz2* were still spread across all four

quadrants, as did the cells transfected with the control plasmid ($p = 0.31$, Figure 7f-j). We also looked at P15, and again, found comparable distributions between the two conditions (Figure 7k-o). Therefore, the somal mispositioning of *Zmiz2*-overexpressing cells must occur later in development, during the third postnatal week.

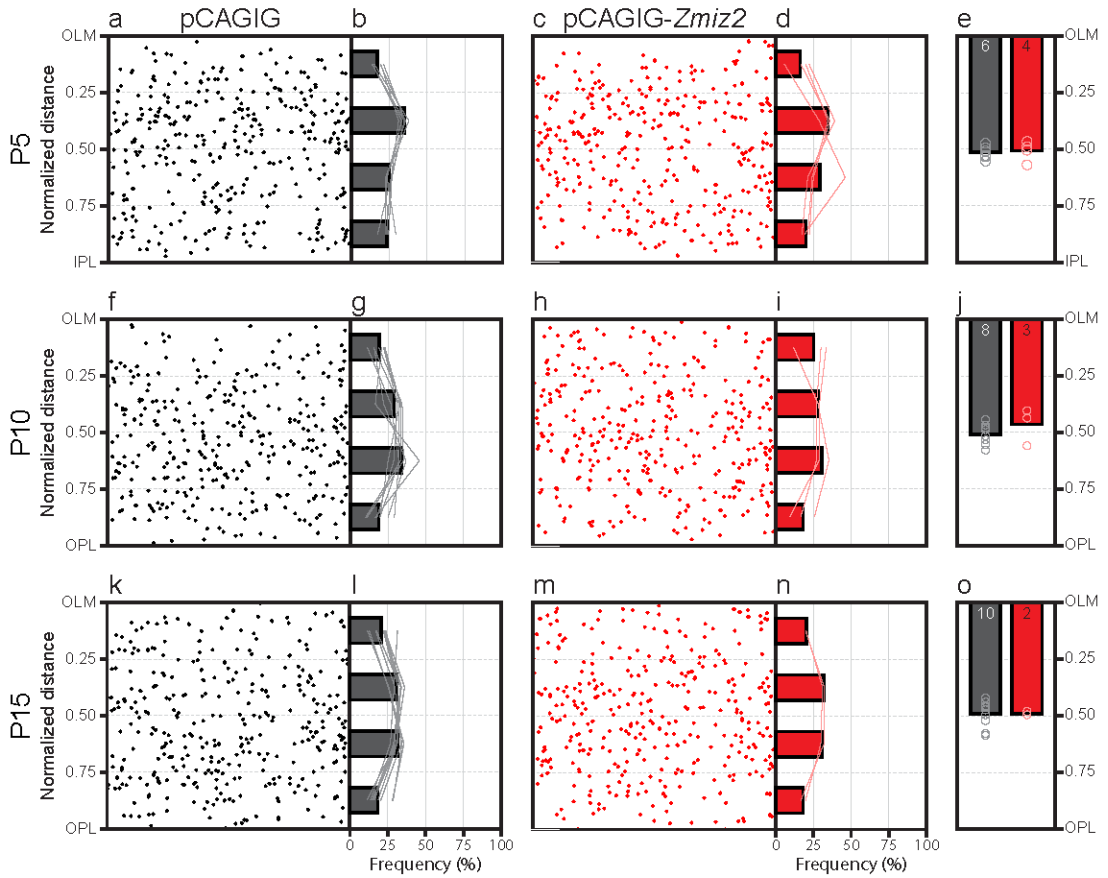

Figure 7: Overexpression of *Zmiz2* on P2 does not prevent photoreceptors from translocating normally into the ONL. There was comparable distribution across the ONL relative to those from retinas receiving control plasmids, as early as P5 (a-e), and still present at their normal depths at P10 (f-j) and P15 (k-o). Conventions as in figure 5. a, c; f, h; k, m: Plot of the position of GFP-positive cells within the NBL (P5) or ONL (P10, P15) from retinas that had been electroporated with control (black) or *Zmiz2*-encoding (red) plasmids on P2 (n = 342 cells from retinas receiving control versus Zmiz2-encoding plasmids, drawn randomly from samples in order to present comparable densities in these plots). b, d; g, i; l, n: Percentage of all labeled cells in each retina positioned in each of the four quarters of the ONL (or NBL at P5) extending from the OLM to the OPL (or to the IPL, at P5). Histograms indicate the mean percentage across all retinas for that quarter, while the individual retinas are indicated by thin connecting lines across the quarters (n = 6 versus 4 retinas at P5; n = 8 versus 3 retinas at P10; n = 10 versus 2 retinas at P15, respectively). e: Histogram comparing the population means derived from the individual retinas contributing these cells (n = 2083 cells from retinas receiving control plasmids versus 1176 cells from retinas receiving *Zmiz2*--overexpressing plasmids at P5 (n = 1397 cells from retinas receiving control plasmids versus 342 cells from retinas receiving *Zmiz2*-overexpressing plasmids at P10; n = 9522 cells from retinas receiving control plasmids versus 519 cells from retinas receiving *Zmiz2*-overexpressing plasmids at P5).

DISCUSSION

The present study identified a possible regulator of translocation of photoreceptors in the developing retina, *Zmiz2*. Difficult to discern, however, is whether endogenous *Zmiz2* plays a role in the positioning of rods in the ONL. *Zmiz2* expression was determined using both bioinformatic and experimental techniques. Using *in situ* hybridization, *Zmiz2* was observed across the entirety of the ONL in maturity, indicating expression in both rod and cone photoreceptors. Using immunofluorescence, ZMIZ2 expression was decidedly greater in the cones in maturity (evidenced by their positioning in maturity, near the OLM), as well as during development, at P10 (evidenced by the known translocation of cone nuclei at this stage). Overexpression of *Zmiz2* in dividing cells yielded a mispositioning of rod photoreceptor nuclei to the outermost portion of the ONL, where cone somata reside in the mature retina (Figure 8). These rod photoreceptors translocated their nuclei into the developing ONL, as normally seen during development, but then aberrantly translocated back to the outermost parts of the ONL, being normal behavior for developing cone photoreceptors (Rich et al. 1997). The cells transfected in the ONL were rod photoreceptors, since these are the only photoreceptor cells generated after birth (Young 1985). Consistent with this, staining of retinal tissue with cone markers hardly ever showed colocalization with the GFP label. As cones are more heavily ZMIZ2-immunopositive relative to rods (Figure 2), their own endogenous *Zmiz2* may participate in controlling this movement of cones back to the outer parts of the ONL; rods in which *Zmiz2* is overexpressed may now be mimicking this cone-like behavior. We suggest that the endogenous heightened Zmiz2 expression in cones may be instrumental in this translocation of the cones.

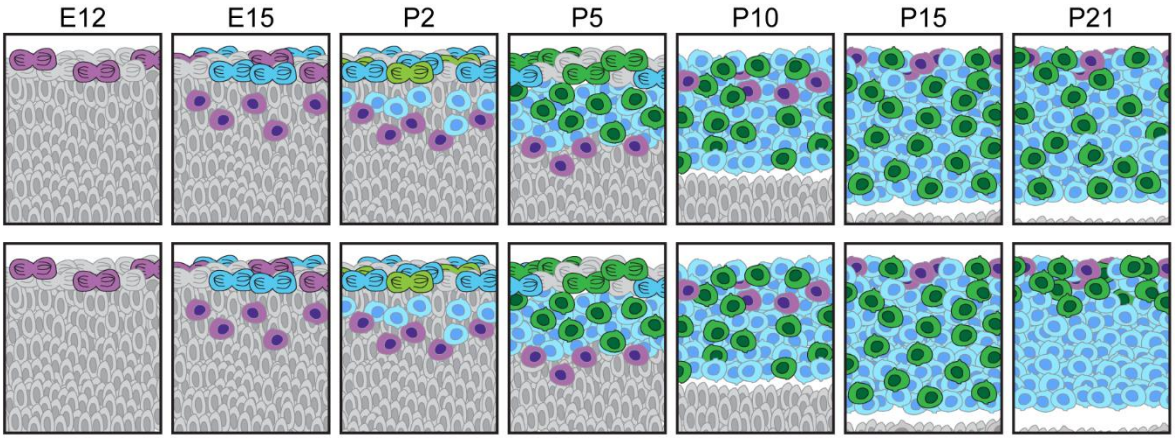

Figure 8: *Zmiz2* overexpressing rods translocate through the ONL and back up to the oONL. Retinas electroporated with control plasmid (top row) or *Zmiz2* (bottom row). Translocation of cones (purple), rods (blue), and electroporated rods (green) are shown from E12 through P21.

The current results raise the question, is *Zmiz2* normally involved in determining the positioning of the rods? Examining the normal sequence of rod photoreceptor development is more difficult, relative to the cones, because of the presence of densely packed rods. Determining whether there is a change in the patterning of rod nuclei would be difficult to discern unless the rods were misplaced in the IPL or INL. Whether or not their initial displacement into the ONL is an active mechanism or simply arises through the stochastic jostling of their nuclei amidst the interkinetic nuclear translocation occurring with ongoing progenitor cells has not been determined. But as some rods are known to migrate back into the ONL after having initially settled in the INL erroneously (Young 1985, Aghaizu et al. 2021), we speculate that endogenous *Zmiz2* may contribute to that direction of movement, and overexpressing it simply exaggerates this effect, driving the cells back to the outermost parts of the ONL.

The mechanism in which ZMIZ2 influences rod nuclei translocation has yet to be determined. ZMIZ2 has not been extensively studied, but what has been explored suggests that it has a role in gene regulation. The protein has been shown to physically interact with androgen receptors, chromatin remodeling proteins, and to impact Wnt signaling (Peng et al. 2010, Lee et al. 2013, Moreno-Ayala et al. 2015, Liu et al. 2021). ZMIZ2 could be acting upon the expression of the machinery that has been recently identified in translocation. LINC complexes, which links the nucleoskeleton to the cytoskeleton, have been shown to participate in the translocation of cone nuclei through the action of cytoskeletal networks and motor proteins within the cytoplasm (Razafsky et al. 2012, Razafsky, Potter and Hodzic 2015), but the orchestration of this

process is unknown. LKB1, a master serine/threonine kinase, and one of its downstream kinases, AMPK, have recently been shown to play a role in the control of nuclear translocation within the cones, as loss-of-function studies show a failure of cone nuclei to translocate back toward the OLM, and these same retinas exhibit reductions in the expression of LINC genes as well as dynein and kinesin (Burger et al. 2020).

Further experiments need to be performed in order to investigate the role of *Zmiz2* in photoreceptor translocation. We observed a change in somal location in rod photoreceptors when there was an overexpression of *Zmiz2* but have yet to determine if there are phenotypic changes, including cellular positioning, if *Zmiz2* is removed. Electroporating cells with a CRISPR/Cas9 gene knockout plasmid would reveal changes in rod photoreceptors, bipolar cells, amacrine cells, and Muller glia, but not cones, since they are post-mitotic at P2. A conditional knockout mouse, in which *Zmiz2* is knocked out of developing cone photoreceptors, would be necessary in order to determine whether *Zmiz2* expression influences the ability for cone somata to correctly translocate. Additionally, candidate genes that could be regulated by *Zmiz2*, such as those that make up LINC-complexes, could be overexpressed via electroporation. Mispositioning of rod somata towards the outer ONL would suggest that ZMIZ2 regulates the expression of that gene. What is clear from this study, however, is that ZMIZ2 is expressed in rods, and to a greater extent, cones, and that it is effective at disrupting the normal migration of rod photoreceptors, possibly by altering the levels of a LINC-complex machinery unit.

CHAPTER 3

SOX5 Regulates Axonal and Dendritic Arbors in Type 7 Cone Bipolar Cells

ABSTRACT

The variety of traits exhibited by the cells of the nervous system are a direct reflection of the heterogeneity of function. These distinguishing characteristics include cell localization, morphology, synaptic partners, and gene expression. Recent advances in transcriptional profiling have enabled researchers to uncover cell-specific genes that may be essential in the development of both the five classes of retinal neurons, as well as the individual types within the classes. The 15 unique types of retinal bipolar cells present an attractive model to study the mechanisms of diversification during neural development, due to the extensive characterization of each of these cell types. Here, we explored the role of *Sox5* in a single bipolar cell type, the Type 7 cone bipolar cell (CBC). We confirmed the expression of SOX5 in the retina as early as the first postnatal day and verified its expression in Type 7 CBCs by the end of the second postnatal week. *Sox5* was conditionally knocked out from bipolar cells by crossing a bipolar cell-specific cre line with mice containing floxed *Sox5* alleles. A *Gustducin-GFP* reporter allele was utilized to identify Type 7 CBCs and to confirm the removal of SOX5 in those cells. The loss of *Sox5* expression during development resulted in cells producing smaller axonal and dendritic arbors. The axonal arbors also contained ectopic sprouts that reached the S5 stratum of the IPL. Dendritic arbors contacted fewer cone pedicles and increased the number of terminals they innervated per pedicle. These changes in morphology generate Type 7 CBCs

with smaller receptive fields from fewer cones, as well as transmit information to a larger range of amacrine and ganglion cell targets in the IPL.

INTRODUCTION

Proper neuronal development requires the coordination of multiple molecular processes at definitive time points. These various mechanisms are controlled by both specialized extrinsic and intrinsic factors. The creation of correct neuronal circuits between cells is no exception. Axonal arbors are influenced by the population of target cells that they aim to synapse with, whereas dendritic arbors are influenced by the density of afferents (Raven et al. 2007, Wässle et al. 2009, Gibson and Ma 2011). These afferents and targets are important in promoting differentiation (Cline and Haas 2008), as well as guiding the growth of these cell's processes (McAllister 2001). The local density of neighboring cells within a population also influences the development of arbors, either through competition for target cells or homotypic interactions between nearby cells (Inberg et al. 2019, Keeley et al. 2021). Cells additionally utilize intrinsic factors to promote differentiation, as well as assure recognition of cues found within the environment (Valnegri, Puram and Bonni 2015, Prigge and Kay 2018).

The bipolar cell class is a desirable model for studying cellular diversity during development. The murine retina contains 15 distinct types of bipolar cells, each with their own unique characteristics: connective partners, stratification, and morphology (Shekhar et al. 2016, Behrens et al. 2016, Keeley et al. 2017, Kautzman et al. 2018, West and Cepko 2022). In contrast, the over 40 ganglion cell types and 50-60 amacrine cell types have not all been studied as thoroughly, and therefore make it difficult to discern similarities or differences in mechanisms that impact their similar or unique traits (Rheaume et al. 2018, Yan et al. 2020). Of the 15 bipolar cell types, 14 of them synapse with cone photoreceptors, and only 1 with rods (Shekhar et al. 2016).

Additionally, the various bipolar cell types terminate at distinct depths within the IPL, where they form synapses with different amacrine and ganglion cells (Euler and Wässle 1998). The divergence in the cell types arise from unique gene expression profiles in development and through maturity (Chow et al. 2001, Shekhar et al. 2016, Suzuki-Kerr et al. 2018).

In the present study, we utilized a single-cell transcriptome database to identify genes that were uniquely expressed in one bipolar cell type, the Type 7 cone bipolar cell (CBC). Based on its selective expression in this bipolar cell, as well as known functions of the gene, we focused our attention on SRY-box transcription factor 5 (*Sox5*). In the nervous system, *Sox5* is affiliated with neuron migration, differentiation, axonal positioning and dendritic arborization (Kwan et al. 2008, Lai et al. 2008, Quiroga et al. 2015, Li et al. 2017, Naudet et al. 2018). We effectively removed expression of *Sox5* from Type 7 CBCs with a conditional knockout mouse that expressed cre in post-mitotic, but still differentiating, bipolar cells (Dy et al. 2008, Nickerson et al. 2011). A mouse line that selectively expressed a reporter gene specific to Type 7 CBCs, *Gustducin-GFP*, was also bred onto these conditional knockout mice, so that the cells of interest could be visualized, and their morphology characterized (Huang et all 2003, Wässle et al. 2009). We identified several phenotypic changes in both the cells' axonal and dendritic morphologies. *Sox5*-CKO Type 7 CBCs maintained the gross morphological characteristics; however, their axonal arbor areas were reduced and displayed additional ectopic sprouts that extended into the S5 stratum of the IPL, instead of being contained to just the S4 stratum. The dendritic arbors also decreased in size, as did the number of cone

pedicles that the Type 7 CBCs contacted. Interestingly, the pedicles that the bipolar cells contacted were hyperinnervated compared to controls. These changes should result in Type 7 CBCs with smaller receptive fields and are no longer restricted to synapsing with primarily ON-OFF and ON Direction Selective RGCs, the dendrites of which are distributed in S4, and may now synapse with a higher proportion of alpha RGCs that stratify in S5 (Martersteck et al. 2017).

METHODS

Mouse Strains and Tissue Preparation

Sox5-floxed mice, in which the endogenous *Sox5* gene was flanked with LoxP sites, were generated in the laboratory of Véronique Lefebvre at The Cleveland Clinic (Dy et al. 2008). These floxed mice were crossed with *Vsx2-cre* mice, where cre recombinase was expressed in post-mitotic bipolar cells (Nickerson et al. 2011). Expression of cre recombinase in Type 7 CBCs was confirmed by crossing the *Vsx2-cre* mice with the *ROSA-tdTomato* mouse. tdTomato expression requires the removal of a loxP-flanked stop site by cre recombinase, thereby confirming expression of cre in the cell type of interest (Madisen et al. 2010). *Gustducin-GFP* mice were crossed with *Sox5*-CTRL and CKO mice, so that Type 7 CBCs could be identified (Wong et al.,1999, Huang et al. 2003). *Gustducin-GFP* mice were also used to confirm selective expression of SOX5 in Type 7 CBCs, as well as profile axonal and dendritic arbor development. The mice were genotyped via PCR using the primers listed in Table 1.

In order to collect adult retinal tissue, 4-8 week old mice were given a lethal dose of sodium pentobarbital (120mg/kg). Once the animals were deeply anesthetized, the temporal side of the cornea was marked with a hot needle to identify orientation. An intracardial perfusion was performed first with 4mL of physiological saline (0.9%), followed by 4% paraformaldehyde in 0.1M sodium phosphate buffer (pH 7.2-7.4) for 15 minutes. Eyes were removed from the orbits and immersion-fixed for an additional 15 minutes. Retinas were dissected out of the eye and four relieving radial cuts were made so that the hemispheric retina could lie flat. Developmental retinal tissue was collected following euthanasia of pups (via decapitation if younger

than P6 or lethal dose of sodium pentobarbital if P7 or older) and eyes were immediately removed from their orbits and fixed in 4% paraformaldehyde in 0.1M sodium phosphate butter (pH 7.2-7.4) for 30 minutes. Retinas were dissected in the same manner as adult retinas.

Developmental retinas (P10) were harvested from eyes following euthanasia via lethal dose of sodium pentobarbital. Retinas were freshly dissected and stored in RNA*later* overnight (Thermofisher Scientific, AM7020). All procedures were approved by the Institutional Animal Care and Use Committee (IACUC) at the University of California, Santa Barbara.

Retinal Sectioning

Dissected retinas were embedded in 5% agarose in 0.1M phosphate buffer. Radial sections 200µm thick were cut using a Pelco easySlicer (Ted Pella, Inc., Redding, CA) and stored in 0.1M phosphate buffer.

Immunofluorescence

In order to prevent non-specific binding of antibodies, whole or sectioned retinas were pre-incubated in 5% Normal Donkey Serum (NDS) for three hours, followed by a series of three washes in cold phosphate-buffered saline (PBS). Samples were incubated in primary antibodies for three days. After an additional three washes in cold PBS, secondary antibodies (diluted 1:200) were added. Samples were incubated overnight, and then washed three times. All incubations were done at 4ºC with gentle agitation. All solutions were made up in 1% Triton in PBS. Hoechst33342 (Invitrogen, #H3570) was used at a dilution of 1:1,000 in order to visualize the nuclear layers of the retina. SOX5 expression patterns in developing and adult retinas were

detected using a rabbit polyclonal antibody (Thermofisher Scientific, #PA5-66331, 1:500) raised against the human SOX5 protein (aa39-aa130), which contained over 90% homology to murine SOX5. We tested three dilutions to determine the suitable working concentration, as well as a negative control to determine background labeling from the secondary antibodies. Two antibodies were to detect and amplify the GFP signal: a rabbit polyclonal antibody conjugated to Alexa Fluor 488 (Thermofisher Scientific, #A21311, 1: 1,000) and a chicken polyclonal antibody (Thermofisher Scientific, #A10262, 1: 1,000). Cones were identified using an affinity-purified rabbit polyclonal antibody to Cone Arrestin (Millipore, #AB15282, 1:10,000) and peanut agglutinin lectin (PNA) conjugated to Alexa Fluor 647 (Thermofisher Scientific, L32460, 1:200). Secondary antibodies raised in donkey and directed to either rabbit IgG conjugated to Alexa Fluor 488 or Alexa Fluor 546 (Invitrogen, #A21206, and #A10040) or chicken IgY conjugated to Alexa Fluor 488 (Jackson ImmunoResearch, 703-545-155) were used to detect primary antibodies.

DiI Injections

Retinal wholemounts were placed in a petri dish and held down by a piece of weigh paper containing a small opening, which enabled the central retina to be accessed for manipulation. The weigh paper was then held down with magnets, and the petri dish was filled with 0.1M phosphate buffer (PB), before being placed on a fixed-stage Nikon microscope equipped with a Burleigh micromanipulator. A glass capillary was pulled to a pipette (0.5µm in diameter) and backfilled with CM-DiI (Invitrogen, V22888). The pipette was brought to GFP-positive somata located in the INL or GFP-positive axon terminals located in the IPL, where a small amount of DiI

was deposited by passing positive current. The DiI began to crystalize in the aqueous solution and subsequently spread in the cellular membranes via lipophilic diffusion. About a dozen cells were injected per quadrant of the retina. The retina was then immersion-fixed for an hour, rinsed three times with PBS, and incubated overnight in PNA-Alexa Flour 647. The following day, the retinas were rinsed an additional three times. Successfully injected cells were imaged on an Olympus Fluoview1000 laser scanning confocal microscope, containing a ×40 oil-immersion objective with a numerical aperture of 1.30.

Morphometric Analysis

Axonal and dendritic arbors from DiI-labeled cells were imaged at 0.5µm optical sections, until their processes were no longer in view. Collapsed Z-stack projections were constructed of the arbors, and a convex polygon was traced around the perimeter to measure the arbor area. Axonal depth was estimated by determining the number of 0.5µm sections that encompassed the axonal processes. Retinal areas and somal areas from DiI-labeled Type 7 CBCs were traced using ImageJ. The density of cone pedicles labeled with mCAR and PNA was measured in sample central and peripheral fields in each quadrant (0.011mm^2), and total cell number was calculated. Fields were sampled using an Olympus Fluoview1000 laser scanning confocal microscope with a ×40 objective.

The number of cones contacted by each cell was detected by the colocalization of the dendrites, labeled with DiI, and cone pedicles, labeled with PNA. Images were manipulated via deconvolution to better visualize individual dendritic terminals. The theoretical point spread function was first calculated for each of the DiI-labeled cells

(https://imagej.net/plugins/diffraction-psf-3d), followed by deconvolution of each image (https://imagej.net/plugins/iterative-deconvolve-3d). All analysis was done with the evaluator blind to condition and with all images randomly interleaved to minimize batch effects.

Quantitative RT-PCR

RNA was extracted from retinas (P10) previously stored in RNAlater using the Qiagen RNeasy Mini Extraction Kit (Qiagen, #74104). cDNA was synthesized using the iScript Reverse Transcription Supermix for RT-PCR (Biorad, #1708840), and final concentrations were determined using a Nanodrop spectrophotometer (Thermofisher Scientific, #ND-2000). Primers (Table 2) for candidate genes were designed and tested for temperature conditions. *Gapdh* and *β2m* were used as standards for the qPCR reactions (Kautzman et al. 2018). qPCR reactions were comprised of SsoAdvanced Universal Inhibitor-Tolerant SYBR Green Supermix (Biorad, #1725270), 20μM of forward and reverse primers, and cDNA from each of the samples. qPCR reactions were run in triplicate alongside a set of standards.

Bioinformatic Databases

Gene expression in bipolar cells was reviewed from single-cell transcription data (Shekhar et al. 2016). Genes with predicted *Sox5* binding sites were found using the following databases: JASPAR Predicted Transcription Factor Targets (https://amp.pharm.mssm.edu/Harmonizome/gene_set/SOX5/JASPAR+Predicted+Transcription+Factor+Targets), MotifMap Predicted Transcription Factor Targets (https://amp.pharm.mssm.edu/Harmonizome/gene_set/SOX5/MotifMap+Predicted+

Transcription+Factor+Targets), and TRANSFAC Curated Transcription Factor Targets (https://amp.pharm.mssm.edu/Harmonizome/gene_set/SOX5/TRANSFAC+Curated+Transcription+Factor+Targets). Gene functions were analyzed using DAVID Bioinformatics Resource (https://david.ncifcrf.gov/), and protein-protein interactions were viewed with STRING functional protein association networks (https://string-db.org/).

Statistics

Student's t-tests were used to determine significant differences between the CTRL and *Sox5*-CKO littermate control mice, using a *p* value of 0.05 as the threshold to reject the null hypothesis.

RESULTS

Sox5 is expressed in the developing and mature murine retina

Sox5 expression was profiled in the developing and mature murine retina, utilizing both bioinformatic databases and immunostaining techniques. In maturity, *Sox5* was selectively expressed in Type 7 CBCs (Figure 1a), as well as a number of amacrine cell types, particularly GABAergic cells, and in a minority of retinal ganglion cell types (Shekhar et al. 2016, Tran et al. 2019, Yan et al. 2020). Immunostaining of adult retinal sections showed expression of SOX5 in cells in both the outer and inner INL (oINL and iINL), where bipolar and amacrine cells reside, respectively (Figure 1c and 1d). Additionally, there was sparse labeling of cells in the GCL (Figure 1b), which corresponded to the previously described bioinformatic data. Adult *Gustducin-GFP* mice, in which GFP was expressed brightly in Type 7 CBCs and faintly in RBCs (Huang et al. 2003), were used to confirm that Type 7 CBCs expressed SOX5 (Figure 1e, e', e'').

To confirm expression during retinal development, expression of SOX5 was profiled in the first two postnatal weeks. At postnatal day 1 (P1), a sparse number of cells was weakly immunopositive for SOX5 (Figure 2a). By P3, SOX5 immunopositive cells had migrated to the amacrine cell layer in the developing INL, as well as the GCL (Figure 2b). As the retinal layers became more pronounced around P7, a population of cells in the oINL, presumably developing Type 7 CBCs, began expressing SOX5 (Figure 2d). Type 7 CBCs, which were identified in development at P13 (when GFP could be readily visualized), colocalized with SOX5 staining (Figure 2g', 2h'). This analysis validated that *Sox5* was expressed in Type 7 cone bipolar cells both in development and maturity.

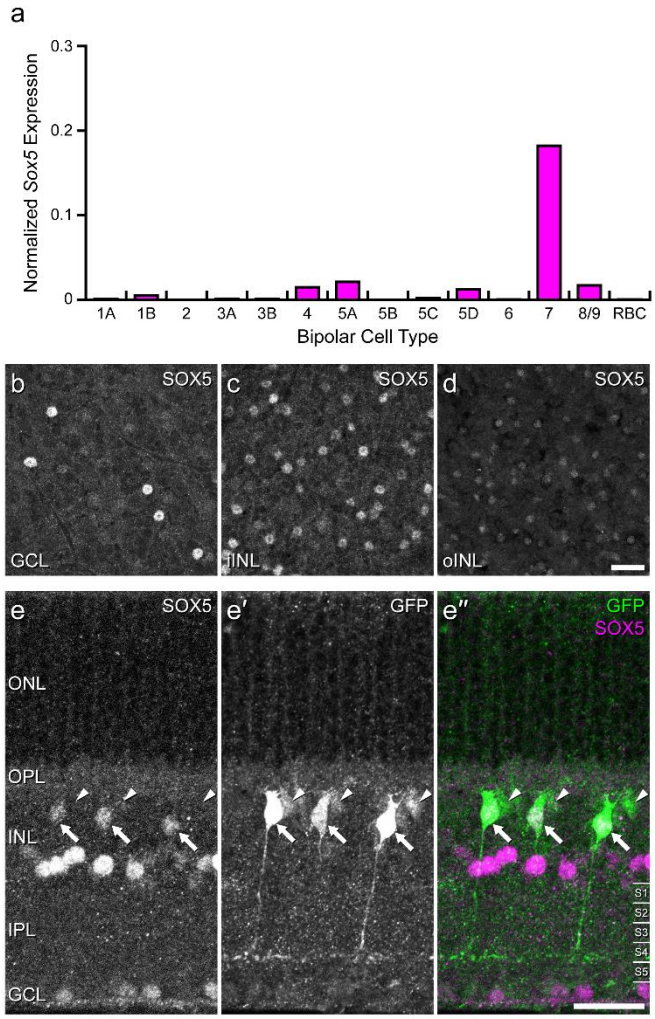

Figure 1: *Sox5* expression in the mature retina. a: Single cell transcriptional profiling of retinal bipolar cells demonstrated that *Sox5* expression was near-selectively expressed in the Type 7 CBC (from Shekhar et al., 2016; accessed from the single cell portal from the Broad Institute). b-d: Immunostaining of mature mouse retinal wholemounts using an antibody to SOX5 revealed sparsely labeled cells in the GCL (b) and in the INL, both in the iINL, being the amacrine cell layer (c) as well as cells in the oINL, being the bipolar cell stratum (d). e-e": Immunostaining Gustducin-gfp transgenic retinas for SOX5 (e, e') confirmed that the SOX5-positive cells in the bipolar cell stratum are also GFP-positive (e", arrows). These are confirmed to be Type 7 CBCs by virtue of their stratifying axonal arbors in S4 of the IPL. GFP-positive cells that do not co-localize with SOX5 in their somata (arrowheads in e-e") are RBCs, evidenced by their dimmer GFP fluorescence and by their axons reaching into S5 of the IPL. Calibration bars = 50 µm.

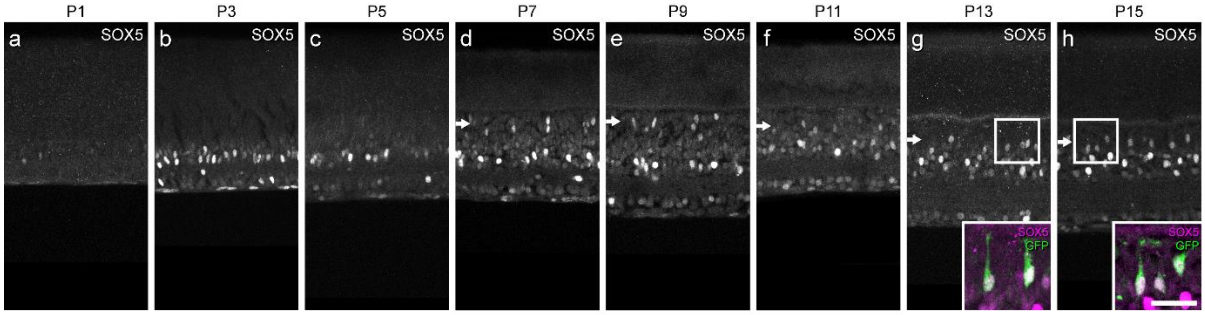

Figure 2: Developmental time-course of SOX5-immunolabeling in the retina, from the day of birth through the first two postnatal weeks. Close to the first postnatal week (d), there were SOX5-immunopositive cells in the emerging bipolar cell stratum and remaining there (horizontal arrows). Panels g' and h' show magnified regions of the INL, confirming that those SOX5-immunopositive cells in the bipolar cell stratum (magenta) are Type 7 CBCs, as they are also GFP-positive, due to the presence of *Gustducin-gfp* (green). Calibration bars = 50 µm.

We next wanted to compare the development of Type 7 CBCs to that of the developmental expression profile of SOX5. Prior to P10, the bipolar cells could not be visualized, due to the lack of *Gustducin-GFP* expression. Beginning at P10, a small number of cells in the oINL began expressing GFP, and a sparse number began producing immature axonal processes (Figure 3a, top and bottom panel). Through the second postnatal week, additional cells began expressing GFP, enabling visualization of their somata and axons (Figure 3b-f, top and bottom panels). As the axons matured, their arbors increased in overall size. There was difficulty visualizing dendrites during these developmental time points, however, prior research has determined that they can be seen as early as P9, using the same reporter (Lee et al. 2011, Dunn and Wong 2012). Together, these results indicate that Type 7 CBCs express *Sox5* early in neural development, prior to their morphological differentiation.

Vsx2-cre can be used to selectively remove SOX5 from retinal bipolar cells

In order to evaluate the importance of *Sox5* expression in the development of Type 7 CBCs, we selectively removed *Sox5* in developing bipolar cells using a conditional knockout mouse. The *Vsx2-cre* mouse line had previously been shown to express cre recombinase in bipolar cells post-mitotically (P3), but not all bipolar cell types had been profiled, including the Type 7 (Nickerson et al. 2011). To verify that Type 7 CBCs expressed cre recombinase, the *Vsx2-cre* mouse was bred with a cre reporter line (*ROSA-tdTomato*). In retinal sections, tdTomato expression was exclusively found in the oINL, where bipolar cell somata reside (Figure 4a). In retinal wholemounts, GFP-positive Type 7 CBCs were also tdTomato-positive, confirming that Type 7 CBCs expressed cre recombinase (Figure 4b, b'). This expression was

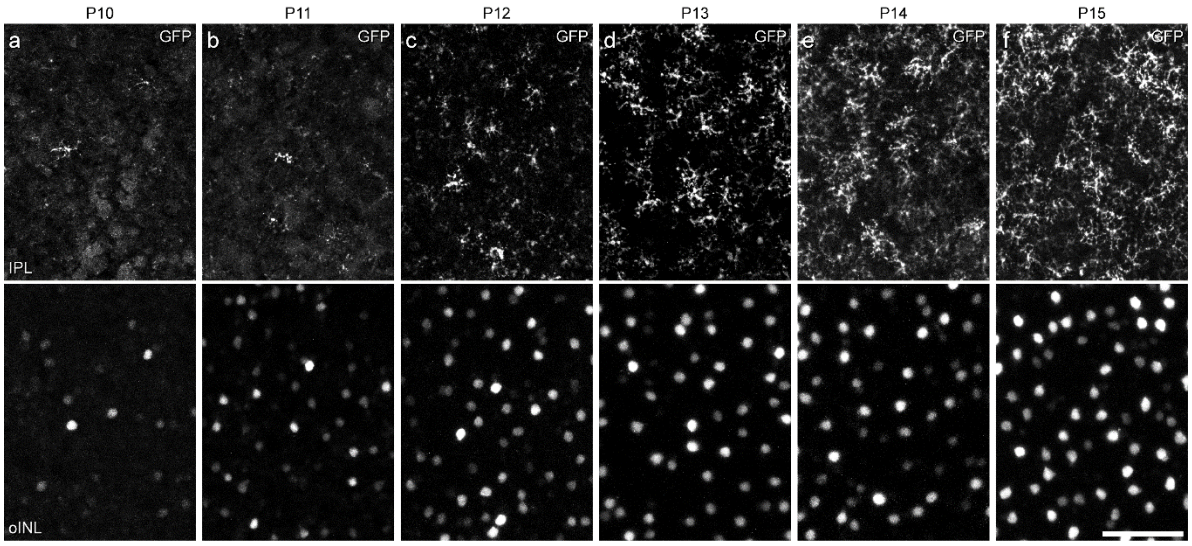

Figure 3: Developmental time-course of Type 7 CBC differentiation, revealed through GFP-labeling of their differentiating axon terminals in S4 of the IPL (top row) and somata in the INL (bottom row). Axonal arbors were first detected at P10 (a), increasing in frequency and size over the following five days (b-f). There remained occasional gaps within the mosaic of axon terminal arbors at P15 due to the incomplete expression of Gustducin-GFP. Calibration bar = 50 µm.

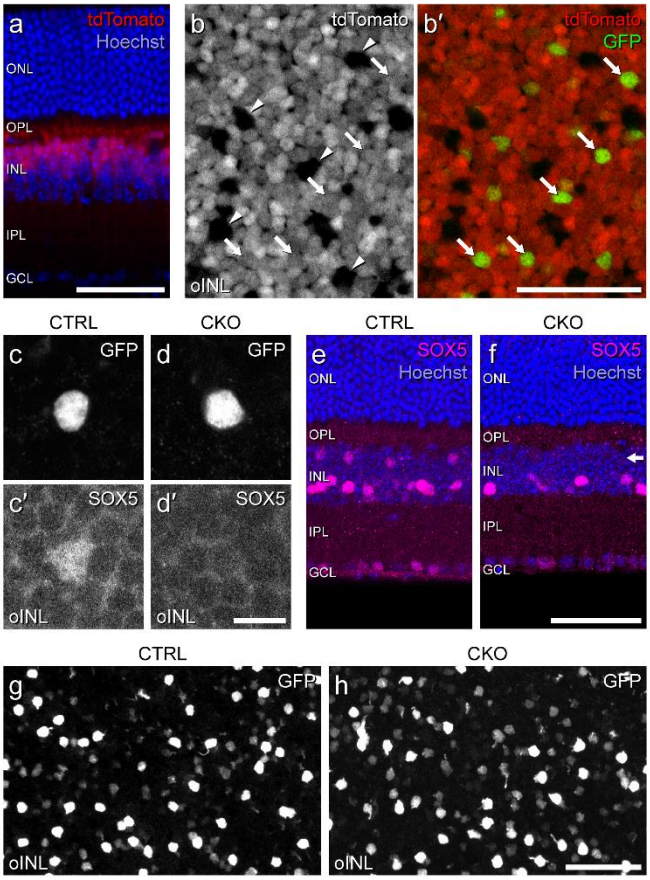

Figure 4: *Sox5*-CKO mice were bred to harbor floxed alleles of *Sox5*, a *Vsx2-cre* transgene, the *ROSA-tdTomato* cre-reporter transgene and Gustducin-gfp Type 7 CBC reporter transgene. a: Retinal cross-section from a mature littermate control mouse revealed the laminar restriction of the tdTomato labeling, confined to the oINL, where primarily bipolar cell somata are located. b, b': Wholemounted retina from a mature littermate control mouse through the bipolar cell stratum of the INL, showing most cells to be tdTomato-positive. Arrowheads indicate cells that were *tdTomato*-negative (b), including horizontal cells, while arrows indicate tdTomato-positive cells that are also GFP-positive (b'), confirming that these were Type 7 CBCs. c, c', d, d': In *Sox5*-CKO retinas, the bright GFP-positive cell soma are no longer SOX5-immunopositive. e, f,: *Sox5*-CKO retinas showed a loss of SOX5 labeling in the bipolar cell stratum of the INL (horizontal arrow), shown in section. g, h: Despite this absence of SOX5-positive cells, the population of GFP-positive cells is not diminished in *Sox5*-CKO retinas. Calibration bars = 50 μm in panels a, b, b', e, f, g and h, and = 10 μm in panels c, c', d, d'.

selective to bipolar cells, as horizontal cells, identified by their larger somal size and location in the inner INL, did not express tdTomato. To remove *Sox5* expression from Type 7 cells, we crossed the *Vsx2-cre* mouse with one that had floxed *Sox5* alleles. In such CKO retinas, GFP-positive Type 7 CBCs no longer expressed SOX5, compared to the CTRL cells that were co-labeled for GFP and SOX5 (Figure 4c, c', d, d'). In CKO retinas, cells in the iINL, presumed to be amacrine cells, still expressed SOX5, even though there was no longer expression of SOX5 in the bipolar cell stratum (Figure 4e, f). Despite the loss of SOX5-positive nuclei in the bipolar cell stratum of *Sox5*-CKO retinas, the incidence of GFP-positive cells therein was comparable to that found in littermate CTRL retinas (Figure 4g, h).

Type 7 CBCs that lack *Sox5* possess smaller axonal and dendritic arbors

Sox5 had previously been studied in nervous system development, pertaining to neuron migration, differentiation, and axon and dendrite formation (Kwan et al. 2008, Lai et al. 2008, Quiroga et al. 2015, Li et al. 2017, Naudet et al. 2018). Because of these known functions of SOX5, as well as the upregulation in the retina that coincided with these developmental processes, we investigated whether removal of *Sox5* impacted the morphology of the Type 7 CBCs. Qualitatively, there seemed to be no discernable differences in the morphology of individual cells between the CTRL and *Sox5*-CKO condition. Every observed cell maintained its bipolar arrangement, which consisted of an axon emerging from the soma into the IPL and a dendritic stalk extending into the OPL. The axonal arbor projected into the S4 stratum of the IPL, where the arbors then extend to the tips of their immediate like-type neighbors, tiling the S4 stratum (Wässle et al. 2009). A dendritic stalk extended from the soma and

branched into the OPL, where those dendrites also extend to the tips of their neighbors, each innervating the cone pedicles within their dendritic fields. But because not all Type 7 CBCs express this GFP reporter, we could not establish whether the axons or dendrites extended to reach their neighbors directly.

Following amplification of the GFP signal by immunostaining, axonal and dendritic arbor areas were measured in both conditions (Figure 5a, d). In the CTRL retinas, axonal area averaged 396 μm^2 (n = 44 cells). There was a 19% reduction in axonal arbor area in the *Sox5*-CKO condition (n=49 cells, $p<0.001$, Figure 5b). We confirmed that this reduction was not related to the eccentricity of the cell within the retinal wholemount, suggesting that the effect seen was not due to a bias in sampling location (Figure 5c). Likewise, dendrites from the same cells also exhibited an 18% decrease in area, from 250 μm^2 to 206 μm^2 ($p=0.008$, Figure 5e). In the CTRL retinas, there was no correlation between a cell's axonal and dendritic arbor area. Interestingly, in the CKO retinas, there was a positive correlation between the sizes of the dendritic and axonal arbor areas (Figure 5g).

The axonal and dendritic arbor areas measured were somewhat smaller than those measured in prior studies (Lee et al. 2011, Dunn and Wong 2012), and we wondered whether the GFP signal was sufficiently expressed in the entirety of each arbor. We noticed when crossing a mouse that contained both the *Gustducin-GFP* and the *Vsx2-cre* transgenes to a mouse that had neither, half the offspring contained the GFP allele and the other half contained the cre allele, but never both. This was true of both male and female offspring. We suspected that both transgenes were located on the same autosomal chromosome, therefore preventing any cre-positive

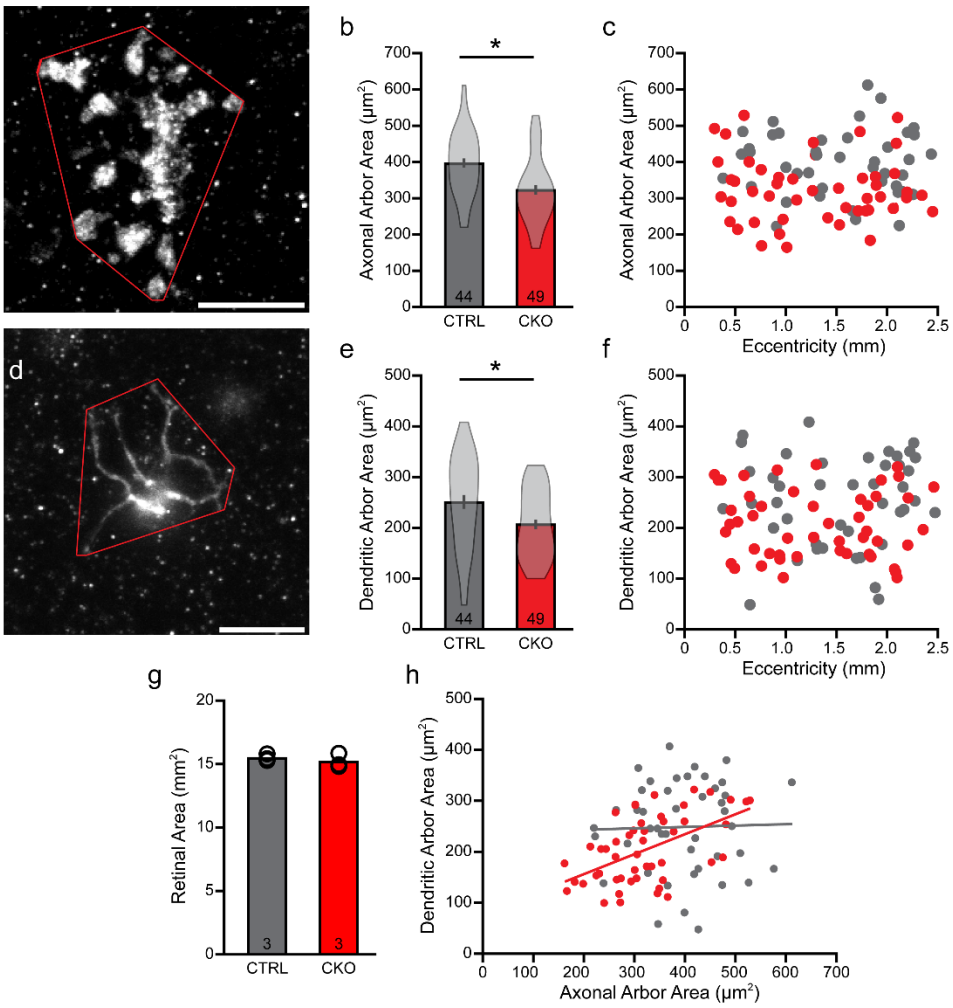

Figure 5: Morphological analysis of Type 7 CBC via GFP signal. Examples of GFP-labeled Type 7 CBC axonal (a) and dendritic (d) arbors, enclosed in a convex polygon (red). The axonal arbor area was significantly reduced in Sox5-CKO retinas (b), sampled at comparable retinal eccentricities (c). Similarly, there was a significant reduction in dendritic arbors (e), from cells with comparable eccentricities (f). Dendritic arbor area vs. axonal arbor area shows no correlation in the CTRL retina, but a positive correlation in the *Sox5*-CKO (h). Means and standard errors are shown within the violin plots in b and e. Calibration bar = 10 µm. n = number of cells (b, e) or retinas (g) sampled.

mouse from obtaining two copies of the *Gustducin-GFP* transgene, resulting in a weaker GFP signal. To guarantee visualization of the finer details of the arbors, GFP-positive cells were injected with a lipophilic dye, DiI, either at the level of the axonal arbors to visualize dendritic arbors, or at the somata to label axonal arbors. This provided us with individually labeled cells that could be analyzed in greater detail.

We measured the axonal and dendritic field areas of cells labeled with DiI, using the same analysis that was previously described (Figure 6a, b, c, d). Similar to the GFP arbors, there was a reduction in axonal areas in the CKO cells (n = 20 cells), when compared to the CTRL condition (n = 28 cells). This effect was larger in the DiI-labeled cells, there being a 25% reduction ($p < 0.001$, Figure 7a). We again confirmed that the reduction observed was not related to the eccentricity of the cell within the retinal wholemount ($p = 0.24$, Figure 7b). Dendritic arbor areas were also measured in the DiI-labeled Type 7 CBCs. There was a 41% decrease in dendritic area in *Sox5*-CKO cells (n = 29 cells) compared to the CTRL cells (n = 32 cells), from an average of 331μm^2 to 197μm^2 ($p < 0.001$, Figure 8a). The arbor areas in both conditions were larger than those measured utilizing the amplified GFP signal, and the decrease in arbor area was still present. The increase in size in both conditions was most likely due to better visualization of dendrites in DiI-labeled cells, which may have been missed when using GFP. Again, the effect was not due to a sampling location bias ($p = 0.81$, Figure 8b). Somal areas were also measured from these cells, showing a slight, if non-significant reduction in their sizes in the *Sox5*-CKO retinas ($p = 0.07$, Figure 8d).

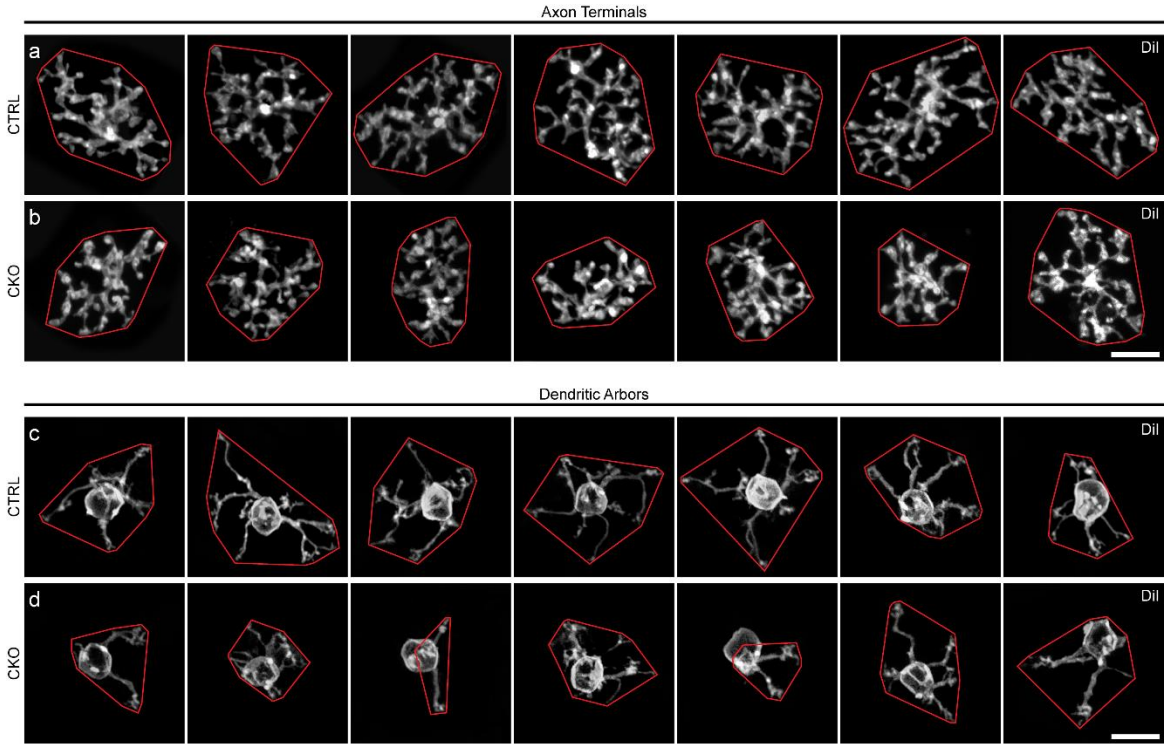

Figure 6: DiI-labeled axons and dendrites. a-d: Examples of DiI-labeled axon terminals (a, b) and dendritic arbors (c, d) from *Sox5*-CKO (b, d) and littermate control (a, c) retinas, in Z-stack projections from retinal wholemounts. Note the smaller areal domains of both axonal and dendritic territories in the *Sox5*-CKO retinas, enclosed here by convex polygons (red). Calibration bar = 10 µm.

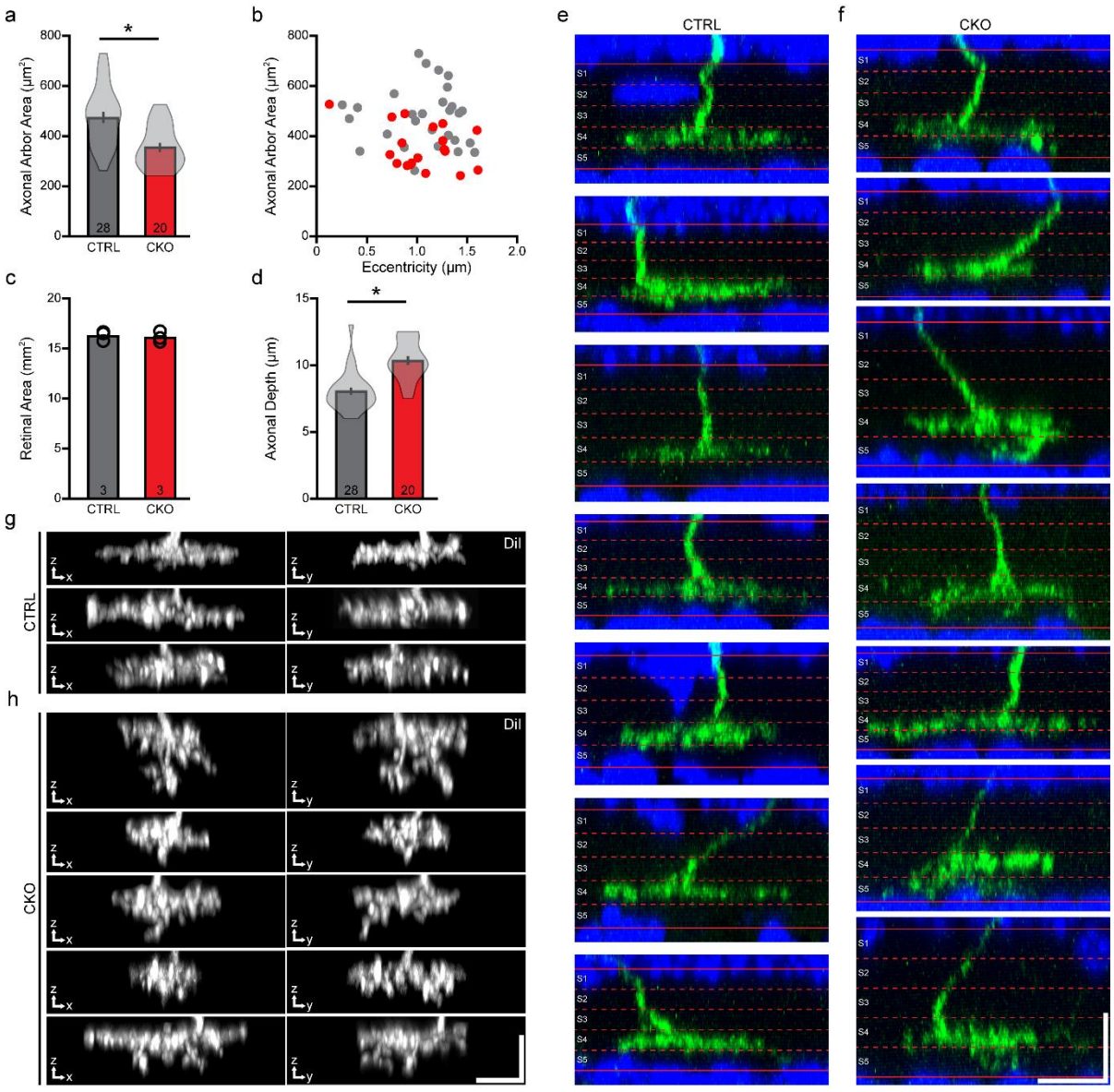

Figure 7:Axonal arbors are smaller and contain ectopic sprouts in *Sox5*-CKO cells. a-c: The areas occupied by the axonal arbors were significantly reduced in the *Sox5*-CKO retinas (a), measured from populations of labeled cells drawn from comparable retinal eccentricities (b) and in retinas showing no difference in overall areal size (c). e,f: Positioning of these axonal arbors, relative to the boundaries of the IPL defined by Hoechst staining, was found to be typical of Type 7 CBCs, in S4 of the IPL, but for the ectopic sprouting extending into S5.The stratification of these arbors was significantly broadened across the depth of the IPL (d), largely due to the presence of vertical sprouts descending from the arbor (g,h). Each pair of images shows the X-Z and Y-Z projection of the entire axonal arbor, for multiple cells in each condition. g, h: Calibration bars = 10 µm. Means and standard errors are shown within the violin plots in a and d, while means and individual retinas are indicated in b. n = the number of cells (a, d) or retinas (c) sampled.

Sox5-CKO Type 7 CBCs show ectopic sprouts in their axonal arbors

Bipolar cell axons stratify into different sublaminae of the IPL, thereby forming synapses with dendrites of precise amacrine and ganglion cell types. In order to assess whether *Sox5*-CKO cells stratified correctly, we reconstructed GFP-labeled axonal arbors relative to the boundaries of the IPL and determined their stratification. CTRL axons were restricted to the S4 sublamina of the IPL, however, the *Sox5*-CKO cells appeared to encroach into the S5 layer (Figure 7e, f). We utilized the DiI-labeled axonal arbors in order to measure the thickness of the spread of those individual axonal processes (Figure 7g, h). There was a 29% increase in the thickness of the arbors of CKO cells, which appeared to come from ectopic sprouts extending from S4 into the S5 stratum of the IPL (Figure 7d. Dendritic stratification and thickness were not measured because all CBCs contain definitive targets confined to a single stratum in the OPL, the cone pedicles, whereas axons are required to target particular strata within the IPL). This change suggests that *Sox5* is involved in restricting the stratification of axons to the S4 layer, by regulating downstream genes that enable Type 7 CBCs to target their correct synaptic partners.

Sox5-CKO cells contact fewer cones, and hyperinnervate those they do contact

Because there was a reduction in dendritic area, we next wanted to determine if there was an effect in the ability of the CBCs to synapse with their partners in the OPL, the cone pedicles. Cone pedicles, labeled with PNA, enabled us to visualize whether the DiI-labeled Type 7 CBC dendritic arbors synapsed with them, or generated aberrant terminals with rod spherules. We observed an occasional terminal that was not colocalized to a pedicle (CTRL = 21/995, CKO = 13/725), but over 97%

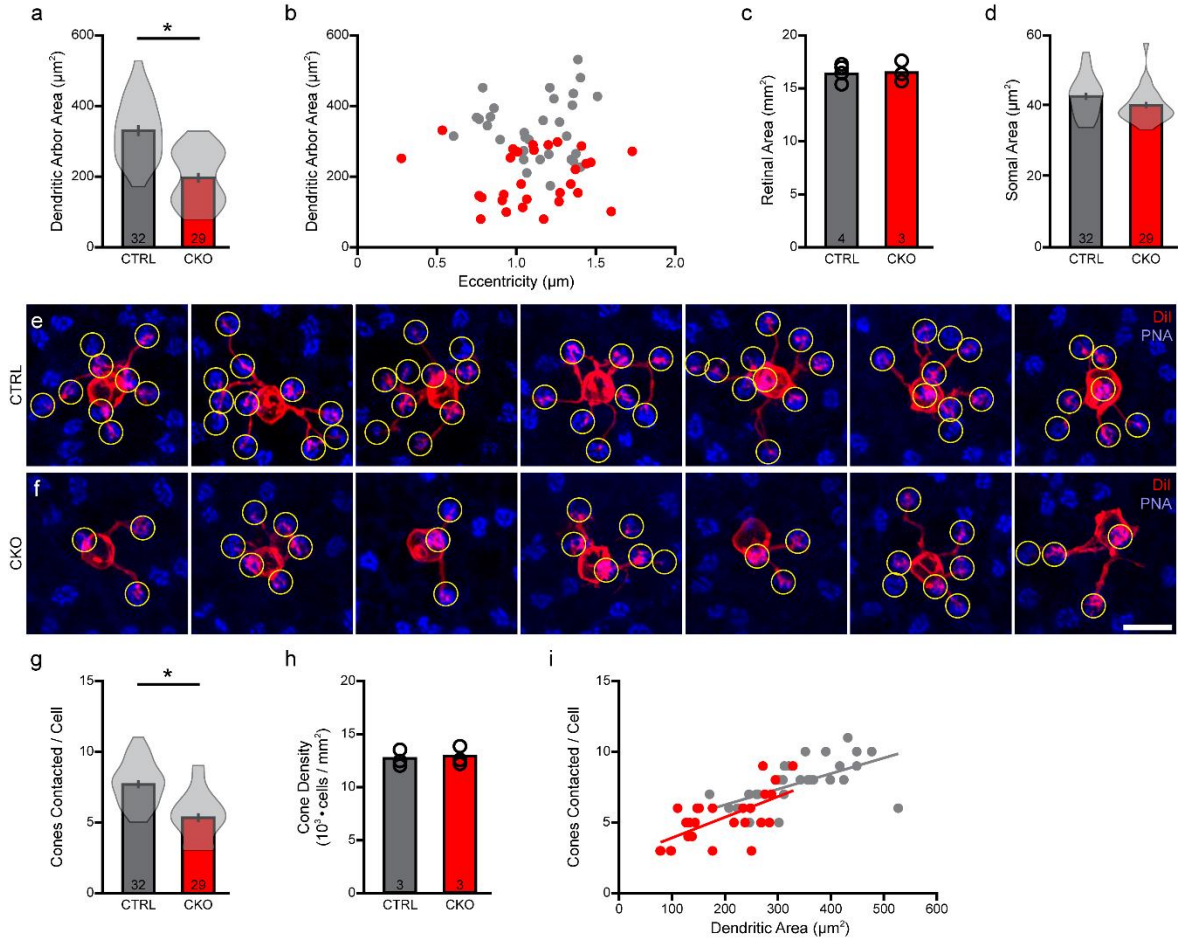

Figure 8: Dendritic arbors are smaller and hyperinnervate cone pedicles in *Sox5*-CKO cells. The areas occupied by the dendritic arbors were significantly reduced (a), drawn from samples of cells distributed across similar retinal eccentricities (b) from retinas of comparable areas (c). Soma sizes were also determined, revealing a slight but non-significant reduction in somal area (d). e, f: Fields containing DiI-labeled dendritic arbors (red) were also labeled for PNA-positive cone pedicles (blue), in order to quantify the number of pedicles contacted (yellow circles) in *Sox5*-CKO (f) and littermate control (e) retinas. Calibration bar = 10 µm. g: The number of cone pedicles contacted by those dendritic arbors was significantly reduced in the *Sox5*-CKO retina. h: Average cone densities were unchanged in the *Sox5*-CKO retina. i: The number of cone pedicles contacted increased with the areal size of the dendritic arbor, in both groups. Means and standard errors are shown within the violin plots in a, d and g, while means and individual retinas are indicated in c and h. n = the number of cells (a, d, g) or retinas (c, h) sampled.

of the terminals counted contacted a pedicle. We next wanted to determine whether the decrease in dendritic arbor area influenced the number of cones that the cell contacted (Figure 8e, f). There was a 31% reduction in the number of cones contacted in *Sox5*-CKO retinas, from an average of 7.72 cones in the CTRL retinas to 5.34 cones in the CKO ($p < 0.001$, Figure 8g). Not surprisingly, the number of cones contacted positively correlated to the size of the dendritic area in both conditions; cells with larger dendritic areas contacted more cones (Figure 8i). In order to determine whether this decrease in cone contacts might be due to a decrease in the number of cones present in the CKO retina, we determined the cone density in both CTRL and CKO retinal wholemounts. There was no change in the densities ($p = 0.52$), confirming that the decrease in cone contacts must be due to the decrease in dendritic arbor area (Figure 8h).

As each dendrite targets a nearby pedicle, it forms fine dendritic tips that invaginate the pedicle at ribbon synapses (Dunn and Wong 2012). These individual tips can be quantified in DiI-labeled cells (Figure 9a, b, c, d). As seen in previous studies, there was a wide range of terminals contacted per pedicle, from as few as one terminal, to as many as twelve (Wässle et al. 2009, Keeley and Reese 2010). Additionally, the number of terminals decreased as the distance from the soma to the pedicle increased (Keeley and Reese 2010, Figure 9e, f). Because the CKO dendrites had a smaller dendritic arbor and contact fewer cones, it was not surprising that there was a 22% decrease in the total number of terminals made by Type 7 CBCs in the *Sox5*-CKO condition compared to the CTRL cells ($p < 0.001$, Figure 9g). However, the total number of terminals *per pedicle* increased in these CKO cells ($p = 0.02$), as

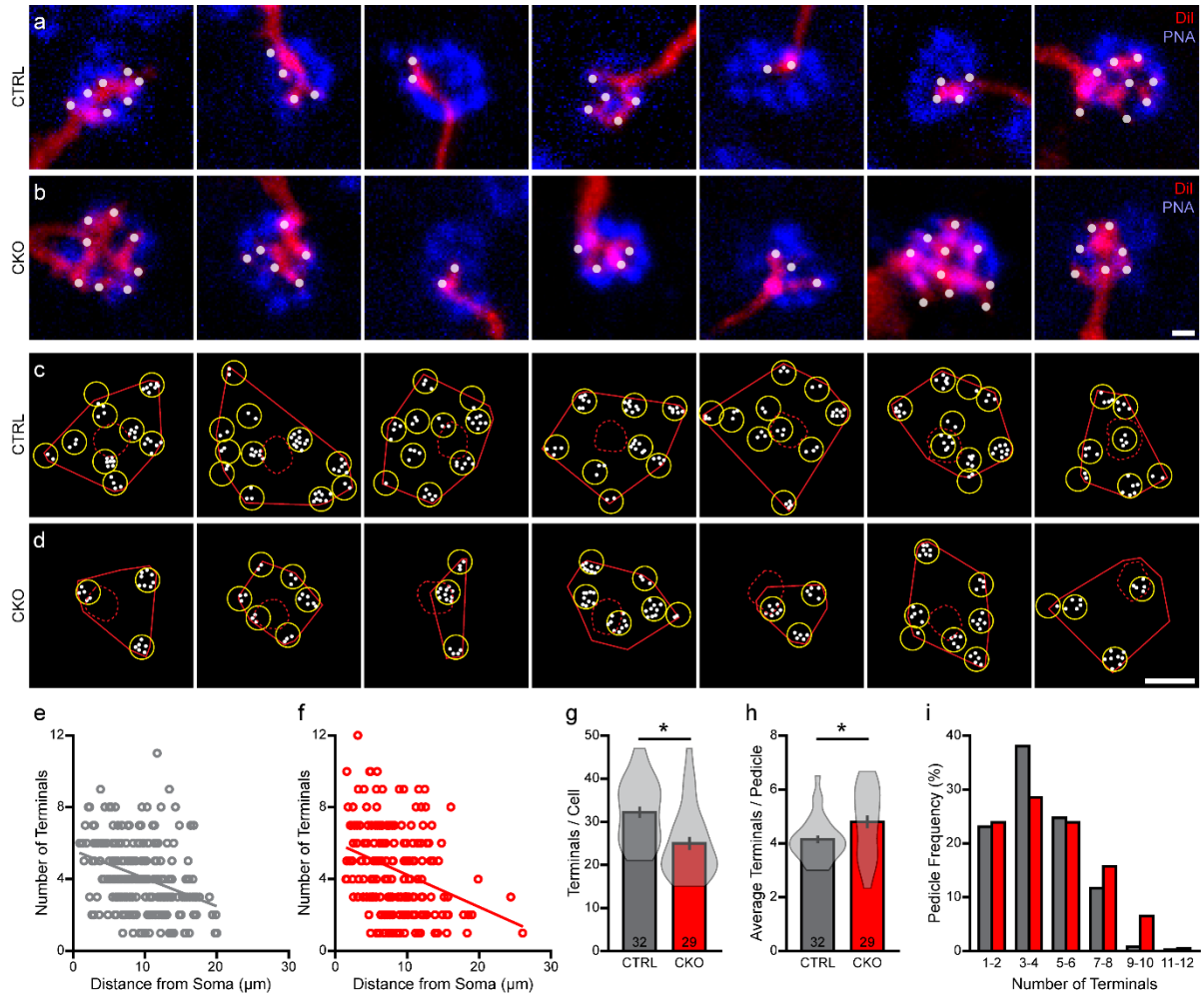

Figure 9: *Sox5*-CKO cells hyperinnervate cone pedicles. The number of DiI-labeled dendritic endings (white dots) at individual PNA-labeled cone pedicles (blue) (a, b) across dendritic fields (c, d), in both littermate control (a, c) and in Sox5-CKO retinas (b, d). Calibration bar = 1 µm in panel a and b, and = 10 µm in panel c and d. e, f: The number of terminals per pedicle declined gradually with distance from the labeled Type 7 soma, in both conditions. g, h: The total number of dendritic terminals contacting all of the pedicles by a cell was significantly reduced in the *Sox5*-CKO retina (g), but the average number at each pedicle per cell was significantly increased (h). That average number of dendritic terminals at each pedicle per cell is more variable in the *Sox5*-CKO retinas, due primarily to the presence of hyper-innervated pedicles (h). i: Pooling the entire population of sampled pedicles, the frequency distribution of the number of pedicles with a given number of terminals is shifted to the right in the *Sox5*-CKO retinas. Means and standard errors are shown within the violin plots in g and h.

did the variance of average number of terminals per pedicle (Figure 9h, i). These results indicate that the connectivity between the Type 7 CBCs and cones is altered; there is a decrease in dendritic arbor area, and the dendrites hyperinnervate many of the pedicles that they do contact.

Sox5-CKO dendritic arbors are smaller due to an outgrowth deficit, not an overpruning of dendrites

Type 7 CBC arbors develop through an over-extention of their dendritic arbor areas, invading the field areas of homotypic neighbors, followed by retrenchment, so that they do not overlap with one another, and instead tile next to their neighbors (Wässle et al. 2009, Lee et al. 2011, Dunn and Wong 2012). The decrease seen in the *Sox5*-CKO dendritic arbor areas could come from either a defect in the initial outgrowth of the arbors, or an increase in the amount of pruning that these arbors undergo as they retract their fields. We attempted to inject GFP-positive cells with DiI in developmental tissue but were unsuccessful due to the difficulty visualizing the native GFP signal. Instead, we utilized the amplified GFP expression to view the cell's morphology as best as possible. Postnatal day 18 was the earliest time that we could detect dendrites with the amplified GFP signal, and we proceeded to measure the areas of those cells. The average dendritic arbor area for the developmental CTRL condition was 281µm^2, which was greater than the adult CTRL (250µm^2). The CKO retinas at P18 still showed a reduction in average dendritic arbor area, by 36%, to 181µm^2 (Figure 10a). Interestingly, the number of cones contacted at P18 was greater than in the adult, in both the CTRL and CKO conditions (Figure 10b). These results suggest that the difference in arbor area between the CTRL and CKO cells occurred

before P18, and that there was additional pruning after P18, in both conditions. Previous studies have shown that this decline in dendritic field area occurs between P13 and P30 (Lee et al. 2011, Dunn and Wong 2012), which coincided with our results. Defective outgrowth followed by comparable pruning, rather than comparable outgrowth followed by excessive pruning, appears to be responsible for the reduction in dendritic area in the *Sox5*-CKO retina.

Candidate genes downstream of *Sox5* were identified via bioinformatics analysis, but could not be confirmed using whole-retinal samples

Because *Sox5* is a known transcription factor involved in several developmental processes, we set out to determine the downstream genes *Sox5* was regulating in the Type 7 CBCs. We utilized the same expression databases and obtained a list of the top 20% of genes that were expressed in Type 7 CBCs. We narrowed down the list of candidate genes by selecting genes that contained predicted SOX5 binding domain. Genes were further scrutinized based on their known functions, and functions that contained phrases such as neuron migration, differentiation, dendrite, axon, or neuron development were ranked higher than those that did not have any known developmental and/or neuronal functions. A final list of 6 candidate genes was compiled based on these factors, including *Ncam1, Clstn3, Sptan1, App, Cntn1,* and *Epha5*. Neural cell adhesion molecule 1 (*Ncam1*), EPH Receptor A5 (*Epha5*), and Spectrin alpha, non-erythrocytic 1 (*Sptan1*) all contained DAVID functional terms that pertained to axon guidance, projection, and cytoskeleton. Amyloid beta precursor protein (*App*) which is most well-known for its involvement in Alzheimer's Disease, is also involved in proper neuronal development, particularly in

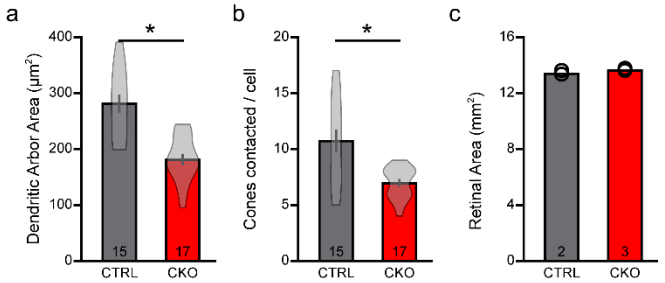

Figure 10: P18 *Sox5*-CKO cells showed decreased dendritic arbor areas and total cone pedicles contacted. The dendritic arbors of developmental Type 7 CBCs was reduced in *Sox5*-CKO retinas (a), as was the number of cones overlaid by dendrites (b). Means and standard errors are shown within the violin plots in a and b. n = number of cells (a, b) or retinas (c) sampled.

processes such as neurite outgrowth and guidance (Salbaum and Ruddle 1994, Young-Pearse et al. 2008). Calsyntenin 3 (*Clstn3*) is a synaptic adhesion protein that is necessary for proper synapse formation during development (Um et al. 2014). Contactin 1 (*Cntn1*) knockout mice show defects in dendritic projections and axon guidance in granule cells (Berglund et al. 1999). We collected RNA from P10 CTRL and CKO mice, at the time the first axon arbors were seen, and measured the expression levels of the six candidate genes via quantitative RT-PCR (Figure 11a, b). Disappointingly, there was no significant difference in quantitative gene expression of any of the candidate genes between the CTRL and CKO retinas, although there was a decrease in *Sox5* expression in the CKO retinas.

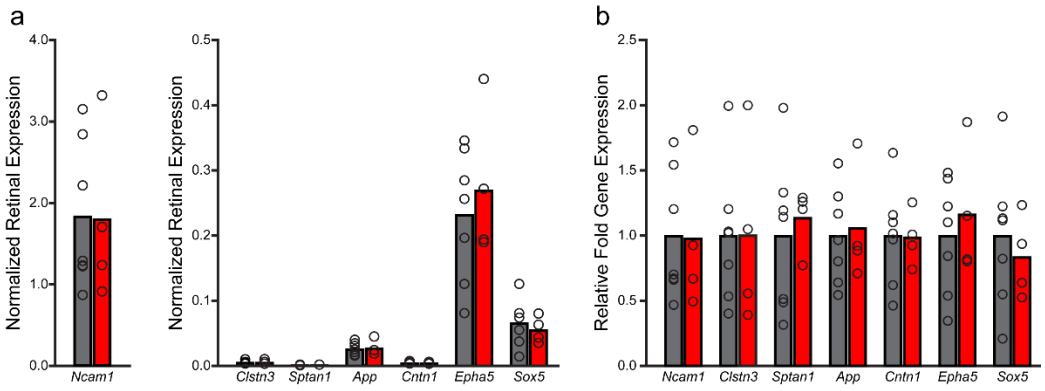

Figure 11: Quantitative RT-PCR of candidate genes. a: Normalized retinal expression of 6 candidate genes and *Sox5* in postnatal day 10 (P10) retinas from CTRL and *Sox5*-CKO retinas. Expression was normalized to two housekeeping genes, *Gapdh* and *β2m* b: Relative fold gene expression of CKO retinas, relative to CTRL retinas. n = number of samples (7 CTRL, 4 CKO), each sample was run in triplicate.

DISCUSSION

The developmental trajectories of the different types of CBCs appear to be distinct, differentiating their respective morphologies at varying rates, some acquiring their mature dendritic connectivity early while others continuing to refine their dendritic connectivity weeks later (Dunn and Wong 2012). The present study explored the role of *Sox5* in Type 7 CBCs, by studying the effects of knocking out the gene in this cell type. Research had previously shown that *Sox5* participated in the differentiation of deep cortical layer neurons in mouse (Kwan et al. 2008). Loss of its orthologue in Drosophila resulted in a reduction in terminal bouton number in motor neurons, as well as a reduction in the size and complexity of the dendritic arbors of DA neurons (Li et al. 2017). Furthermore, SOX5 had been shown to function as a transcriptional activator of the cytoskeletal regulator, *Crmp5*, modulating the differentiation of hippocampal cells *in vitro* (Naudet et al. 2018).

Our results show that the removal of *Sox5* resulted in significantly reduced axonal and dendritic arbors (Figure 12). Despite the reduced sensitivity of the GFP signal, utilizing it allowed us to measure both axonal and dendritic arbor areas of the same cell. Interestingly, there was a positive correlation between the two arbor areas in the *Sox5*-CKO cells, but no correlation in the CTRL cells. Because we do not know the downstream genes that *Sox5* uses to regulate the differentiation of the Type 7 cell, it is difficult to determine how this correlation arises. The P18 data suggests that the dendritic arbors in the CKO are always smaller than those of the CTRL ones. The increased number of cones that are contacted at P18 (both in CTRL and CKO conditions) compared to the mature retina suggests that subsequent pruning occurs

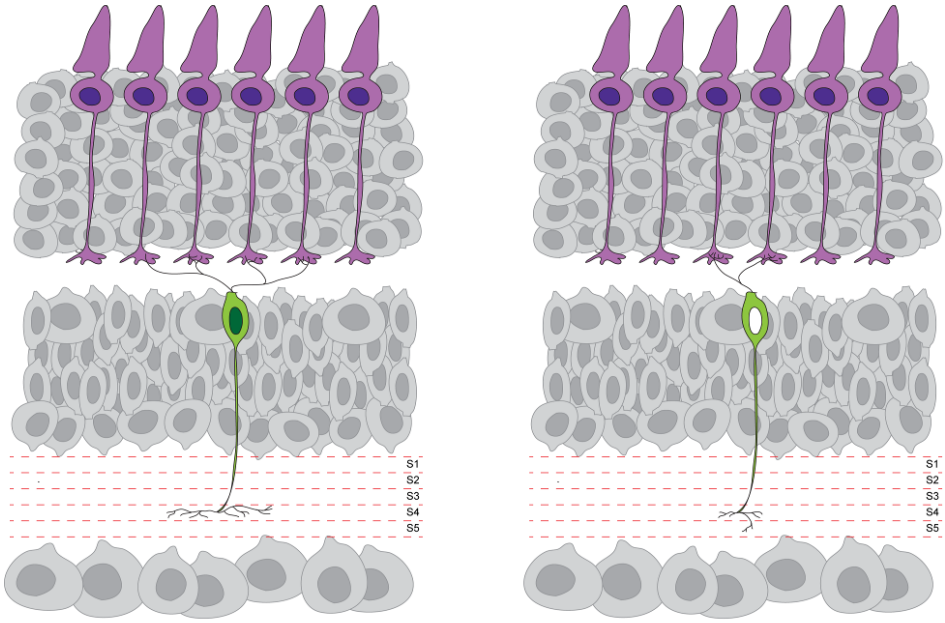

Figure 12: Summary schematic of CTRL and *Sox5*-CKO Type 7CBCs morphologies. Cells lacking *Sox5* produced smaller axonal arbors that ectopically protruded into the S5 sublaminae of the IPL. Additionally, dendritic arbor areas decreased in size and hyperinnervated the pedicles that they contacted. The hyperinnervation is thought to arise from the lack of shared pedicle contacts with neighboring Type 7 dendrites, due to the reduced dendritic arbor size.

after P18 in both cases. Cell intrinsic mechanisms coordinate both axonal and dendritic arbor size, but perhaps this is lost once the arbors grow large enough and must compete for space and prevent overlap of one another. The *Sox5*-CKO arbors never grow large enough for those extrinsic factors to influence their size, so the correlation is still visible in maturity.

Having ultimately colonized a smaller domain that contains fewer cone pedicles due to the loss of this outgrowth-promoting function of *Sox5*, many of these Type 7 CBCs make more contacts per pedicle, on average, than they would otherwise have made. Occasional pedicles have been reported to connect to the dendritic arbors of two neighboring Type 7 cells at the borders of adjacent dendritic fields (Behrens et al. 2016, Wässle et al. 2009). As the number of dendritic contacts with a pedicle made by a Type 7 CBC tends to decline with distance from the soma, shared pedicles presumably receive a reduced number of dendritic terminals from each of two neighboring cells. The fact that the most hyper-innervated pedicles reside closer to the soma in the *Sox5*-CKO retinas is not at odds with this, because bipolar cells in the mouse retina appear to be arranged upon the retina no better than a random distribution of cells (Keeley et al. 2017, Keeley et al. 2020), and dually innervated pedicles are occasionally present nearby individual Type 7 somata (Wässle et al. 2009). The increase in the average number of dendritic terminals per pedicle in the *Sox5*-CKO retina may therefore reflect a loss of such dually-contacted pedicles now being colonized by only one Type 7 cell, still leaving no pedicles free of contact and thus maintaining complete functional coverage of the retina (Figure 13).

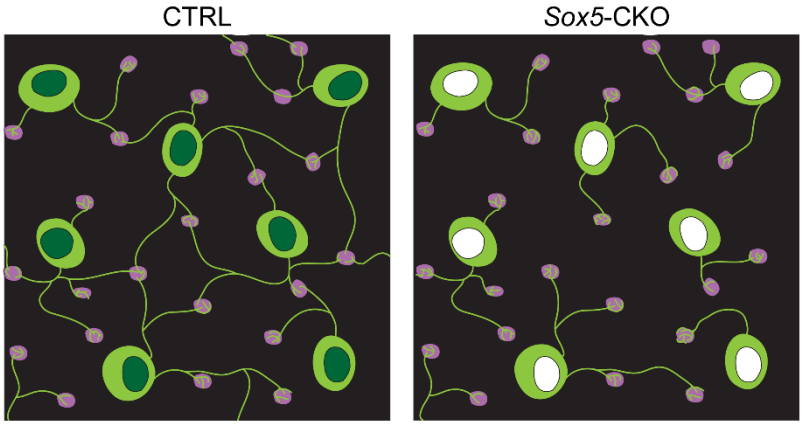

Figure 13: Smaller dendritic area of *Sox5*-CKO Type 7 CBCs resulted in less shared pedicles, but still complete coverage of the retina. CTRL cells acquire larger dendritic areas, and share more pedicles with neighboring cells, and innervate these pedicles with fewer terminals (a). Sox5-CKO cells hyperinnervate pedicles, and have a smaller dendritic area, although there is still complete coverage of the retina (b).

The genes regulated by *Sox5* controlling these features of the Type 7 CBC morphology remain to be determined. Quantitative PCR, which measures mRNA levels of gene expression, showed no difference in expression of any of the candidate genes in the CTRL and *Sox5*-CKO developmental retinas. Differences in expression could be difficult to detect, however, since we collected RNA from the entire retina and Type 7 CBCs make up a small portion of the entire retinal cell population; therefore, more refined techniques could be used to assess gene expression levels in the future, for instance single-cell transcriptomic profiling of GFP-positive cells from the two conditions. Additionally, single-cell transcriptomic profiling would enable us to take a non-biased approach, measuring expression levels of a greater number of genes, rather than only the highest ranked candidate genes.

The limited gene expression to one single bipolar cell type makes it attractive as an identifier for this CBC type, especially since *Gustducin-GFP* expression is not expressed in every Type 7 CBC. However, further research is necessary to identify the downstream genes that *Sox5* regulates and to determine the underlying mechanisms influencing the morphology of Type 7 CBCs.

Table 1: List of primer sequences for genotyping.

Gene	Primers	Size
Vsx2-cre	5'-CTCCCAACCCCAGAGGTAGT-3' 5'-CTATAGGGCCTGGGTCAGTG-3' 5'-CAAACCTGGCTGTTTCACCT-3' 5'-CAGGTTCTTGCGAACCTCAT-3'	Tg: 420bp Ctrl: expected 324bp, band seen at 175bp
Gustducin-GFP	5'-GGTGAGCTTTCCGTATGTGGC-3' 5'-GGGCCCCTCTGCTAACC-3' 5'-ACAACATTCTGCCTCCAAAG-3' 5'-TATGCTCATTCACCCACTTAC-3'	Tg: 420bp Ctrl: 250bp
ROSA-tdTomato	5'-AAGGGAGCTGCAGTGGAGTA-3' 5'-CCGAAAATCTGTGGGAAGTC-3' 5'-GGCATTAAAGCAGCGTATCC-3' 5'-CTGTTCCTGTACGGCATGG-3'	Tg: 196bp Ctrl: 297bp
Sox5-flox	5'-GGCATGGGCCCAAGATGTTTAAGA-3' 5'-CGATGCACATGATCACAGTTGGGT-3'	Fx: 423bp Wt: 319bp

Table 2: List of primer sequences for quantitative RT-PCR.

Gene	Primers (5' to 3')	Product Length	Melting Temperature
Ncam1	5'-GCGGTAAATTCAGTGCCTTCC-3' 5'-TGTCACTCATTCTCCGCTCAG-3'	164bp	60°C
Clstn3	5'-CCTCGCCACAGTCATAAGCC-3' 5'-TGTGATCCTGGACAAGGCAA-3'	113bp	66°C
Sptan1	5'-CCGTCACTATCCGCTGC-3' 5'-GCTGCTGAGGAAAAAGATGCG-3'	71bp	66°C
App	5'-AGGAGCAGTGCCAAGCTG-3' 5'-ATCTTCCACTCGCACACGG-3'	73bp	66°C
Cntn1	5'-ATGAATAACGGGGACGTGGA-3' 5'-CAGGCAGTAGTACACCCCAG-3'	111bp	66°C
Epha5	5'-GCACACAAGAGAAGGCACG-3' 5'-AGGGTAGTAGAAAATGCGGGG-3'	162bp	60°C
Sox5	5'-TGACCCCTACTCTCTCCAGC-3' 5'-CCCAAACTCCAAGTGCCTCT-3'	88bp	60°C
Gapdh	5'-AACTTTGGCATTGTGGAAGG-3' 5'-GGATGCAGGGATGATGTTCT-3'	132bp	63°C
β2m	5'-GAGCCCAAGACCGTCTACTG-3' 5'-GCTATTTCTTTCTGCGTGCAT-3'	134bp	63°C

CONCLUSIONS

In this dissertation, we studied three different genes involved in various developmental processes in the retina. We reaffirmed that population sizes are genetically controlled, and variation between murine strains arise from specific gene variants. Using QTL mapping, we generated a list of genes that could then be researched and experimentally tested, resulting in *Dixdc1* as a final candidate. The functionality of the translated protein containing one of two variants (a splice or a missense variant) was tested using an *in vitro* approach. This sets the stage for future work to determine the mechanism underlying cell number, and the result of the gene variant on this mechanism. Future work will test each variant's effect on cell number, by overexpressing them postnatally in a murine model. One shortcoming of this method, however, is that the cell type that was studied, the AII amacrine cell, is primarily born embryonically, and therefore an embryonic electroporation technique will need to be used.

We have begun to elucidate the genes that are involved in the regulation of neuronal migration. The proteins that make up the machinery that promotes migration have been recently discovered, but the genes that regulate the expression of them has yet to be determined. Whether the mechanism is cell-type specific, or is used by numerous cell types, is yet to be seen. Knocking out the gene in select cell types, either through the use of a conditional knockout mouse or CRISPR-Cas9 knockdown approach, could be used to determine whether removal of the gene influences migration of that cell type.

The formation of axonal and dendritic arbors is necessary for the formation of neuronal circuitry throughout the retina. We discovered a transcription factor that was cell-type specific, *Sox5*, and determined that the removal of it affected both the axonal and dendritic arbors. The arbors of the Type 7 CBC tile, ensuring complete coverage of the retina. Investigating whether they continue to be capable of completely covering the retina with their smaller arbors has yet to be determined, since we currently do not have a way of labeling the entire population. Determining the genes that are regulated by SOX5 may help in deciphering the mechanism underlying the formation of arbors.

Understanding the genes that regulate proper development of the retina is critical in developing therapies to combat diseases that result in retinal degeneration. Researchers are working on “growing” functional retinas *in vitro*, so that they can replace damaged and degenerated retinas. In order to design these retinas, the genes involved in the production of each cell type and formation of proper circuitry is critical. The results presented in the dissertation provide additional information pertaining to the development of the retina.

REFERENCES

Aghaizu, N. D., K. M. Warre-Cornish, M. R. Robinson, P. V. Waldron, R. N. Maswood, A. J. Smith, R. R. Ali & R. A. Pearson (2021) Repeated nuclear translocations underlie photoreceptor positioning and lamination of the outer nuclear layer in the mammalian retina. *Cell Rep*, 36, 109461.

Akimoto, M., H. Cheng, D. Zhu, J. A. Brzezinski, R. Khanna, E. Filippova, E. C. Oh, Y. Jing, J. L. Linares, M. Brooks, S. Zareparsi, A. J. Mears, A. Hero, T. Glaser & A. Swaroop (2006) Targeting of GFP to newborn rods by Nrl promoter and temporal expression profiling of flow-sorted photoreceptors. *Proc Natl Acad Sci USA*, 103, 3890-5.

Amini, R., A. Bhatnagar, R. Schlüßler, S. Möllmert, J. Guck & C. Norden (2022) Amoeboid-like migration ensures correct horizontal cell layer formation in the developing vertebrate retina. *Elife*, 11.

Babinet, C. (2000) Transgenic mice: an irreplaceable tool for the study of mammalian development and biology. *J Am Soc Nephrol*, 11 Suppl 16, S88-94.

Baye, L. M. & B. A. Link (2008) Nuclear migration during retinal development. *Brain Res*, 1192, 29-36.

Behrens, C., T. Schubert, S. Haverkamp, T. Euler & P. Berens (2016) Connectivity map of bipolar cells and photoreceptors in the mouse retina. *ELife*, 5, e20041.

Beliakoff, J. & Z. Sun (2006) Zimp7 and Zimp10, two novel PIAS-like proteins, function as androgen receptor coregulators. *Nucl Recept Signal*, 4, e017.

Berglund, E. O., K. K. Murai, B. Fredette, G. Sekerková, B. Marturano, L. Weber, E. Mugnaini & B. Ranscht (1999) Ataxia and abnormal cerebellar

microorganization in mice with ablated contactin gene expression. *Neuron*, 24, 739-50.

Blackshaw, S., S. Harpavat, J. Trimarchi, L. Cai, H. Huang, W. P. Kuo, G. Weber, K. Lee, R. E. Fraioli, S. H. Cho, R. Yung, E. Asch, L. Ohno-Machado, W. H. Wong & C. L. Cepko (2004) Genomic analysis of mouse retinal development. *PLoS Biol*, 2, E247.

Bloomfield, S. A. & R. F. Dacheux (2001) Rod vision: pathways and processing in the mammalian retina. *Prog Retin Eye Res*, 20, 351-84.

Bonfanti, L., E. Strettoi, S. Chierzi, M. C. Cenni, X. H. Liu, Martinou J-C, L. Maffei & S. A. Rabacchi (1996) Protection of retinal ganglion cells from natural and axotomy-induced cell death in neonatal transgenic mice overexpressing bcl-2. *J Neurosci*, 16, 4186-94.

Burger, C. A., J. Alevy, A. K. Casasent, D. Jiang, N. E. Albrecht, J. H. Liang, A. A. Hirano, N. C. Brecha & M. A. Samuel (2020) LKB1 coordinates neurite remodeling to drive synapse layer emergence in the outer retina. Elife, 9.

Cagan, R. (2009) Principles of Drosophila eye differentiation. *Curr Top Dev Biol*, 89, 115-35.

Carter-Dawson, L. D. & M. M. LaVail (1979a) Rods and cones in the mouse retina. I. Structural analysis using light and electron microscopy. *J Comp Neurol*, 188, 245-62.

Carter-Dawson, L. D. & M. M. LaVail (1979b) Rods and cones in the mouse retina. II. Autoradiographic analysis of cell generation using tritiated thymidine. *J Comp Neurol*, 188, 263-72.

Cepko, C. L., C. P. Austin, X. Yang, M. Alexiades & D. Ezzeddine (1996) Cell fate determination in the vertebrate retina. *Proc Natl Acad Sci USA*, 93, 589-95.

Choi, J. H., X. Zhong, W. McAlpine, T. C. Liao, D. Zhang, B. Fang, J. Russell, S. Ludwig, E. Nair-Gill, Z. Zhang, K. W. Wang, T. Misawa, X. Zhan, M. Choi, T. Wang, X. Li, M. Tang, Q. Sun, L. Yu, A. R. Murray, E. M. Y. Moresco & B. Beutler (2019) LMBR1L regulates lymphopoiesis through Wnt/β-catenin signaling. *Science*, 364.

Chow, R. L., B. Snow, J. Novak, J. Looser, C. Freund, D. Vidgen, L. Ploder & R. R. McInnes (2001) Vsx1, a rapidly evolving paired-like homeobox gene expressed in cone bipolar cells. *Mech Dev*, 109, 315-22.

Chow, R. W., A. D. Almeida, O. Randlett, C. Norden & W. A. Harris (2015) Inhibitory neuron migration and IPL formation in the developing zebrafish retina. *Development*, 142, 2665-77.

Cline, H. & K. Haas (2008) The regulation of dendritic arbor development and plasticity by glutamatergic synaptic input: a review of the synaptotrophic hypothesis. *J Physiol*, 586, 1509-17.

Dacey, D. M. (1999) Primate retina: cell types, circuits and color opponency. *Prog Retin Eye Res*, 18, 737-63.

Demb, J. B. & J. H. Singer (2012) Intrinsic properties and functional circuitry of the AII amacrine cell. *Vis Neurosci*, 29, 51-60.

Dräger, U. C. (1985) Birth dates of retinal ganglion cells giving rise to the crossed and uncrossed optic projections in the mouse. *Proc R Soc Lond B Biol Sci*, 224, 57-77.

Dunn, F. A. & R. O. Wong (2012) Diverse strategies engaged in establishing stereotypic wiring patterns among neurons sharing a common input at the visual system's first synapse. *J Neurosci*, 32, 10306-17.

Dy, P., Y. Han & V. Lefebvre (2008) Generation of mice harboring a Sox5 conditional null allele. *Genesis*, 46, 294-9.

Edqvist, P. H. & F. Hallböök (2004) Newborn horizontal cells migrate bi-directionally across the neuroepithelium during retinal development. *Development*, 131, 1343-51.

Euler, T. & H. Wässle (1998) Different contributions of GABAA and GABAC receptors to rod and cone bipolar cells in a rat retinal slice preparation. *J Neurophysiol*, 79, 1384-95.

Famiglietti, E. V. & H. Kolb (1975) A bistratified amacrine cell and synaptic cirucitry in the inner plexiform layer of the retina. *Brain Res*, 84, 293-300.

Farajian, R., M. A. Raven, K. Cusato & B. E. Reese (2004) Cellular positioning and dendritic field size of cholinergic amacrine cells are impervious to early ablation of neighboring cells in the mouse retina. *Vis Neurosci*, 21, 13-22.

Fujimura, N. (2016) WNT/β-Catenin Signaling in Vertebrate Eye Development. *Front Cell Dev Biol*, 4, 138.

Gamlin, C. R., C. Zhang, M. A. Dyer & R. O. L. Wong (2020) Distinct Developmental Mechanisms Act Independently to Shape Biased Synaptic Divergence from an Inhibitory Neuron. *Curr Biol*, 30, 1258-1268.e2.

Gibson, D. A. & L. Ma (2011) Developmental regulation of axon branching in the vertebrate nervous system. *Development*, 138, 183-95.

Guo, Y., X. Chen, R. Xing, M. Wang, X. Zhu & W. Guo (2018) Interplay between FMRP and lncRNA TUG1 regulates axonal development through mediating SnoN-Ccd1 pathway. *Hum Mol Gene*t, 27, 475-485.

Hamburger, V. & H. L. Hamilton (1951) A series of normal stages in the development of the chick embryo. *J Morphol*, 88, 49-92.

Harman, A. M. & J. Ferguson (1994) Morphology and birth dates of horizontal cells in the retina of a marsupial. *J Comp Neurol*, 340, 392-404.

Harris, W. A. (1997) Cellular diversification in the vertebrate retina. *Curr Opin Genet Dev*, 7, 651-8.

Hartveit, E. & M. L. Veruki (2012) Electrical synapses between AII amacrine cells in the retina: Function and modulation. *Brain Res*, 1487, 160-72.

Holt, C. E., T. W. Bertsch, H. M. Ellis & W. A. Harris (1988) Cellular determination in the Xenopus retina is independent of lineage and birth date. *Neuron*, 1, 15-26.

Huang, L., M. Max, R. F. Margolskee, H. Su, R. H. Masland & T. Euler (2003) G protein subunit G gamma 13 is coexpressed with G alpha o, G beta 3, and G beta 4 in retinal ON bipolar cells. *J Comp Neurol*, 455, 1-10.

Huang, C. Y., J. Beliakoff, X. Li, J. Lee, M. Sharma, B. Lim & Z. Sun (2005) hZimp7, a novel PIAS-like protein, enhances androgen receptor-mediated transcription and interacts with SWI/SNF-like BAF complexes. *Mol Endocrinol*, 19, 2915-29.

Inberg, S., A. Meledin, V. Kravtsov, Y. Iosilevskii, M. Oren-Suissa & B. Podbilewicz (2019) Lessons from Worm Dendritic Patterning. *Annu Rev Neurosci*, 42, 365-383.

Jeon, C. J., E. Strettoi & R. H. Masland (1998) The major cell populations of the mouse retina. *J Neurosci*, 18, 8936-46.

Jimeno, D., C. Gómez, N. Calzada, P. de la Villa, C. Lillo & E. Santos (2016) RASGRF2 controls nuclear migration in postnatal retinal cone photoreceptors. *J Cell Sci*, 129, 729-42.

Johnson, P. T., R. R. Williams, K. Cusato & B. E. Reese (1999) Rods and cones project to the inner plexiform layer during development. *J Comp Neurol*, 414, 1-12.

Jusuf, P., W. A. Harris & L. Poggi (2013) Imaging retinal progenitor lineages in developing zebrafish embryos. *Cold Spring Harb Protoc*, 2013.

Kautzman, A. G., P. W. Keeley, C. R. Ackley, S. Leong, I. E. Whitney & B. E. Reese (2018) Modulates Bipolar Cell Number in the Mouse Retina. *Front Neurosci*, 12, 876.

Kay, J. N., M. W. Chu & J. R. Sanes (2012) MEGF10 and MEGF11 mediate homotypic interactions required for mosaic spacing of retinal neurons. *Nature*, 483, 465-9.

Keeley, P. W. & B. E. Reese (2010) Role of afferents in the differentiation of bipolar cells in the mouse retina. *J Neurosci*, 30, 1677-85.

Keeley, P. W., B. J. Sliff, S. C. Lee, P. G. Fuerst, R. W. Burgess, S. J. Eglen & B. E. Reese (2012) Neuronal clustering and fasciculation phenotype in Dscam- and Bax-deficient mouse retinas. *J Comp Neurol*, 520, 1349-64.

Keeley, P. W., N. R. Madsen, A. J. St John & B. E. Reese (2014a) Programmed cell death of retinal cone bipolar cells is independent of afferent or target control. *Dev Biol*, 394, 191-6.

Keeley, P. W., I. E. Whitney, N. R. Madsen, A. J. St John, S. Borhanian, S. A. Leong, R. W. Williams & B. E. Reese (2014b) Independent genomic control of neuronal number across retinal cell types. *Dev Cell*, 30, 103-9.

Keeley, P. W., J. J. Kim, S. C. S. Lee, S. Haverkamp & B. E. Reese (2017) Random spatial patterning of cone bipolar cell mosaics in the mouse retina. *Vis. Neurosci.*, 34, e002.

Keeley, P. W., S. J. Eglen & B. E. Reese (2020) From random to regular: Variation in the patterning of retinal mosaics. J Comp Neurol, 528, 2135-2160.

Keeley, P. W., M. C. Lebo, J. D. Vieler, J. J. Kim, A. J. St John & B. E. Reese (2021) Interrelationships between Cellular Density, Mosaic Patterning, and Dendritic Coverage of VGluT3 Amacrine Cells. *J Neurosci*, 41, 103-117.

Kim, Y., D. Y. Kim, H. Zhang, C. R. Bae, D. Seong, J. Song, Y. M. Kim & Y. G. Kwon (2022) DIX domain containing 1 (DIXDC1) modulates VEGFR2 level in vasculatures to regulate embryonic and postnatal retina angiogenesis. *BMC Biol*, 20, 41.

Kivimäe, S., P. M. Martin, D. Kapfhamer, Y. Ruan, U. Heberlein, J. L. Rubenstein & B. N. Cheyette (2011) Abnormal behavior in mice mutant for the Disc1 binding partner, Dixdc1. *Transl Psychiatry*, 1, e43.

Kolb, H. & E. V. Famiglietti (1974) Rod and cone pathways in the inner plexiform layer of cat retina. *Science*, 186, 47-9.

Kryger, Z., L. Galli-Resta, G. H. Jacobs & B. E. Reese (1998) The topography of rod and cone photoreceptors in the retina of the ground squirrel. *Vis Neurosci*, 15, 685-91.

Kwan, K. Y., M. M. Lam, Z. Krsnik, Y. I. Kawasawa, V. Lefebvre & N. Sestan (2008) SOX5 postmitotically regulates migration, postmigratory differentiation, and projections of subplate and deep-layer neocortical neurons. *Proc Natl Acad Sci USA*, 105, 16021-6.

Lai, T., D. Jabaudon, B. J. Molyneaux, E. Azim, P. Arlotta, J. R. Menezes & J. D. Macklis (2008) SOX5 controls the sequential generation of distinct corticofugal neuron subtypes. *Neuron*, 57, 232-47.

Lee, S. C., E. J. Cowgill, A. Al-Nabulsi, E. J. Quinn, S. M. Evans & B. E. Reese (2011) Homotypic regulation of neuronal morphology and connectivity in the mouse retina. *J Neurosci*, 31, 14126-33.

Lee, S. H., C. Zhu, Y. Peng, D. T. Johnson, L. Lehmann & Z. Sun (2013) Identification of a novel role of ZMIZ2 protein in regulating the activity of the Wnt/β-catenin signaling pathway. *J Biol Chem*, 288, 35913-24.

Li, A., B. Hooli, K. Mullin, R. E. Tate, A. Bubnys, R. Kirchner, B. Chapman, O. Hofmann, W. Hide & R. E. Tanzi (2017) Silencing of the Drosophila ortholog of SOX5 leads to abnormal neuronal development and behavioral impairment. *Hum Mol Genet*, 26, 1472-1482.

Linden, R., & Reese, B. (2006). Programmed cell death. In E. Sernagor, S. Eglen, B. Harris, & R. Wong (Eds.), *Retinal Development* (pp. 208-241). Cambridge: Cambridge University Press. doi:10.1017/CBO9780511541629.013.

Liu, H., S. Thurig, O. Mohamed, D. Dufort & V. A. Wallace (2006) Mapping canonical Wnt signaling in the developing and adult retina. *Invest Ophthalmol Vis Sci*, 47, 5088-97.

Liu, Y., Y. Wang, W. Yuan, F. Dong, F. Zhen, J. Liu, L. Yang, X. Qu & R. Yao (2021) Reelin promotes oligodendrocyte precursors migration via the Wnt/β-catenin signaling pathway. Neurol Res, 43, 543-552.

Liu, Y. T., Q. J. Dan, J. Wang, Y. Feng, L. Chen, J. Liang, Q. Li, S. C. Lin, Z. X. Wang & J. W. Wu (2011) Molecular basis of Wnt activation via the DIX domain protein Ccd1. *J Biol Chem*, 286, 8597-608.

Livesey, F. J. & C. L. Cepko (2001) Vertebrate neural cell-fate determination: lessons from the retina. *Nat Rev Neurosci*, 2, 109-18.

Macosko, E. Z., A. Basu, R. Satija, J. Nemesh, K. Shekhar, M. Goldman, I. Tirosh, A. R. Bialas, N. Kamitaki, E. M. Martersteck, J. J. Trombetta, D. A. Weitz, J. R. Sanes, A. K. Shalek, A. Regev & S. A. McCarroll (2015) Highly Parallel Genome-wide Expression Profiling of Individual Cells Using Nanoliter Droplets. *Cell*, 161, 1202-1214.

Madisen, L., T. A. Zwingman, S. M. Sunkin, S. W. Oh, H. A. Zariwala, H. Gu, L. L. Ng, R. D. Palmiter, M. J. Hawrylycz, A. R. Jones, E. S. Lein & H. Zeng (2010) A robust and high-throughput Cre reporting and characterization system for the whole mouse brain. *Nat Neurosci*, 13, 133-40.

Marc, R. E., J. R. Anderson, B. W. Jones, C. L. Sigulinsky & J. S. Lauritzen (2014) The AII amacrine cell connectome: a dense network hub. *Front Neural Circuits*, 8, 104.

Martersteck, E. M., K. E. Hirokawa, M. Evarts, A. Bernard, X. Duan, Y. Li, L. Ng, S. W. Oh, B. Ouellette, J. J. Royall, M. Stoecklin, Q. Wang, H. Zeng, J. R. Sanes & J. A. Harris (2017) Diverse Central Projection Patterns of Retinal Ganglion Cells. *Cell Rep*, 18, 2058-2072.

Martin, P. M., R. E. Stanley, A. P. Ross, A. E. Freitas, C. E. Moyer, A. C. Brumback, J. Iafrati, K. S. Stapornwongkul, S. Dominguez, S. Kivimäe, K. A. Mulligan, M. Pirooznia, W. R. McCombie, J. B. Potash, P. P. Zandi, S. M. Purcell, S. J. Sanders, Y. Zuo, V. S. Sohal & B. N. R. Cheyette (2018) DIXDC1 contributes to psychiatric susceptibility by regulating dendritic spine and glutamatergic synapse density via GSK3 and Wnt/β-catenin signaling. *Mol Psychiatry*, 23, 467-475.

Matsuda, T. & C. L. Cepko (2004) Electroporation and RNA interference in the rodent retina in vivo and in vitro. *Proc Natl Acad Sci USA*, 101, 16-22.

Matsuda, T. & C. L. Cepko (2007) Controlled expression of transgenes introduced by in vivo electroporation. *Proc Natl Acad Sci USA*, 104, 1027-32.

McAllister, A. K. (2001) Neurotrophins and neuronal differentiation in the central nervous system. *Cell Mol Life Sci*, 58, 1054-60.

Moreno-Ayala, R., D. Schnabel, E. Salas-Vidal & H. Lomelí (2015) PIAS-like protein Zimp7 is required for the restriction of the zebrafish organizer and mesoderm development. *Dev Biol*, 403, 89-100.

Mosinger Ogilvie, J., T. L. Deckwerth, C. M. Knudson & S. J. Korsmeyer (1998) Suppression of developmental retinal cell death but not of photoreceptor degeneration in Bax-deficient mice. *Invest Ophthalmol Vis Sci*, 39, 1713-20.

Mulligan, K. A. & B. N. Cheyette (2012) Wnt signaling in vertebrate neural development and function. *J Neuroimmune Pharmacol*, 7, 774-87.

Naudet, N., A. Moutal, H. N. Vu, N. Chounlamountri, C. Watrin, S. Cavagna, C. Malleval, C. Benetollo, C. Bardel, M. A. Dronne, J. Honnorat, C. Meissirel & R. Besançon (2018) Transcriptional regulation of CRMP5 controls neurite outgrowth through Sox5. *Cell Mol Life Sci*, 75, 67-79.

Nickerson, P. E., K. Ronellenfitch, J. McEwan, H. Kim, R. R. McInnes & R. L. Chow (2011) A transgenic mouse line expressing cre recombinase in undifferentiated postmitotic mouse retinal bipolar cell precursors. *PLoS One*, 6, e27145.

Oltvai, Z. N., C. L. Milliman & S. J. Korsmeyer (1993) Bcl-2 heterodimerizes in vivo with a conserved homolog, Bax, that accelerates programmed cell death. *Cell*, 74, 609-19.

Peng, Y., J. Lee, C. Zhu & Z. Sun (2010) A novel role for protein inhibitor of activated STAT (PIAS) proteins in modulating the activity of Zimp7, a novel PIAS-like protein, in androgen receptor-mediated transcription. *J Biol Chem*, 285, 11465-75.

Peters, L. L., R. F. Robledo, C. J. Bult, G. A. Churchill, B. J. Paigen & K. L. Svenson (2007) The mouse as a model for human biology: a resource guide for complex trait analysis. *Nat Rev Genet*, 8, 58-69.

Petridou, E. & L. Godinho (2022) Cellular and Molecular Determinants of Retinal Cell Fate. *Annu Rev Vis Sci*, 8, 79-99.

Poché, R. A., K. M. Kwan, M. A. Raven, Y. Furuta, B. E. Reese & R. R. Behringer (2007) Lim1 is essential for the correct laminar positioning of retinal horizontal cells. *J Neurosci*, 27, 14099-107.

Poché, R. A., M. A. Raven, K. M. Kwan, Y. Furuta, R. R. Behringer & B. E. Reese (2008) Somal positioning and dendritic growth of horizontal cells are regulated by interactions with homotypic neighbors. *Eur J Neurosci*, 27, 1607-14

Prada, C., L. Puelles, J. M. Genis-Gálvez & G. Ramírez (1987) Two modes of free migration of amacrine cell neuroblasts in the chick retina. *Anat Embryol* (Berl), 175, 281-7.

Prigge, C. L. & J. N. Kay (2018) Dendrite morphogenesis from birth to adulthood. *Curr Opin Neurobiol*, 53, 139-145.

Péquignot, M. O., A. C. Provost, S. Sallé, P. Taupin, K. M. Sainton, D. Marchant, J. C. Martinou, J. C. Ameisen, J. P. Jais & M. Abitbol (2003) Major role of BAX in apoptosis during retinal development and in establishment of a functional postnatal retina. *Dev Dyn*, 228, 231-8.

Quiroga, A. C., C. C. Stolt, R. Diez del Corral, S. Dimitrov, S. Pérez-Alcalá, E. Sock, J. A. Barbas, M. Wegner & A. V. Morales (2015) Sox5 controls dorsal progenitor and interneuron specification in the spinal cord. *Dev Neurobiol*, 75, 522-38.

Rapaport, D. H. & R. I. Dorsky (1998) Inductive competence, its significance in retinal cell fate determination and a role for Delta-Notch signaling. *Semin Cell Dev Biol*, 9, 241-7.

Raven, M. A., S. B. Stagg, H. Nassar & B. E. Reese (2005) Developmental improvement in the regularity and packing of mouse horizontal cells: implications for mechanisms underlying mosaic pattern formation. *Vis Neurosci*, 22, 569-73.

Raven, M. A., E. C. Oh, A. Swaroop & B. E. Reese (2007) Afferent control of horizontal cell morphology revealed by genetic respecification of rods and cones. *J Neurosci*, 27, 3540-7.

Razafsky, D., N. Blecher, A. Markov, P. J. Stewart-Hutchinson & D. Hodzic (2012) LINC complexes mediate the positioning of cone photoreceptor nuclei in mouse retina. *PLoS One*, 7, e47180.

Razafsky, D., C. Potter & D. Hodzic (2015) Validation of a Mouse Model to Disrupt LINC Complexes in a Cell-specific Manner. *J Vis Exp*, e53318.

Reese, B. E., W. F. Thompson & J. D. Peduzzi (1994) Birthdates of neurons in the retinal ganglion cell layer of the ferret. *J Comp Neurol*, 341, 464-75.

Reese, B. E., A. R. Harvey & S. S. Tan (1995) Radial and tangential dispersion patterns in the mouse retina are cell-class specific. *Proc Natl Acad Sci USA*, 92, 2494-8.

Reese, B. E. (2012) Retinal Mosaics: Pattern Formation Driven by Local Interactions between Homotypic Neighbors. *Front Neural Circuits*, 6, 24.

Reese, B. E. & P. W. Keeley (2015) Design principles and developmental mechanisms underlying retinal mosaics. *Biol Rev Camb Philos Soc*, 90, 854-76.

Rheaume, B. A., A. Jereen, M. Bolisetty, M. S. Sajid, Y. Yang, K. Renna, L. Sun, P. Robson & E. F. Trakhtenberg (2018) Single cell transcriptome profiling of retinal ganglion cells identifies cellular subtypes. *Nat Commun*, 9, 2759.

Rich, K. A., Y. Zhan & J. C. Blanks (1997) Migration and synaptogenesis of cone photoreceptors in the developing mouse retina. *J Comp Neurol*, 388, 47-63.

Rosso, S. B. & N. C. Inestrosa (2013) WNT signaling in neuronal maturation and synaptogenesis. *Front Cell Neurosci*, 7, 103.

Salbaum, J. M. & F. H. Ruddle (1994) Embryonic expression pattern of amyloid protein precursor suggests a role in differentiation of specific subsets of neurons. *J Exp Zool*, 269, 116-27.

Sharrocks, A. D. (2006) PIAS proteins and transcriptional regulation--more than just SUMO E3 ligases? *Genes Dev*, 20, 754-8.

Shekhar, K., S. W. Lapan, I. E. Whitney, N. M. Tran, E. Z. Macosko, M. Kowalczyk, X. Adiconis, J. Z. Levin, J. Nemesh, M. Goldman, S. A. McCarroll, C. L. Cepko, A. Regev & J. R. Sanes (2016) Comprehensive Classification of Retinal Bipolar Neurons by Single-Cell Transcriptomics. *Cell*, 166, 1308-1323.e30.

Shiomi, K., H. Uchida, K. Keino-Masu & M. Masu (2003) Ccd1, a novel protein with a DIX domain, is a positive regulator in the Wnt signaling during zebrafish neural patterning. *Curr Biol*, 13, 73-7.

Shiomi, K., M. Kanemoto, K. Keino-Masu, S. Yoshida, K. Soma & M. Masu (2005) Identification and differential expression of multiple isoforms of mouse Coiled-coil-DIX1 (Ccd1), a positive regulator of Wnt signaling. *Brain Res Mol Brain Res*, 135, 169-80.

Shuai, K. & B. Liu (2005) Regulation of gene-activation pathways by PIAS proteins in the immune system. *Nat Rev Immunol*, 5, 593-605.

Sidman RL. Histogenesis of mouse retina studied with thymidine-H3. In: Smelser GK, editor. *The Structure of the Eye.* 1961. pp. 487–506.

Singh, K. K., X. Ge, Y. Mao, L. Drane, K. Meletis, B. A. Samuels & L. H. Tsai (2010) Dixdc1 is a critical regulator of DISC1 and embryonic cortical development. *Neuron*, 67, 33-48.

Snow, R. L. & J. A. Robson (1994) Ganglion cell neurogenesis, migration and early differentiation in the chick retina. *Neuroscience*, 58, 399-409.

Soma, K., K. Shiomi, K. Keino-Masu & M. Masu (2006) Expression of mouse Coiled-coil-DIX1 (Ccd1), a positive regulator of Wnt signaling, during embryonic development. *Gene Expr Patterns*, 6, 325-30.

Strettoi, E., E. Raviola & R. F. Dacheux (1992) Synaptic connections of the narrow-field, bistratified rod amacrine cell (AII) in the rabbit retina. *J Comp Neurol*, 325, 152-68.

Strettoi, E. & M. Volpini (2002) Retinal organization in the bcl-2-overexpressing transgenic mouse. *J Comp Neurol*, 446, 1-10.

Suzuki-Kerr, H., T. Iwagawa, H. Sagara, A. Mizota, Y. Suzuki & S. Watanabe (2018) Pivotal roles of Fezf2 in differentiation of cone OFF bipolar cells and functional maturation of cone ON bipolar cells in retina. *Exp Eye Res*, 171, 142-154.

Tran, N. M., K. Shekhar, I. E. Whitney, A. Jacobi, I. Benhar, G. Hong, W. Yan, X. Adiconis, M. E. Arnold, J. M. Lee, J. Z. Levin, D. Lin, C. Wang, C. M. Lieber, A. Regev, Z. He & J. R. Sanes (2019) Single-Cell Profiles of Retinal Ganglion

Cells Differing in Resilience to Injury Reveal Neuroprotective Genes. *Neuron*, 104, 1039-1055.e12.

Turner, D. L. & C. L. Cepko (1987) A common progenitor for neurons and glia persists in rat retina late in development. *Nature*, 328, 131-6.

Turner, D. L., E. Y. Snyder & C. L. Cepko (1990) Lineage-independent determination of cell type in the embryonic mouse retina. *Neuron*, 4, 833-45.

Um, J. W., G. Pramanik, J. S. Ko, M. Y. Song, D. Lee, H. Kim, K. S. Park, T. C. Südhof, K. Tabuchi & J. Ko (2014) Calsyntenins function as synaptogenic adhesion molecules in concert with neurexins. *Cell Rep*, 6, 1096-1109.

Valnegri, P., S. V. Puram & A. Bonni (2015) Regulation of dendrite morphogenesis by extrinsic cues. *Trends Neurosci*, 38, 439-47.

Vekrellis, K., M. J. McCarthy, A. Watson, J. Whitfield, L. L. Rubin & J. Ham (1997) Bax promotes neuronal cell death and is downregulated during the development of the nervous system. *Development*, 124, 1239-49.

Voinescu, P. E., P. Emanuela, J. N. Kay & J. R. Sanes (2009) Birthdays of retinal amacrine cell subtypes are systematically related to their molecular identity and soma position. *J Comp Neurol*, 517, 737-50.

Wang, X., L. Zheng, Z. Zeng, G. Zhou, J. Chien, C. Qian, G. Vasmatzis, V. Shridhar, L. Chen & W. Liu (2006) DIXDC1 isoform, l-DIXDC1, is a novel filamentous actin-binding protein. *Biochem Biophys Res Commun*, 347, 22-30.

West, E. R. & C. L. Cepko (2022) Development and diversification of bipolar interneurons in the mammalian retina. *Dev Biol*, 481, 30-42.

Wetts, R. & S. E. Fraser (1988) Multipotent precursors can give rise to all major cell types of the frog retina. *Science*, 239, 1142-5.

Whitney, I. E., P. W. Keeley, M. A. Raven & B. E. Reese (2008) Spatial patterning of cholinergic amacrine cells in the mouse retina. *J Comp Neurol*, 508, 1-12.

Whitney, I. E., M. A. Raven, D. C. Ciobanu, R. W. Williams & B. E. Reese (2009) Multiple genes on chromosome 7 regulate dopaminergic amacrine cell number in the mouse retina. *Invest Ophthalmol Vis Sci*, 50, 1996-2003.

Whitney, I. E., M. A. Raven, L. Lu, R. W. Williams & B. E. Reese (2011) A QTL on chromosome 10 modulates cone photoreceptor number in the mouse retina. *Invest Ophthalmol Vis Sci*, 52, 3228-36.

Wässle, H. & H. J. Riemann (1978) The mosaic of nerve cells in the mammalian retina. *Proc R Soc Lond B Biol Sci*, 200, 441-61.

Wässle, H., C. Puller, F. Müller & S. Haverkamp (2009) Cone contacts, mosaics and territories of bipolar cells in the mouse retina. *J. Neurosci*., 29, 106-117.

Wong, G. T., L. Ruiz-Avila & RF Margolskee (1999) Directing Gene Expression to Gustducin-Positive Taste Receptor Cells.

Yan, W., M. A. Laboulaye, N. M. Tran, I. E. Whitney, I. Benhar & J. R. Sanes (2020) Mouse retinal cell atlus: Molecular identification of over sixty amacrine cell types. *J Neurosci*.

Young, R. W. (1985) Cell differentiation in the retina of the mouse. *Anat Rec*, 212, 199-205.

Young-Pearse, T. L., A. C. Chen, R. Chang, C. Marquez & D. J. Selkoe (2008) Secreted APP regulates the function of full-length APP in neurite outgrowth through interaction with integrin beta1. *Neural Dev*, 3, 15.

Zolessi, F. R., L. Poggi, C. J. Wilkinson, C. B. Chien & W. A. Harris (2006) Polarization and orientation of retinal ganglion cells in vivo. *Neural Dev*, 1, 2.